STABILITY CHARACTERIZATION OF ADVANCED INJECTORS

FINAL REPORT ON PHASE III OF CONTRACT NAS 8-20672

Prepared For

MARSHALL SPACE FLIGHT CENTER
Huntsville, Alabama

Report 20672-P3F

February 1971

AEROJET LIQUID ROCKET COMPANY
A DIVISION OF AEROJET-GENERAL
SACRAMENTO, CALIFORNIA

STABILITY CHARACTERIZATION OF

ADVANCED INJECTORS

FINAL REPORT ON PHASE III OF
CONTRACT NAS 8-20672

Prepared For

MARSHALL SPACE FLIGHT CENTER
Huntsville, Alabama

Report 20672-P3F

February 1971

TABLE OF CONTENTS

TABLE OF CONTENTS (cont.)

TABLE LIST

FIGURE LIST

FIGURE LIST (cont.)

FIGURE LIST (cont.)

I INTRODUCTION

The objective of this program is the evaluation of the combustion stability characteristics of advanced oxygen/hydrogen injectors. The program was initiated in December 1966 with an investigation of the effect of high velocity in the combustion chamber on stability. This report covers the third and final phase which was begun in July 1969. The feasibility of a new research tool, the transverse excitation chamber, as a method of characterizing the stability sensitivity of an injector was demonstrated in Phase I. Phase II continued this effort by characterizing the stability of a triplet injector. Additionally, a comprehensive design manual combining combustion stability theory with practical design applications was completed during Phase II.

Phase III consisted of the following four tasks:

Task I - The formulation of analytical models for the characterization of combustion stability in cylindrical and annular combustors, extensions of theory to include chamber Mach numbers up to 0.50 and the evaluation of this model applied to gas-gas combustion.

Task II - An experimental investigation of the response of the injector to combustion by testing it in the transverse excitation chamber. Two injectors were evaluated: a coaxial injector as previously tested in cylindrical and annular hardware on Phase I of this program and on Contract NAS 8-11741, and a HIPERTHIN injector.

Task III - The extension of the formulation of design criteria started during Phase II by improving the correlation equations with data from recent testing, both that from Task II of this program and from other investigations, and by including the analytical developments of Task 1.

Task IV - A preliminary evaluation of gaseous hydrogen/gaseous oxygen stability characteristics and current gas-gas stability models.

I Introduction (cont.)

The task shall include empirical evaluation of gas-gas stability at two regimes of chamber pressure: 300 psia and 15 psia. The objectives of this task are to attempt to determine the rate controlling mechanism of combustion stability with gaseous propellants and to identify areas where further work is required.

II SUMMARY

This phase of the contract continued the efforts of previous investigations (NAS 8-4008 and NAS 8-20672 Phases I and II) into the combustion stability of various oxygen/hydrogen injector designs. Previously coaxial, triplet and multi-orifice designs had been characterized. The purpose of the evaluations presented herein was to provide data for injectors to be used in future advanced cryogenic engines.

The objective of Phase III was to determine the transverse mode stability characteristics of coaxial and HIPERTHIN injectors in a transverse excitation chamber. The transverse excitation chamber is a research tool developed during Phase I to evaluate the response of injectors to purely transverse modes of instability. In addition, the Sensitive Time Lag Theory was to be extended to include operation at high Mach numbers. At the conclusion of the original contract period there were funds remaining and the scope of the contract was increased to include a investigation of the stability characteristics of gaseous oxygen/gaseous hydrogen propellants at moderate and low chamber pressures (300 and 15 psia).

II Summary (cont.)

A. COAXIAL TESTING

Coaxial injector testing in a transverse excitation chamber was conducted using an injector element previously tested on Phase I of this program and also on Contract NAS 8-11741. Twenty-four tests were conducted during this test program. The results compared favorably with predicted stability characteristics using correlations based on Sensitive Time Lag Theory.

B. HIPERTHIN TESTING

Combustion stability characteristic of HIPERTHIN injectors were also obtained during this phase. Previous test history on Advanced Injectors Development Program (Contract NAS 8-21052) showed instabilities occurring at high frequencies using the same injector pattern as tested on this program. This indicated that the sensitive frequency for this injector pattern was too high for the excitation chamber used for coaxial injector tests. Consequently, smaller, heat sink excitation chambers were built for evaluation of HIPERTHIN injectors. The fundamental mode frequency for these excitation chambers ranged from 4500 Hz to 16,00 Hz.

Four different sizes of excitation chambers and ten injectors were built and twenty-eight tests were conducted with them. The test results showed that some of the injector/chamber configurations were spontaneously unstable and others were dynamically stable. On the unstable tests the instability growth rates were used to characterize the system. In the case of the stable tests, a non-directional bomb was discharged during the steady-state portion of the test and the decay rates of the pressure spike were used to characterize the system.

II Summary (cont.)

C. GAS-GAS TESTING

Two series of tests were conducted in the investigation of gaseous oxygen/gaseous hydrogen stability characteristics. Both utilized hardware built previously for ALRC IR&D projects. The first consisted of twelve tests at nominal and peripheral operating conditions for the proposed Auxiliary Propulsion System (APS) engines for the Space Shuttle Vehicle. Testing was conducted at 300 psia chamber pressure and mixture ratios from two to six. All tests used a non-directional bomb for dynamic stability testing. Although each test experienced spontaneous pressure oscillations, they had peak to peak values less than five percent of the chamber pressure. In addition no sustained instabilities were caused by the bomb and pressure oscillations caused by the pressure spike dissipated within 10 msec. The data indicated the time required for the oscillations to decay from a bomb induced pressure spike was proportional to the mixture ratio with little dependence on fuel temperature.

The second series of tests was conducted at a chamber pressure of 15 psia and mixture ratios of approximately 2.7. This series was designed to investigate the interaction of the feed system and chamber in an engine with gaseous propellants. There were 40 tests, 27 of which were successful. All tests were unstable with a 1500 Hz oscillation predominating. No oscillation successfully damped by use of a fuel system resonator. There was no effect evident due to increases in the feed system pressure drops. The data obtained in this test series did not lead to any direct conclusion regarding gaseous feed systems other than the appearance of some coupling to produce the 1500 Hz oscillations.

II Summary (cont.)

D. ANALYTICAL MODELS

The Sensitive Time Lag Theory was extended to include operation at high Mach numbers in the combustion zone. A model was formulated which characterized the response of a staged combustion system to high frequency instability. A model for the tap-off portion of feed system for the hot gas tap-off cycle was also developed.

III CONCLUSIONS

A. Coaxial Injector Tests

1. The objective of characterizing coaxial injectors in the transverse excitation chamber was met. The decay rate data from the pulse was demonstrated as a realistic representation of the responsiveness of the system to the coupling of combustion with system acoustics.

2. All tests were dynamically stable. By post-test visual inspection it was determined that combustion had occurred a considerable distance downstream. By considering the effect of non-uniform injection it was estimated that at the point where combustion was occurring the mechanism by which the combustion coupled with the system acoustics was only 43 percent effective. The likelihood of spontaneous instabilities would markedly increase if the combustion chamber used to test these injectors were specifically designed to account for the relatively long precombustion distance necessary, e.g. a chamber whose convergent section did not begin until the combustion was completed.

3. The correlations for coaxial injectors based on sensitive time lag theory produced an accurate expression for the sensitive frequency of the system. There appears to be a slight change in system response (or damping) due to the effects of mixture ratio.

B. HIPERTHIN Injector Tests

1. The objective of evaluating HIPERTHIN injectors in transverse excitation chambers was met satisfactorily. Both stable and spontaneously unstable tests were conducted. The data indicated a general dependency on chamber pressure for system stability.

2. Successful fabrication of ten HIPERTHIN injector platelet stacks was achieved. One problem was encountered in the brazing operation. The fuel manifold of one injector apparently was not adequately brazed

III Conclusions (cont.)

to the injector and failed during a test resulting in damage to the injector.

3. Four copper heat sink combustion chambers were satisfactorily manufactured. The hafnia flame barrier coating in the combustion zone was unsatisfactory since it flaked and spalled off the chamber walls during the test program. The use of heat sink excitation chambers was completely satisfactory even with the unsatisfactory coating performance. There was a minimum of streaking and erosion and the throats of each chamber withstood many test firings with a minimum change in dimension.

C. Analytical Model Development

Two new analytical models were completed and programmed for the computer; the gas tap-off model and the staged combustion model. In addition the analytical models presented in Ref. 8 have been extended to include the effects of operation at high Mach numbers. The computer program given in Ref. 8 has undergone extensive revision and is being issued in a revised edition which will reflect changes such as those for high Mach number operation (Ref. 16). The gas-tapoff and staged combustion models and computer programs will be included as Appendices to Ref. 16.

D. Gas-Gas Testing

Two series of tests using gaseous oxygen/gaseous hydrogen propellants were completed with hardware developed previously on ALRC IR&D programs. The tests were designed to simulate anticipated operating conditions of the Auxiliary Propulsion Systems of the proposed space shuttle vehicle. There are two distinct categories of the APS; high pressure at 300 psia chamber pressure and low pressure at 15 psia.

The initial series of twelve tests was designed to investigate the dependence of dynamic combustion stability on mixture ratio and propellant

III CONCLUSIONS (cont.)

temperature at a constant chamber pressure of 300 psia. All tests were dynamically stable with a relatively low performing (≃ 95% C*) injector. The tests all showed low level (< 10% of chamber pressure) oscillations observed before and after perturbations induced by a non-dimensional bomb. The damping rates from the bomb induced overpressures increased with increasing mixture ratio. There was very little effect of propellant temperature on the damping time of the overpressures. It appears that high frequency stability characteristics at the 300 psia APS conditions are adequate with low performing injectors. This conclusion, however, does not rule out the possibility of problems with high performing injectors.

The remaining tests were designed to investigate feed system associated instability at a chamber pressure of 15 psia. High frequency instability was not evaluated during these tests. The use of a passive damping device similar to a quarter-wave tube to alter the admittance of the fuel feed system in an attempt to damp low frequency instabilities was unsuccessful. No attempt to evaluate oxidizer feed system admittance changes was made. Increases in the oxidizer feed system pressure drop appeared to have no effect on low frequency oscillations.

IV RECOMMENDATIONS

As a result of the efforts of this contract an experimental technique, using the transverse excitation chamber, has been developed. Continued use of this device is recommended when new propellant combination or unique injector designs are being evaluated.

Currently there is little or no experimental data or correlations relating injector design to specific physical processes felt to be important in determining the stability characteristics of gaseous propellants. These data are required if the mechanistic type stability models are to be used. Any experimental work in this area should first emphasize measurement techniques for identification of the significant rate controlling processes. This should then be followed by experiments designed to relate injector design characteristics to the rate controlling processes.

The excitation chamber because of the ability to vary its acoustic mode frequency is an excellent high sound level source for the evaluation of resonators under realistic rocket engine conditions. This device should be used to determine the response of representative designs over a broad frequency range.

V HARDWARE AND TEST FACILITIES

A. Coaxial Hardware

1. Injector

A major part of the test activity of this program was concentrated on the characterization of the high frequency response of a coaxial injector to combustion. The injector design selected for this testing was a coaxial element which had been tested previously and characterized for combustion stability in both a cylindrical combustion chamber (14 in. diameter, Contract NAS 8-11741) and 10.5-in. outside diameter by 6.15-in. inside diameter annular combustion chamber during Phase I of this program. The coaxial element tested in the transverse excitation chamber is shown in Figure 1 installed on Test Stand J-1 prior to a test firing. A photograph of the coaxial element used in the excitation chamber is shown in Figure 2. A section view of the coaxial element used in excitation chamber testing is shown in Figure 3 along with a sectional view of the coaxial elements used in the annular injector in Phase I of this program.

The durability of the triplet injector was significantly improved during Phase II of this program when the stainless steel face was replaced with an all-copper face. Photographs of the stainless steel triplet injector after two tests are shown in Figure 4a. The same injector pattern in an all-copper face after a maximum of fifteen tests is shown in Figure 4b. This test experience provided the principal reason for selection of an all-copper face for the coaxial injector for this phase of the program. A transient thermal analysis conducted on the copper coaxial injector resulted in the predictions shown in Figures 5 and 6. Figure 5 shows the predicted transient heating of the injector at a cross section through the coaxial element. Figure 6 shows a cross section through the injector body at a location other than the injection element.

The stress characteristics of the copper face were investigated because of the propensity of copper to plastic deformation.

V Hardware and Test Facilities (cont.)

There was concern that deformation of the face would produce a distortion at the fuel annulus sufficient to alter the flow characteristics. A finite element program was run in which temperatures from the thermal analysis were used and strain levels predicted at each station. Results of this analysis indicated that deformations due to the strain levels of normal operation would not be noticeable until after 20 test firings if the test durations were each less than two seconds. To increase the duration capability of the copper face and to reduce plastic deformation, a thin coating of zironium oxide coating was applied to the face of each injector. The major function of this coating was to reduce the temperature of the copper face. The effectiveness of the coating was apparent from the fact that after 24 tests the coating was intact and no noticeable deformation had occurred.

2. Transverse Excitation Chamber

Transverse modes of instability are pressure perturbations perpendicular to the direction of flow in a combustion chamber. The modes of a cylindrical combustion chamber included in this category are: tangential modes, radial modes, and pocket modes for baffled compartments. A combustion chamber (transverse excitation chamber) was designed and demonstrated on Phase I of this program for the sole purpose of evaluating these modes of instability.

The transverse excitation chambers used for triplet and coaxial injector evaluations on this program are shown disassembled in Figures 7 and 8. The chamber in Figure 7 was able to incorporate up to seven injector inserts and had a large arc distance across the injector face and therefore a low fundamental mode frequency (approximately 2000 Hz). The other chamber, shown in Figure 8 and used exclusively on this phase of the program, had a shorter arc distance producing a fundamental mode near 2800 Hz.

V Hardware and Test Facilities (cont.)

The transverse chamber contour was designed so that losses for transverse modes would be low and losses for longitudinal modes would be high. The vertical transverse mode located perpendicular to the mode across the arc portion of the chamber, was at frequency of approximately 13,000 Hz and was above the sensitive frequency of most in-injector configurations. The excitation chamber, therefore, provided a direct evaluation of combustion response to the fundamental mode frequency. An acoustic pressure profile for the transverse modes of instability and the transverse mode plus the first radial mode are shown on Figure 9.

The injector for the transverse excitation chamber consisted of a series of injector inserts such as that shown in Figure 2. The chamber angle (arc distance across the injector) was varied by use of wedges. Once a chamber angle had been selected for a test series, the wedge was placed in the chamber, secured to the chamber wall, and sealed to the chamber lid. The injector inserts were placed in the ports not covered by the wedge to make the injector for that chamber configuration. Figure 8 shows one coaxial injector insert in an injector port and a wedge covering two of the injector insert ports. A similar wedge exposing only two injectors and another exposing four injectors were also used. The combustion zone was protected by using a zirconium oxide coating on the portion of the chamber near the injector and ablative liners on the downstream section of the chamber. A series of ablative nozzles of different throat sizes were available for attachment to the aft flange of the chamber, and a lid was bolted on this assembly and sealed by an O-ring in the groove shown.

A pyrotechnic igniter consisting of an Alclo grain with a burn duration of 1.0 sec, was used to ignite the engine. A pulse gun was used to provide a pressure perturbation during the test. The pulse gun used a conventional 300 H&H magnum cartridge and contained 40 grains of No. 2 Bullseye pistol powder. This cartridge was fired with a squib-driven firing pin. A 20,000 psi burst diaphragm downstream of the pulse charge allowed a pressure buildup prior to discharge into the combustion chamber. The burst diaphragm also provided thermal isolation between the pulse charge and combustion gases.

V Hardware and Test Facilities (cont.)

3. Fabrication of Test Hardware

a. Coaxial Injectors

A stainless steel body was used for the coaxial injector. The stainless steel central oxidizer tube was furnace brazed into the injector body. The partially assembled injector was then fitted with the copper face which formed the fuel annulus around the oxidizer tube; this fitting procedure was crucial in providing an accurate fuel annulus. The assembly was then furnace brazed using a lower melt temperature braze alloy than in the previous braze cycle. Finally, the manifold tubes were attached, producing the finished part as shown in Figure 2.

b. Transverse Excitation Chambers

Two excitation chambers were constructed of all-stainless steel. The chambers were machined from a forged billet. The nozzle flanges were later welded to the chambers. The chamber lid was machined from a plate of stainless steel. Wedges were made of mild steel as were nozzle housings. The ablative pieces, both liners and nozzles, were made of a silica phenolic compound designated WBC-2230 (Western Backing Corp.) which has been used on many applications at ALRC with satisfactory results. During low chamber pressure testing, the exit flange was used as the throat. An ablative plate of silica phenolic was attached to the aft portion of the chamber to provide thermal protection of the hardware. Silicon O-rings were used for the hot gas seal at the following locations in the chamber: (1) the seal between the chamber and chamber lid, (2) the nozzle flange and the chamber, and (3) the shaft seal between the injector and the chamber in two locations.

4. Test Apparatus & Procedure

a. Test Stand Setup

V Hardware and Test Facilities (cont.)

Coaxial injector testing in the transverse excitation chamber was conducted at ALRC Test Stand J-1. A photograph of the excitation chamber installed on the test stand prior to testing is shown in Figure 1. A schematic flow and instrumentation diagram for Test Stand J-1 is shown in Figure 10. Propellant was supplied to the test stand by a 60-gallon nitrogen pressurized oxygen tank and a vacuum jacketed 100-gallon cryogenic hydrogen vessel pressurized with gaseous hydrogen.

Liquid oxygen was used for all tests. Hydrogen temperature at the injector was 80°R for the greater part of testing and 200°R for the remaining tests. The hydrogen temperature was varied in order to evaluate the effect of operation at two velocity ratios of the injected propellants. All tests were planned for mixture ratios between 4 and 6. Minor changes in the temperature of the propellants in the system produced significant density variations resulting in mixture ratio variations from test to test. The extent of this variation may be seen in the test data in Table 1.

The hydrogen temperature was maintained by preconditioning the propellant in the hydrogen vessel to the desired temperature after the system (lines, valves, flanges, etc.) had been sufficiently chilled to maintain a constant propellant temperature during the test firing. This preconditioning was accomplished during the pressurization of the hydrogen run vessel through a diffuser at the bottom of the tank; this allowed the warmer gaseous hydrogen to transfer heat to the liquid hydrogen.

The propellant temperature was monitored during the foregoing procedures and a test firing was initiated when the desired propellants temperature was reached. The run vessel was allowed to reach the desired pressure before final hydrogen temperature was reached. The run vessel was then vented slightly to allow the temperature to rise with the entry of additional pressurization gas. This was repeated until the desired

V Hardware and Test Facilities (cont.)

temperature was obtained.

b. Instrumentation

The stability characterization of coaxial injectors depends largely upon comparison of results with existing correlating equations. Data required for these correlations were considered of primary importance to the test program. The test measurements included in this category were:

Dynamic pressure measurements to determine accurately the mode of instability, the ampltiude, and growth or decay rate of the instability;

Static measurement of pressure in the combustion chamber, fuel and oxidizer manifolds for establishing the chamber pressure operating point and the low frequency parameter (injection pressure drop divided by operating chamber pressure);

The temperature and static pressure of the propellant and the rate propellant discharge in order to calculate velocity ratio of the propellants at the injection point;

Propellant flow rates for determining mixture ratio.

(1) Pressure Measurements

The most important parameter to be measured was the dynamic pressure measurements in the combustion zone. These data were recorded with helium bleed Kistler Model 615A high frequency pressure transducers. When testing with a wedge in the chamber these transducers were located at two locations; on the side of the chamber near the pulse gun and on the lid near the centerline of the chamber. These two locations may

V Hardware and Test Facilities (cont.)

be seen in Figure 9a. When testing without a wedge, a third Kistler was installed in the chamber wall opposite the pulse gun. The Photocon Model 352A used during the Phase I and II testing give data equal to that of the Kistler Model 615A when flush mounted to the combustion zone. The photocon transducer, however, has a 1-inch diameter water cooled flame shield exposed to combustion which sustained severe damage on several tests during Phase I and was replated by the helium bleed Kistler at that time. The Kistler transducer demonstrated satisfactory frequency response characteristics when located close to combustion. The transducer was exposed to combustion through an 0.060 in. diameter bleed orifice through which helium flowed to provide improved compatibility when compared to the Photocon installation.

The sensor in the Kistler pressure transducer has an extremely high natural frequency (on the order of 100,000 Hz). When installed with a helium bleed system the frequency response of the transducer is similar to that shown in Figure 24.a. Pressure perturbations were introduced during the test by firing a 40-grain pulse tangentially to the transverse mode.

Static pressure transducers were used to measure operating chamber pressure at the injectors and fuel and oxidizer manifolds.

(3) Temperature Measurements

Temperature measurements, when coupled with flow rate and pressures at the injector, were used to obtain velocity ratio data. The response of the temperature measuring equipment was crucial in obtaining the data at the time in a test when an instability occurred. The temperature measuring device selected to obtain these data was a 0.020 in. diameter sheathed copper constantan thermocouple. The thermocouple wires were .004 in.-diameter and when installed in a probe had a response time of 50 msec. The probe measuring fuel temperature was placed as close as possible to the point of entry to the combustion zone since the change in fuel density

V Hardware and Test Facilities (cont.)

is large in response to only slight changes in temperature. The oxidizer was not subject to as severe a density change, hence placement of the thermocouples in the oxidizer manifold posed no problems.

(3) Flow Measurements

Conventional turbine type flow meters were used to obtain volumetric flow data for both fuel and oxidizer circuits; pressure and temperatures upstream of the flow meter were monitored to obtain mass flow rates.

c. Test Procedure

Both the hydrogen and oxygen tanks were chilled down using the cryogenic liquid of each propellant until liquid was observed out of the vent stack. The insulated oxygen line and vacuum-jacketed fuel line were then chilled down. Both fuel and oxidizer manifolds were prechilled using liquid nitrogen through an external jacket.

Testing was initiated after the system was cooled down. A fuel lead was used to minimize the compatibility problems associated with high temperature operation through stoichiometric mixture ratio. Ignition was obtained by initiating a pyrotechnic igniter. The 40-grain pulse was discharged 50 milliseconds prior to FS-2, and the test duration was nominally one second. Gaseous nitrogen injector purges were turned on manually prior to FS-1 and were checked by system pressures until they had decayed below a predetermined level, at which point the purges began to flow until closed manually.

B. HIPERTHIN Hardware

1. Injector

V. Hardware and Test Facilities (cont.)

The HIPERTHIN injector was designed to duplicate injection characteristics of an injector from Contract NAS 8-21052, Advanced Injector Concepts Investigation (AICI). This injector contained an integral heat exchanger for increasing the temperature of the oxidizer by removing heat from heated hydrogen. The design of the injector for AICI was conducted concurrently with the combustion stability investigations of this program; as a result, changes were incorporated into the design as it progressed. Detailed features of this design are identified in Reference 3. Some general design characteristics are:

Propellants	O_2/H_2
Maximum operating chamber pressure	1500 psia
Throttling range	33:1
H_2 inlet temperature to the heat exchanger	200 to 500°R
Mixture ratio	4 to 6

The injector used for the combustion stability evaluations contained the same injection characteristics as the AICI injector. The major difference was in the heat exchanger portion of the injector. The stability evaluation injector had a short stainless heat exchanger rather than the relatively long nickel heat exchanger of the AICI injector; therefore, preconditioned propellants were used to produce an outlet temperature similar to that expected from the AICI injector.

The basic concept of a HIPERTHIN injector is to provide an injector with a uniform injector pattern of well-mixed propellants. The injectors were built from a series of thin platelets of stainless steel consisting of 0.020-in. thick, separator platelets, 0.006-in.-thick fuel metering platelets, and 0.008-in.-thick oxidizer metering platelets.

An injector assembly was made up of a oxidizer metering platelet followed by a separator platelet, a fuel metering platelet, and

V. Hardware and Test Facilities (cont.)

another separator platelet. This arrangement is shown in Figure 11. An injector was constructed by repeated assembly of such units.

The injector for this program was designed to duplicate the pressure drop section and part of the heat exchanger section of the AICI injector. A comparison of the fuel injection portion of the injector tested on this program and a similar fuel platelet from the AICI injector is seen in Figure 12.

A photograph of the series of platelets used in the HIPERTHIN injector is shown in Figure 13. The fuel separator platelet contains through-etched manifold passages and depth-etched distribution passages which feed through-etched fuel metering passages in the fuel metering platelet. The fuel metering platelet contains through-etched manifold and metering passages and was plated with braze alloy to an accurately controlled thickness. The oxidizer separator platelet was constructed in the same manner as the fuel separator platelet; however, the distribution grooves originate in the opposite manifold passage. The oxidizer metering platelet was also accurately plated with braze alloy and contains through-etched metering passages which are fed by the depth-etched distribution passages of the separator platelet. The width of the metering groove in the pressure drop section of the metering platelet was carefully controlled to produce uniform propellant distribution and an accurate, predictable pressure drop.

A computer program developed on the AICI program predicted the heat transfer characteristics of the heat exchanger portion of the injector. This program was used to predict the propellant temperature at the heat exchanger outlet. This was used to determine the desired propellant conditions at the manifold of the injector used on this program. The action of the propellants within the injector is as follows. The preconditioned propellants enter the fuel and oxidizer manifolds and are distributed throughout the injector by the depth-etched distribution grooves

V. Hardware and Test Facilities (cont.)

of the fuel and oxidizer separator platelets. The propellants then flow atlow velocities through the distribution section of the injector to the metering section. At the pressure drop section of the metering platelets the velocity of the propellant is increased significantly to produce the desired pressure drop for the injector. The velocity is then reduced by enlarging the flow passage to its original size. The propellants are then injected into the combustion chamber.

Injection velocities under normal operating conditions were 300 to 400 ft/sec for the fuel and 70 to 100ft/sec for the oxidizer. These velocities coupled with mass discharge produced a ratio of momentum of injected fuel to oxidizer from 0.75 to 1.00 over the range of operational conditions used during the test program described in Section V,B,4.

Many sets of platelets were used to produce a completed injector. The first platelet set started with a oxidizer passage and the last platelet set ended with an fuel passage; one additional set of fuel metering and separator platelets were added to each injector so that both outside passages were fuel. The intent of adding the fuel passage was to increase the compatibility between the injector chamber and to provide a slightly fuel-rich zone at the junction between the injectors when more than one injector was used in a combustion chamber. The first four injectors had 34 sets of platelets; the next four injectors increased the platelet sets to 35 to provide a slight increase in injector width because it had been found that the shrinkage of the platelet assembly during the first braze operation was greater than had been anticipated. These eight injectors had final face dimensions of approximately 0.75 to 2.0 in. Two other injectors were built with 52 sets of platelets producing an injector face 0.75 to 3.0 in.

Following is a list of design details common to all of the injectors;

V. Hardware and Test Facilities (cont.)

	Oxidizer	Fuel
Depth of distribution passages	0.008	0.006
Width of distribution passages	0.050	0.050
Depth of metering passages	0.008	0.006
Width of metering passages	0.028	0.034
Depth of injection passages	0.008	0.006
Width of injection passages	0.050	0.050
No. of orifices per platelet	8	8

2. Excitation Chamber

Selection of a chamber size for evaluation of the HIPERTHIN injectors first required an estimate of the frequencies at which the HIPERTHIN injector would couple with combustion. The large excitation chamber for testing coaxial injectors operates at fundamental modes frequencies as low as 2600 Hz. The vertical transverse mode, which is perpendicular to this first mode, is near 13,000 Hz. The frequency band between these extremes is adequate to evaluate the most conventional injector patterns; however, for the extremely fine pattern, as in the HIPERTHIN injector, sensitive frequencies could occur near 13,000 Hz. If so, this would require an excitation chamber capable of testing at higher frequencies to verify that the injector response had actually reached a maximum. Test data from Phase II of the Advanced Injector Concepts Investigation and previous test history with the excitation chamber using triplet injectors were used to predice a frequency range within which the sensitive frequency range from 4000 Hz to 16,000 Hz was determined to be adequate to characterize the injector. The resulting minimum injector face dimensions of 2.0 in. by 0.75 in. was determined to meet the frequency range requirement.

Since the vertical mode frequency of the transverse excitation chamber used for coaxial injector characterization was too near the predicted sensitive frequency of the HIPERTHIN injector, smaller heat

V. Hardware and Test Facilities (cont.)

sink chambers were designed for these tests. A selection was made of four chamber sizes, producing four fundamental mode frequencies between 4000 and 16,000 Hz. A constant angle of 36 deg. was selected for the converging part of the two-dimensional excitation chambers. The non-converging height of the chamber was 0.75 inches for the entire length of the chamber. The The major variables in the four transverse excitation chambers were the chamber radius and arc distance across the face of the injector.

The chambers were designed to accommodate a modular assembly of common size injectors to construct the injector face of varied arc distances. The 2-in. by 0.75 in. injector was chosen for construction of three of the four excitation chambers. A schematic representation of the largest chamber, which had an 8-in. face composed of four of the injectors is shown in Figure 14. A chamber with a 4-in. face used two injectors, and a chamber with a 2-in. face had one injector. A fourth chamber with a 3-in. face used one injector 3 in. wide.

The chamber contour was typical of the transverse excitation chamber design. The chamber walls converged at a constant 36^{o} angle to the injector face. When the four injector modules were placed in the largest excitation chamber, the face of the injector approximated an arc; a similar situation existed for the two injector module chamber. In the two smallest chambers, which accept only a single injector module a flat face injector results. The assembled chambers are shown in Figure 15.

A heat sink type combustion chamber was selected as the best candidate for the types of tests planned for the HIPERTHIN injectors. Copper was selected as the chamber material because of its heat sink capability. A thermal analysis of the chambers indicated that, at high chamber pressures (P_c of 1500 psia), only very short (0.1 sec) tests could be conducted if free-standing copper was used, whereas at low chamber pressures ($P_c < 500$ psia) test durations to 1.0 sec were practical. A refractory coating of hafnia (HfO_2) appeared to be a practical means for extending the duration capability of the

V. Hardware and Test Facilities (cont.)

copper chamber. It was predicted that a thickness of 0.005 in. to 0.007 in. would be adequate to thermally protect the copper for test durations of 1.0 sec at 1500 psia chamber pressure.

3. Fabrication

a. HIPERTHIN Injector

The platelets used in the fabrication of HIPERTHIN injectors are shown in Figure 13. The metering platelets, both fuel and oxidizer, were plated to a carefully controlled thickness of copper. This plating served as braze alloy for the platelet assembly. The first four injectors were brazed together without structural end plates. The brazed platelet stack was then machined flat in preparation for end plate braze. The platelet stack was checked for leakage before brazing the end plates to the stack. The end plates were fitted to the platelet stack and furnace brazed with a lower melting temperature braze alloy. The side of the injector assembly was machined to open the manifolds. The inlet portions of the injector passages were inspected visually at this point to insure that the passages were open and there were no inter-manifold leaks. A plate with associated manifold tubing was brazed over the open manifold using a still lower temperature braze alloy than the previous braze operation. A photo of the face of two finished injectors is shown in Figure 16.

The first four injectors were measured for flatness before the end plate braze operation. This measurement showed that the platelet assembly was flat and the end plates could have been brazed to the platelet assembly during the first braze cycle. The next four injectors were assembled so that the end plate braze operation was conducted concurrently with the platelet braze. This assembly procedure was satisfactory since no leakage problems were encountered during subsequent leak-checks. The 3-in. wide injectors were brazed in the same manner and no problems were noted.

V. Hardware and Test Facilities (cont.)

When leak-checking the injectors with the manifolds open for visual inspection, small inter-manifold leaks were noted on several injectors. There seemed to be an equal degree of susceptibility to these leaks on both injectors which had end plates brazed on during the first braze cycle and injectors assembled by two separate braze cycles. To eliminate the possibility of inter-circuit leakage during testing, a vent slot was machined in every injector between the two manifolds. The slot was filled with braze alloy prior to the last braze cycle. The vent slot allowed the leakage to vent to atmosphere if the braze alloy did not fill or block the leak passages. This modification apparently repaired most of these minor leaks. Only one injector showed that the braze alloy did not stop the leak, and it was leaking slightly out the vent at moderate pressures.

After brazing the two manifolds cover plates over the fuel and oxidizer manifolds it was discovered that slight leakage also occurred through this braze joint. A retainer groove was machined around this joint and a repair braze conducted. The injectors were then leak checked and proof tested prior to test firing.

After the injector braze operations were completed, the part of the injector that inserted into the chamber was machined to final contour. The injector passages were machined open and the face was electropolished to clear the passages of small burrs. A photograph of the two sizes of completed injectors is shown in Figure 17.

b. Excitation Chamber

The transverse excitation chambers built for characterization of HIPERTHIN injectors were brazed assemblies of OFHC copper plate. The plates for the flat parts of the chamber were first reinforced with steel ribs to provide a higher rigidity across the unsupported sections of the chamber. These ribs also prevented the chamber from sagging when the

V. Hardware and Test Facilities (cont.)

flat plates were brazed to the side pieces which formed the chamber contour. A photograph of the largest chamber is shown in Figure 18. During the assembly of the chambers, the internal contour at the combustion zone was coated with hafnia (HfO_2) prior to the final braze cycle. The two smallest chambers are shown in Figure 19, after the coating was applied and prior to final brazing.

To evaluate the effect of subjecting copper coated with hafnia to a braze cycle, test samples were made with various coating thicknesses, with and without a base coating and subjected to an experimental braze cycle. Five 0.375 x 3.0 x 5.0 plates of OFHC copper were prepared with the following coating details:

(1) 0.003 in. thick hafnia on 0.004 in. thick Nichrome base

(2) 0.005 in. thick hafnia on 0.004 in. thick Nichrome base

(3) 0.005 in. thick hafnia on parent copper

(4)& (5) 0.005 in. thick hafnia on 0.004 in. thick Nichrome base on one-half of the plate. The other half was uncoated parent cooper.

The two plates which were only coated on half of the plate were used to make an experimental lap-joint where the two surfaces of parent metal were brazed together.

All of the coated parts survived the furnace braze cycle. No evidence of peeling, flaking, or separation from the parent surface was observed. The experimental braze joint was satisfactory. No evidence of cracking or deterioration of strength of the joint was noted nor was there detected any intrusion of braze material into the coating. It was concluded from these experiments that the bond of the coating to the chamber would not deteriorate seriously during a braze cycle.

V. Hardware and Test Facilities (cont.)

As a result of the above experiments, all the excitation chambers received a 0.004 to 0.006 in. coating of hafnia on the parent copper prior to the final braze cycle. The coating was applied to the combustion zone and tapered off under the injectors.

c. Ancillary Hardware

This hardware included: manifolds, igniter, and pulsing device.

Manifolds for feeding four injectors simultaneously were made for both fuel and oxidizer systems. These manifolds were balanced for uniform propellant discharge by selected fitting of the orifices to the discharge ports. This same piece of hardware served as manifold for the 2-injector chamber by capping two of the discharge ports.

The propellants were ignited by a pyrotechnic igniter which screwed into a standard 1/4-inch fitting. The igniter selected for these tests had a 10 msec burning time. This igniter was selected because of its size and a history of satisfactory use of experimental test programs.

A non-directional bomb containing 100 mg of RDX explosive was designed specifically for this program and may be seen on Figure 15 installed in the 3-in. excitation chamber. The bomb was inserted through a 1/4-inch Swagelock fitting and sealed on a stainless steel shaft. Details of the bomb design are seen in Figure 20. The explosive was encased in a Teflon sleeve and contained an electrical squib for ignition so that the bomb would discharge on command during the test. The majority of the tests did not use a pulsing device since spontaneous instabilities were obtained during the early part of the test program. Later in the test program, however,

V. Hardware and Test Facilities (cont.)

when testing was conducted at higher frequencies (smallest chambers) the bombs were necessary in order to obtain stability data.

4. Test Apparatus and Procedure

a. Test Stand Setup

Testing of HIPERTHIN injectors on this program was conducted in ALRC Research Physics Laboratory, Bay No. 7. A photograph of a chamber containing a single 3-in.-wide injector installed on the test stand is shown in Figure 21. A flow diagram schematically showing the test system and instrumentation locations in Bay No. 7 is included as Figure 22.

Temperature conditioned hydrogen was supplied to the combustion chamber by a cooling tower. The tower consisted of a pressure vessel filled with copper rings with temperature probes at top, bottom, and center. Nitrogen, at the desired temperature was injected at the bottom of the cooling tower, cooling the copper rings as it passed through the bed and out the vent. When the temperature probes at the three stations along the tower sensed the desired temperature the system was ready to receive gaseous hydrogen. Gaseous hydrogen for testing was injected at the top of the tower and passed through the tower, cooling the hydrogen to the temperature of the cooled copper rings.

Oxygen preconditioning was done by mixing ambient gaseous oxygen with liquid oxygen until the desired temperature for testing was attained. This mixing was done by setting the pressure regulator of the ambient gaseous oxygen at the upstream pressure of the main-line flow venturi to the pressure required for test flow rates. Liquid oxygen was then bled in through a separate flow system until the desired mixture temperature

V. Hardware and Test Facilities (cont.)

was attained. A test was initiated once the run system (lines and fitting) was cooled to constant temperature by flowing oxygen at the desired temperature.

b. Instrumentation

The test parameters required to characterize the HIPERTHIN injector were: propellant mass flow rate, injection temperatures, injection pressures, static combustion chamber pressure measurements, and dynamic pressure measurements in the combustion zone.

(1) Pressure Measurements

Dynamic pressure measurements in the combustion zone were singularily the most important measurements of the test program. To make this measurement, helium bleed Kistler model 615A high-frequency pressure transducers were used on the excitation chambers at locations shown in Figure 23. Reasons for selection of this particular transducer are given in Section V,A,4,b,(1). The transducer's sensor element was located approximately 0.25 inch from the combustion. The gain versus frequency characteristic for the Model 615A transducers used on the two largest excitation chambers is shown in Figure 24. It was necessary to improve the gain versus frequency characteristics of the transducers for use in the two smallest chambers. This was done by machining the tip of the transducer body to the configuration shown in Figure 25. This modification allowed the sensor to be located closer to the combustion zone, thereby increasing its resonant frequency and giving a gain versus frequency curve as shown in Figure 24b.

Static pressure transducers were located near the injector in the combustion chamber and in the fuel and oxidizer manifolds.

V. Hardware and Test Facilities (cont.)

(2) Temperature Measurements

Rapid response, 20-mil, sheathed copper constantan thermocouples were located at the fuel and oxidizer manifolds. Conventional thermocouples were located upstream of the flow venturis in both the fuel and the oxidizer systems.

(3) Flow Measurements

Flow venturis were located in the run line upstream of the thrust chamber valve. Pressures, both upstream and downstream of the venturi and the temperature upstream were recorded for each test. These data were input for a program which calculated the mass flow rate by using the venturi calibration curve and propellant transport property data.

c. Test Procedure

Both hydrogen and oxygen were used as cooled gases for the testing on this program. A detailed description of the equipment used in obtaining the preconditioned propellants is included in the description of the test hardware in paragraph V,B,4,a.

The firing sequence was controlled by the temperature of the propellants in the fuel and oxidizer manifolds. Following is a description of a test sequence which occurred after fire switch had been activated.

The hydrogen run line through the injector was chilled down using preconditioned hydrogen from the cooling tower until the temperature of the fuel manifold reached the predetermined temperature for test operation. The fuel thrust chamber valve was then closed.

V. Hardware and Test Facilities (cont.)

After a 0.5 second delay the oxygen thrust chamber valve and a bleed valve were actuated to allow the temperature of the oxidizer manifold to reach a predetermined value. The oxidizer thrust chamber valve was then closed.

The recording devices were activated.

After a 0.5 second delay the injector purges (both fuel and oxidizer) were actuated for 1 second.

Firing was initiated with a slight (0-10 msec) fuel lead. The igniter was initiated about 30 msec after the fuel manifold pressure increased.

Shutdown occurred after 1.00 sec firing (or at higher chamber pressures, 0.5 seconds) with the oxidizer valve closing first.

C. Gas-Gas Hardware

1. High Pressure (300 psia)

a. Hardware

The hardware used for this portion of the program was fabricated on a previous ALRC IR&D program. It had been designed for gaseous oxygen/gaseous hydrogen propellants at nominal operating conditions of the Space Shuttle High Pressure APS: chamber pressure of 300 psia and mixture ratio of 4. The objective of this program was to test dynamic stability of an engine operating with gaseous propellants at nominal and peripheral operating conditions of the APS.

(1) Injector

The injector was an impinging swirl-cup coaxial

V. Hardware and Test Facilities (cont.)

injector. It is so named because the manifolding results in the fuel being injected normal to the axially directed oxidizer streams. The fuel enters the mixing cup through two tangential ports thus swirling the flow in the cup as shown schematically in Figure 26. This injector concept uses a concentric ring manifold system which is attached to a face plate assembly which contains internal fuel passages. The oxidizer channels discharge into holes which go through the face plate. The fuel channel feed into a labyrinth of passages in the face plate which provide regenerative cooling as well as fuel entry into each element. A photograph of the injector mounted on the test stand is included as Figure 27.

(2) Chamber

The chamber was a 4.25 in. diameter, 4 in. long copper chamber with a 2-in. extension ring added at the injector end. Of the original chamber wall thermocouples, ten were still in operating condition.

b. Test Apparatus and Procedure

(1) Test Stand Setup

The testing of the impinging swirl cup coaxial injector was conducted on the test stand in ALRC Research Physics Laboratory Bay 7. A photograph of the engine on the stand is shown in Figure 28. A flow diagram schematically showing the test system and instrumentation in Bay 7 is included as Figure 29.

The preliminary test plan was to fire twelve tests at both nominal and peripheral APS operating conditions. The operating conditions for these tests are shown in Table 6. The propellants for the ambient temperature tests were delivered through the system without the activation of the cooling procedures. In the case of chilled propellants the

V. Hardware and Test Facilities (cont.)

following steps were implemented. Temperature conditioned hydrogen was supplied to the combustion chamber by a cooling tower. The tower consists of a pressure vessel filled with copper rings with temperature probes at top, bottom, and center. Nitrogen, at the desired temperature was injected at the bottom of the cooling tower, cooling the copper rings as it passed through the bed and out the vent. When the temperature probes at the three stations along the tower sensed the desired temperature the system was ready to receive gaseous hydrogen. Gaseous hydrogen for testing was injected at the top of the tower and passed through the tower, cooling the hydrogen to the temperature of the cooled copper rings.

Oxygen preconditioning was accomplished by mixing ambient gaseous oxygen with liquid oxygen and bleeding the mixture through the test apparatus until the desired test temperature was attained. The test was conducted once the entire apparatus was cooled to a desirable test temperature.

(2) Instrumentation

The test parameters required to characterize the injector were: propellant mass flow rate, injection temperatures, injection pressures, static combustion chamber pressure measurements, and dynamic pressure measurements in the combustion zone.

Dynamic pressure measurements were made with two water cooled Model 307 Photocons in the chamber and one in each of the two propellant feed lines. The two chamber Photocons were located at 0^{o} and 270^{o} from vertical and approximately 1 inch downstream of the injector. In both tests 2 and 3 the instrument at the 270° position was destroyed for no apparent reason. After losing two instruments in succession it was decided to continue the test program with a single high frequency instrument in the chamber and the two in the feed lines.

V. Hardware and Test Facilities (cont.)

Static pressure transducers were located in the chamber and in each of the propellant manifolds.

A total of 10 operational rapid response 0.020 in. sheathed chromel-alumel thermocouples were in three axial rows in the chamber walls. It was anticipated that the data from these thermocouples would provide some insight into the question of combustion efficiency as a function of axial distance.

Conventional thermocouple were located upstream of the flow venturies and in the two propellant manifolds. Flow metering venturis were located in the run line upstream of the thrust chamber valve. Pressures, both upstream and downstream of the venturi and the temperature upstream were recorded for each test. These data were the input for a computer program which calculated the mass flow rate by using the venturi calibration curve and propellant transport property data.

(3) Test Procedure

There were slight variations in the test procecures resulting from the varying propellant temperature requirements. When there was a need to chill the propellants they were preconditioned in accordance with the procedures mentioned in paragraph V,C,1,c,(1).

The firing sequence was controlled by propellant temperature when preconditioned propellants were necessary. The following is a description of the test sequence. The referenced operations regarding preconditioned propellants are naturally eliminated from tests where the propellants are at ambient temperatures.

V. Hardware and Test Facilities (cont.)

The hydrogen run line through the injector was chilled down using preconditioned hydrogen from the cooling tower until the temperature of the fuel manifold reached the predetermined temperature for test operation. The fuel thrust chamber valve was then closed.

After minimal delay the oxygen thrust chamber valve and a bleed valve were actuated to allow the temperature of the oxidizer manifold to reach a predetermined value. The oxidizer thrust chamber valve was then closed.

Fire Switch (The sequence began with this step when there was no requirement for preconditioned propellants).

The recording devices were activated.

After a 1 second delay the two thrust chamber valves were actuated simultaneously. The pyrotechnic igniter was ignited after a 200 msec delay and a non-directional bomb was ignited after another 200 msec. This bomb is the same design as used in the HIPERTHIN testing and is discussed in detail in Section V,B,3,c.

Shutdown occurred approximately 500 msec after ignition with the oxidizer valve closing first.

2. Low Pressure (15 psia)

a. Hardware

The hardware used on this portion of the program was also fabricated on a previous ALRC IR&D program. It had been designed for gaseous oxygen/gaseous hydrogen at nominal operating conditions for the Space Shuttle Low Pressure APS: chamber pressure 15 psia and mixture ratio

V. Hardware and Test Facilities (cont.)

2.5. The objective of these tests was to obtain data regarding feed system coupling with acoustic modes of the combustion chamber.

(1) Injector

The injector used for these tests consists of a steel coaxial injector body with removable fuel sleeves and oxidizer tubes. The parameter variations possible with this hardware (shown in Figures 30 and 31) in conjunction with minor feed system changes are: mixture ratio, chamber length, chamber diameter, fuel injection velocity, oxidizer injection velocity, oxidizer tube end location, fuel circuit resistance and oxidizer system resistance.

The hardware was assembled so to closely simulate the injector element geometry on the APS. Accordingly, the injector was designed to produce a fuel injection velocity of approximately 1400 ft/sec and an oxidizer velocity of 100 ft/sec. Also the mixture ratio was in the range of 2.5 - 3.2 and the oxidizer injection tube was recessed approximately a distance equivalent to its inner radius.

(2) Chamber

As was the case for the injector this hardware was design for parameter studies and therefore there are several chambers and nozzles available.

The chamber selected for use was the largest diameter (1.75 in.) shortest length (4.00 in.) chamber available. This choice was made to attempt to preclude conditions favorable to the establishment of a longitudinal chamber mode which could possibly mask the feed system data.

V. Hardware and Test Facilities (cont.)

(3) Ancillary Hardware

The ignition system consisted of a surface gap spark plug mounted in the chamber wall immediately upstream of the convergent nozzle entrance. It is fired at 50 H_z by a GLA Variable Energy Three Point Spark Gap system delivering 50 millijoules per spark.

Since the objective of this test series was to obtain data regarding feed system coupling with chamber acoustic modes, there was some hardware modifications which had to be made. The incoming fuel feed line was equipped with a tee into which 6-in. sections of 3/8 in. tubing could be added to create a resonator of varying dimensions based on the concept of the quarter-wave tube. The maximum length of the resonator was 54 in. This length plus the 14 in. from the injector face to the start of the resonator was equivalent to a quarter-wave tube designed to resonate at approximately 200 H_z. This system was assumed to be acoustically isolated from the remainder of the feed system due to the inclusion of flow metering venturi upstream of the entrance to the resonator.

b. Test Apparatus and Procedure

(1) Test Stand Setup

The testing of the uni-element coaxial injector was conducted on the test stand in Research Physics Lab Bay 1. This bay is equipped with an altitude simulation facility capable of obtaining a test pressure of approximately 1.5 psia. A schematic diagram of this facility is shown in Figure 32. A photograph of the uni-element hardware on the test stand is shown in Figure 33. The propellants for all tests in this series were at ambient conditions thus there was no preconditioning equipment. The feed system resonator as shown in Figure 33 was a variable in length from a minimum of zero inches to a maximum of 54 inches in 6 in. increments.

V. Hardware and Test Facilities (cont.)

(2) Instrumentation

The evaluation of the chamber-feed system acoustic coupling was the primary interest in this series of tests. The principal parameters to be measured therefore, were the high frequency pressure oscillations in both the chamber and the feed systems. These dynamic pressure measurements were made with model 601H Kistler high frequency pressure transducers. There was a Kistler in each of three locations: the chamber wall, to record chamber high frequency data; the oxygen feed system directly adjacent to the tap for POJ measurement, and; the end of the hydrogen feed system resonator. Later in the testing a fourth Kistler was added at the injector hydrogen manifold.

Flow venturis were located between the thrust chamber valves and the chamber. Pressures and temperatures were recorded immediately upstream and downstream of the venturi in the oxygen line and upstream of the venturi and in the manifold in the hydrogen line. These data allow for calculation of mass flow rates of the propellants.

Additionally, there was a steady state pressure transducer located in the chamber wall to measure chamber pressure.

(3) Test Procedure

The objective of this test program was to attempt to evaluate acoustic coupling of the feed system with the chamber. This was to be accomplished by means of feed system geometry changes and therefore, no changes were made to the original flow rates as the series progressed.

The sequence of events which transpired from the start of the test to the end will be discussed in detail here. The test sequence used throughout was as follows:

V. Hardware and Test Facilities (cont.)

Recording devices were activated

Approximately 900 msec later the spark plug was energized.

30 msec later the oxidizer valve was opened.

Approximately 40 msec later the fuel valve opened.

150 msec later the spark plug energy system was switched off.

310 msec later the ox valve was closed.

10 msec later the fuel valve was closed.

500 msec later the records were switched off

After completion of a successful test the length of the resonator built into the fuel system was either lengthened or shortened by a six inch section and the above sequence was repeated.

VI TEST RESULTS

A. Coaxial Injector Testing

1. Test Results

Twelve tests were planned for evaluation of the coaxial injector. Variations in velocity ratio between 3 and 10 were planned as a result of varying hydrogen temperature between 200 and 600 psia were planned.

Twelve additional tests were conducted to obtain additional

VI Test Results (cont.)

data at some of the original operating conditions as well as data at other chamber pressures. The following is a description of the tests by test series. The first series used a chamber configuration with five injectors for evaluations at the lowest fundamental mode frequency. The second series used two injectors and a corresponding wedge for testing at the highest possible fundamental mode frequency. The third and fourth series used three and four injectors respectively with corresponding wedges for testing at intermediate fundamental mode frequencies. A test-by-test tabulation of steady state operation conditions for each test is shown in Table 1.

The first four tests used the chamber with five injectors and no wedge. The first test was ignited by the pulse; consequently, no decay rate data were recorded. The remaining three tests were satisfactory and decay rates were recorded for each test. The low mixture ratio on the third test was due to a malfunctioning oxidizer flowmeter.

The next series of tests was conducted using the same chamber as in the first test series except that the widest available wedge was fitted into the excitation chamber, exposing only two injectors. This chamber configuration produced a frequency of 6500 Hz in the fundamental mode. Five tests were conducted during this test series. Difficulties were encountered in obtaining the desired fuel temperature at the injectors. The problem was largely the result of operation at the low flow rates required for only two injectors. This, coupled with higher heat flux to the propellant than anticipated, produced lower fuel flow rates than predicted and therefore high mixture ratios. Pulse decays were recorded on all tests except Test 6 where the pulse was of extraordinarily low amplitude.

The next series used three injectors in the second excitation chamber, which had been fitted with the corresponding wedge. The frequency of the fundamental mode for this chamber was 4200 Hz. The first test (Test 10) was aborted because of a solid nitrogen obstruction in the run line, causing near blockage of fuel flow. The run line was inspected, the fuel in-line filter was cleaned, and testing was continued. Seven tests

VI Test Results (cont.)

were then conducted using this hardware configuration. An unusually high mixture ratio was experienced during Test 11 and an unusually low one during Test 17. Decay rates were recorded on all tests except the aborted test (Test 10). The decay rates were high for all tests of this series except Test 13.

The final test series included Tests 18 through 24. This series was conducted on the chamber fitted with a thin wedge covering only one injector and producing a fundamental mode of 3400 Hz. Seven tests were conducted during this series. Decay rates were obtained for all tests. The steady-state operating conditions during these tests were all satisfactory.

At the conclusion of testing, the test hardware was disassembled and observed for compatibility results. The copper injector faces withstood the test series and showed only slight discoloration and wear. The zirconium oxide coating on both excitation chambers was intact, showing slight erosion around the igniter port and the pulse gun port. On the floor and lid of the excitation chamber, thermal discoloration was visible; however, the coating was intact. Figure 34 shows an excitation chamber after testing. Viewing the side of the chamber, the port nearest the injector was for the pulse gun discharge; the downstream port was for the igniter discharge; the black residue downstream of the igniter port was material discharged by the solid propellant of the igniter.

2. Stability Data and Correlations

All tests of the 24-test series were dynamically stable. As a result it was necessary to cause a pressure disturbance with the pulse gun and measure the rate of decay of the resulting fundamental transverse mode. This data was then used to determine the response of the injector to combustion and to obtain frequency sensitivity information. As a result, the method for determining the response of the injector to combustion and for obtaining frequency sensitivity information was to measure the decay rate

VI Test Results (cont.)

of the fundamental mode for the chamber caused by the pulse discharge. The frequency for the fundamental mode at the operating conditions for a given test was obtained by using a spectral plot of peak to peak pressure versus frequency at the time of the pulse. An example of one such plot is shown in Figure 35.

A primary purpose of this phase of the program was to verify or correct the correlation equation based on sensitive time lag and reported in the Phase I final report for this program (Ref. 1). Sensitive frequency (f_s) values were calculated for each test using the following equation:

$$f_s = 4550\left[\frac{M_c}{d_{ox}}\right]^{0.15}\left[\frac{P_c}{P_{crit}}\right]^{1/3}\frac{1}{F\ (VR \sin \phi)}$$

where;

M_c	=	chamber Mach number at the injector face
Pc/P_{crit}	=	ratio of chamber pressure to the critical pressure of oxygen. This ratio is 1.0 when $Pc \geq P_{crit}$.
d_{ox}	=	diameter of the oxidizer orifice.
F (VR sin ϕ)	=	shown in Figure 36.
VR	=	ratio of the injected fuel velocity to the injected oxidizer velocity
ϕ	=	included angle between fuel and oxidizer streams

A comparison of the test data with predicted results was made by plotting the decay rate data versus the ratio of the sensed frequency divided by the predicted sensitive frequency for a test series on a single chamber setup. First, to eliminate the effect of possible damping from the wedge or associated cavities behind the wedge, the data from the tests with no wedge and only the smallest wedge were compared. These data are shown in Figure 37. The data is given in tabular form in Table 2.

VI Test Results (cont.)

By combining the data from the 4-insert tests with the 5-insert tests, a maximum sensitivity is observed at values of f/fs = 1.0. If only the 4-insert data are considered, there is sufficient spread of the data at values of f/fs < 1.0 to obtain the right hand side of the curve; however, only one point occurs at values of f/fs > 1.0. The location of the minimum value of f/fs cannot therefore be determined accurately. The possible fit indicates a minima should lie between f/fs of 1.0 to 1.3. The curve in Figure 37 was drawn to reflect a minima at 1.0. Adding the 5-insert test data does not compromise the correlation since there is less system damping than in the 4-insert case.

Figure 38 shows all the decay rate data and possible correlations for all chamber configurations tested. It should be noted, however, that the data for the 3-insert tests show a slightly questionable slope. Most of the points at decay rates of 8000 db/sec were at the response speed of the data reduction equipment. The actual decay rates may in fact be higher than the 8000 db/sec shown. Consequently, the points at decay rates of 6000 db/sec are considered valid points, whereas the points at 7000 and 8000 db/sec are considerable as upper limit cases.

These data show good agreement between the predicted sensitive frequency using existing correlation equations and the test data obtained on this phase of the program. Of significznce is Figure 37 in that the minimum decay rates occurred at a f/fs of 1.0 and the result was repeatable with two tests run at nearly the same condition, even though the data is evidently somewhat mixture ratio dependent. The test data presented in this report show high damping for all tests.

To this point only the acoustic characteristics of the excitation chamber have been considered. The following observations discuss the effect of combustion distributed axially along the chamber on the coupling of an instability mode with the acoustics of the system.

VI Test Results (cont.)

Upon completion of the 24-test series, the test hardware was disassembled and examined. A photograph of the hardware after testing is shown in Figure 39. The portion of the zirconium oxide coating nearest the injectors appeared to have received a minimal thermal damage. The marked portion of the chamber shown in Figure 39 is the location where thermal discoloration and erosion appears to have first occurred. This location is approximately 7 inches from the injectors, which is about 25% of the distance from the injector to the throat. Figure 9a shows that the acoustic pressure of the fundamental mode has dropped to a value of about 65% of P_{max} at a point 25% of the distance from the injector to the throat. This accounts for a considerable loss of potential for coupling between combustion and the fundamental mode, whereas the losses are even greater for the combined fundamental and first radial mode. The combustion length of 7 inches for the coaxial injector may be contrasted with that of the triplet which was spontaneously unstable. The discoloration pattern indicates combustion was occurring one inch from the injector face with the triplet. A photograph of the excitation chamber after tests with the triplet is seen in Figure 40. These data are reported in Reference 2.

The degree to which the extended combustion length of the coaxial injector alters the ability of the injector to sustain an acoustic instability in the excitation chamber can be expressed by the term:

$$A_{\nu\eta} = \frac{N_u}{N_{nu}}$$

where:

N_u = combustion response with combustion concentrated at the injector face

N_{nu} = effective combustion response with combustion located a significant distance from the injector face

$A_{\nu\eta}$ = pressure distribution coefficient

VI Test Results (cont.)

A plot of $A_{\nu\eta}$ (partially taken from Reference 2) is shown in Figure 41. The mode shapes shown on this figure are referenced to a cylindrical combustion chamber. When using this plot for an excitation chamber it must be remembered that the fundamental mode of the excitation chamber compares to a sector of a higher mode of a cylindrical chamber and is a function of the excitation chamber angle. For example, the fundamental mode of an excitation chamber with a chamber angle of 36^{o} compares with a sector of a fifth tangential mode in a cylindrical chamber as shown in Figure 42. The value for $A_{\nu\eta}$ at $r_i = 1.0$ coresponds to the value assuming concentrated combustion at that location at the injector face with no axial combustion distribution down the chamber. The distance from the apex of the angle for the transverse excitation chamber to the injectors is approximately 29 inches. If combustion occurred at 7 inches from the injectors as indicated by Figure 39, the value for r_i would be about 0.76. At this value for r_i, $A_{\nu\eta}$ for the fifth tangential mode would be 1.1 whereas the value of $A_{\nu\eta}$ is about 2.55 at $r_i = 1.0$ or

$$\frac{A_{\nu\eta} \quad (r_i = 0.76)}{A_{\nu\eta} \quad (r_i = 1.0)} = \frac{1.1}{2.55} = .43$$

This result means that only 43% of the maximum possible oscillatory combustion energy input for this mode will occur. The maximum energy input would occur if combustion took place at the face ($r_i = 1.0$). This observation suggests that the inability to obtain spontaneous instabilities with the coaxial injectors in the transverse excitation chamber was a result of extended combustion zone of the coaxial injector.

B. HIPERTHIN Injector Testing

1. Test Results

Twelve tests were planned to evaluate HIPERTHIN injectors. Variations in chamber pressure and fuel temperature were primary

VI Test Results (cont.)

the test variables. Four different chamber configurations were used to test at different fundamental mode frequencies. The test plan showing these tests is included as Table 3.

All the test conditions shown in Table 3 were met. An additional 16 tests were conducted making a test series of 28 tests. Repeated test points at certain operating conditions and tests at additional chamber pressure levels were obtained with the additional 16 tests. Steady state test data are shown in Table 4.

The first test series consisted of three tests. The chamber containing two injectors and a 4-inch face was used for these tests. The first test served as a checkout of the system, and due to misranging of the instrumentation for the oxidizer system an unusually high oxidizer flow rate was obtained resulting in a high mixture ratio. Difficulty in separating the high frequency signal from the test with other noise in the electrical system precluded usable high frequency data on this test. With both the high frequency data acquisition and oxidizer tank instrumentation corrected, tests 2 and 3 were conducted. These two tests were planned to operate at a chamber pressure of 100 psia and a mixture ratio of 5.0. The fuel temperature was planned to be 520°R for test 2 and 375°R for test 3 and oxidizer temperature 375°R for all tests. Both tests were unstable throughout in the fundamental mode; however, test 3 went unstable initially in a high order mode at about 14,000 hz, decayed into a pure fundamental mode, and then grew into a complex mode. A reproduction of the unfiltered high frequency record for this test is shown in Figure 43. The amplitude of these instabilities was from 15 to 20 psi peak-to-peak.

The next test series was conducted on the chamber which contained one 3-inch injector. The fundamental mode frequency for this configuration was approximately 13,000 hz. The first two tests of this series was planned to operate at a chamber pressure of 100 psia and mixture ratio 5.0. The desired hydrogen temperature was 375°R for the first test and 520°R for the second test. Tests 6 and 7 were planned to operate at 700 psia and a mixture ratio of 5.0 with the same variation in hydrogen temperature as tests

VI Test Results (cont.)

4 and 5. Test 4 was stable until 810 msec after ignition (200 msec before FS-2) when an unstability occurred in the fundamental mode. Test 5 was unstable from the start; the test was initially unstable in the fundamental mode which decayed and went into a higher order mode for the remainder of the test. The amplitude of the instabilities for these tests was about 20 psi peak to peak. The two high chamber pressure tests of this series were dynamically stable throughout. No organized instabilities of significant amplitudes were observed.

The next test series (Tests 8 - 12) was conducted with the same chamber configuration as Tests 1 - 3. The planned operating chamber pressure for these tests were: Tests 8 - 10, 700 psia; Test 11, 300 psia; and 100 psia on Test 12. All tests were to have a 5.0 mixture ratio and fuel temperature at both 375°R and 520°R as in prior test series. All tests of this series were stable with the exception of Test 12 which experienced an instability near the end of the test in the fundamental mode with an amplitude of 8 psi peak-to-peak.

The stability data obtained from the next test series was the most significant data of the test program since instabilities occurred both above and below the peak response of the system. This series was conducted with the chamber containing four injectors and a total injector face width of 8 inches and a fundamental mode frequency near 5500 Hz. The tests of this series were planned to operate at a mixture ratio of 5.0 and chamber pressures of 700 psia, 300 psia, and 100 psia. Six tests were conducted in this series; a discussion of the stability results follows. Test 13 was invalid due to a failure of the fuel manifold of one injector resulting in a loss of fuel flow therefore causing a severe mixture ratio maldistribution. The post-test hardware examination revealed no chamber damage; however, the injector containing the leaky manifold was damaged beyond repair. A photograph of this injector is shown in Figure 44. The adjacent injectors were only slightly damaged and useable for the remainder of the test series. The remaining five tests of this series were satisfactory and no further hardware

VI Test Results (cont.)

damage was experienced. Test 14 was initially stable and became unstable 500 msec after ignition. The frequency of this instability was about 10,200 Hz with an amplitude of 350 psi peak-to-peak. Test 15 was unstable from about 90 msec after ignition. The frequency of the instability was again at about 10,200 Hz with an amplitude of about 250 psi peak-to-peak. A very slow growth of the fundamental mode occurred during the steady state portion of the test until, about 330 msec after ignition, it had attained an amplitude of 40 psi peak-to-peak. Test 16 was stable throughout with the exception of small instability near the end of the test at a frequency of 10,000 Hz and an amplitude of 2 - 3 psi. Test 17 was similar to test 16; it was stable for the majority of the test but, near the end of the test an unstable oscillation grew to about 45 psi -eak-to-peak at 10,200 Hz. Test 18 was stable except once again, an instability occurred near the end of the test at a frequency of 11,400 Hz with an amplitude of about 13 psi peak-to-peak.

The next test series (Tests 19 - 26) using a single injector with a 2-inch injector face and a fundamental mode frequency of 16,000 Hz. These tests were planned to operate at a mixture ratio of 5.0 and chamber pressures of 100 psia, 500 psia, and 700 psia. Test 19 was unsatisfactory due to low chamber pressure and consequently very low performance. The C* was not sufficiently low to conclude that combustion had not occurred. However, when compared with other tests using the same test hardware, the low performance does negate comparison of this data with other tests in the series. Test 20 was a repeat of Test 19. The test was stable with only a very low amplitude oscillation (about 2 psi). Tests 21 and 22 were stable throughout with no indication of any organized instability. Test 23 experienced an instability at the end of the test which reached an amplitude of 8 psi peak-to-peak. Bombs were used on tests 24, 25, and 26 to observe the decay characteristics of the fundamental mode. Test 24 was stable and the pulse (about 200 psi) produced by the bombs decayed rapidly at 8000 db/sec. The bomb discharged during test 25 did not produce a significant pressure rise (only 5 - 6 psi). At the end of the test, however, an instability reaching 10 psi peak-to-peak was recorded. The pulse on test 26 showed a pressure perturbation of 30 psi and the decay rate was againvery high at 8000 db/sec.

VI Test Results (cont.)

The final two tests 27 and 28, were conducted on the chamber using one injector with a 3-inch injector face. The first test had a nominal operating chamber pressure of 100 psia and a mixture ratio of 5.5. A bomb was discharged 320 msec after ignition producing a pressure perturbation of 15 psi. This pulse exhibited a very high decay rate in the fundamental mode at about 8000 db/sec. Test 28 had a nominal operating chamber pressure of 660 psia and a mixture ratio of 4.7; a pulse fired 303 msec after ignition produced a pressure perturbation of 12 psi which had a high decay rate in the fundamental mode of 8000 db/sec but a lower decay (5000 db/sec) at a higher mode of about 20,000 Hz.

2. Stability Data and Correlations

The high frequency stability data from tests described in the previous paragraphs were analyzed to determine the effects of chamber pressure and hydrogen temperature on the stability of the system. The unfiltered high frequency records from data from the helium bleed Kistler pressure transducers was first analyzed to determine the frequencies present during the tests. From this analysis log decrement plots were produced using a combination of filters to obtain growth and decay rates of the instabilities at selected frequencies. These records were then read and compared with the steady state data to determine the operating conditions at the instant the instabilities occurred. The combustion stability data obtained from the analysis of the test data are shown in Table 5.

The selection of data to be used in the stability characterization of the HIPERTHIN injectors was based on the ability to determine the operating conditions at the time an instability occurred and the magnitude of the instability once it had reached its limiting amplitude. As an example, a growth rate that occurred during the steady-state portion of a test and contained an amplitude greater than 10 percent of nominal chamber pressure was considered valid data whereas a test with an oscillation with a limiting amplitude of 1 to 2 percent of nominal Pc was considered a stable test.

VI Test Results (cont.)

The test data was then correlated by selecting the growth rates of a variety of frequencies a relatively constant chamber pressure and mixture ratio. The most complete set of data for such a correlation is seen in Figure 45 where growth rates at chamber pressures between 300 and 700 psi are plotted versus frequency. At lower chamber pressures a peak frequency such as that in Figure 45 was not reached, but appeared as though it might occur at frequencies lower than those tested in this test series. There then appears to be a chamber pressure relationship present which would account for this shift in peak frequency response.

In reviewing the correlation equations for injectors using oxygen and hydrogen propellants, sensitive frequency is described in general as:

$$f_s \propto (M_c)^a (d)^b (P_c)^c f(VR)$$

where:

M_c = Mach number in the chamber

d = dimension of the orifice for the injection of the least volatile propellant

f(VR) = a velocity ratio term or function of velocity ratio. In some correlations (Ref. 4) this term appears $f(T_{H_2})$

P_c = chamber pressure

Consider this relationship term by term: mach number in the chamber is constant at all test conditions; the dimension of the injection element of the least volatile propellant is fixed by design and therefore constant; the velocity term is by the design of the hardware, small with the exception of variations due to changes in hydrogen temperature; and the chamber pressure term was intentionally varied by test contions. The correlation for this test series then may be reduced to:

VI Test Results (cont.)

$$f_s \propto (P_c)^c \; f\,(VR)$$

When considering the correlation equation for coaxial injectors the pressure relationship appears as a term $\left[\frac{P_c}{P_{crit}}\right]^{1/3}$. This also applies to multi-orifice injection as reported in Refs. 2 and 5. This term may also appear as P_c^{-1} for a diffusion limited droplet burning process as reported in Ref. 6. Attempts to correlate this data with P_c^{-1} met with no success and, thus, further consideration of that correlation parameter was abandoned.

Considering first the pressure term as

$$\left[\frac{P_c}{P_{crit}}\right]^{1/3} = Pr^{1/3}$$

the correlation for f_s may then be written as

$$f_s = K\,(Pr)^{1/3}\; f\,(VR)$$

By arbitrarily assuming a constant for the correlation equation, calculating the ratio of the measured acoustic mode frequency to the calculated sensitive frequency and plotting this ratio versus growth rate, the data should maximize if the correlation is correct and determine a correction factor for correlation constant. A value of 10^4 was assumed for K.

Considering first the data from a single set of test hardware to minimize scatter of the data due to hardware variations, the data from the chamber using four injectors with the fundamental mode frequency near 5500 Hz was selected. These data are shown in Figure 46 and a peak response is observed near f/fs = 1.2.

VI Test Results (cont.)

Data from the entire test program was considered as shown on Figure 47. The envelope for all the data and the best fit curve shows a peak response near f/fs = 1.6. There is apparently only a 25 percent variation in the correlation of all the data from f/fs = 1.6 to f/fs = 1.2. For a design criteria this amount of variation in f_s does not pose serious problems. For conservative design the highest value should be used or in terms of sensitive frequency a value of K would become 1.6×10^4. The correlation equation may then be written as:

$$f_s = 1.6 \times 10^4 \, Pr^{1/3} \, f(VR)$$

In the correlation for the coaxial injectors the velocity term was expressed as the product of injected propellant velocity ratio and the sine of the included angle between the oxidizer and fuel streams. Assuming that the same form would apply here the correlation equation becomes:

$$f_s = 1.6 \times 10^4 \, P_r^{1/3} \, F(VR \sin \phi)$$

The included angle of the HIPERTHIN injector is difficult to determine but at best it is quite small as is the sine of the angle. In order to establish the relative importance of the velocity term it is assumed that, $\sin \phi = 0.1$. The velocity ratio of the tests from which the data for Figures 46 and 47 was obtained varied from 4.2 to 5.4. Referring to Figure 36 it can be seen that F (VR sin ϕ) will range from 1.33 to 1.23 for values of VR sin ϕ of 0.42 to 0.54. This spread is well within the 25% variation of the constant K already determined from Figures 46 and 47 and thus may safely be included as part of this constant. The final correlation from the HIPERTHIN testing from this program is then

$$f_s = 1.6 \times 10^4 \, P_r^{1/3}$$

This interpreted in terms of f_s would produce a sensitive frequency of 16,000 Hz when chamber pressure is 700 psia, and fs = 8500 Hz when chamber pressure is 100 psia.

VI Test Results (cont.)

C. Gas-Gas Testing

1. High Pressure

a. Test Results

A total of twelve tests were planned to evaluate the dynamic stability of the impinging swirl cup injector using gaseous oxygen/ gaseous hydrogen propellants. There were to be two groups of tests as shown in Table 6; the first series at nominal high pressure APS conditions and the second series at peripheral conditions. All twelve tests were completed and the steady state data are shown in Table 7. All twelve tests were spontaneously unstable at a low level (less than 5% peak to peak of Pc). The first five tests were conducted with ambient temperature propellants. The mixture ratio in these tests ranged from 2.07 to 6.16.

The first test was 1 second in duration with the bomb electrically detonated at approximately 500 msec after FS1. The high frequency pressure data showed a precessing first tangential mode at 6000 Hz and 10 - 15 psi peak to peak. The bomb created a maximum overpressure of approximately 120 psi which decayed to the original level in 1 msec. The Photocons in the feed lines indicated unorganized oscillations at 10 - 25 KHz and 10 - 20 psi peak to peak.

The second test was a 0.5 second test with the bomb detonated at 250 msec after FS1. The high frequency data showed an possible second tangential mode at 8000 - 10000 Hz and approximately 10 psi peak to peak. A maximum pressure spike of approximately 95 psi decayed to the original conditions in 1 msec. The Photocons in the feed line indicated an irregular 8500 Hz in each line at 5 psi peak to peak in the hydrogen and 20 psi in the oxygen line.

VI Test Results (cont.)

The Photocon located at the 270° position was destroyed near the end of this test for no obvious reason. The injector and chamber both appeared free of any indication of overheating in this region. Therefore, it was decided that the failure could have been a fluke and another Photocon was installed for Test 3.

Test 3 again indicated a very low level oscillation at 8600 Hz an 6 psi peak to peak in the chamber. The bomb produced a 55 psi overpressure which decayed in 2 msec to the original steady state conditions. The feed lines each indicated the pesence of the 8600 Hz oscillation at 5 psi in the hydrogen line and 15 psi in the oxygen line. The Photocon was again destroyed.

Tests 4 and 5 were almost identical to Test 3 with an approximately 8000 Hz oscillation at 6 psi peak to peak. The bomb created a 50 psi spike decaying in 4.5 msec and a 60 psi spike decaying in 6 msec in Tests 4 and 5 respectively. The feed lines showed oscillations at the same frequency as the chamber at 15 psi peak to peak in the oxygen line and 4 psi peak to peak in the hydrogen line.

Tests 6 and through 10 were a series of tests conducted with ambient oxygen and preconditioned hydrogen with mixture ratios ranging from 2.21 to 6.56.

Tests 6 and 7 reacted similar to the previous three tests. The chamber oscillation was 8000 - 8500 Hz at 4 psi with the bomb producing a 40 psi spike in test 6 and a 55 psi spike in Test 7 which decayed in 2 and 3.5 sec respectively. The feed lines all indicated oscillations of approximately 8000 Hz at 5 - 15 psi.

Tests 8 and 9 behaved very much alike however somewhat different from the remainder of the series. The chamber frequency increased to 9500 - 10,000 Hz at 5 - 10 psi peak to peak steady state. The bomb created a 95 - 100 psi spike in the chamber in each case which decayed in 5.2 msec in Test 8 and 4 sec in Test 9. The fuel feed line had a steady state oscillation of 7500 Hz at 10 - 15 psi. The oxygen fuel line instrumentation indicated a

VI Test Results (cont.)

8000 - 8500 Hz oscillation at approximately 25 psi peak to peak in each case. In Test 9 there was also a 1600 Hz, 40 psi peak to peak pressure oscillation observed in the oxygen feed line.

Test 10 was the last of the group of ambient oxygen, preconditioned hydrogen tests. The spontaneous oscillations in the chamber were at 8000 Hz and 6 psi peak to peak. The bomb produced an overpressure of 165 psi which decayed to the steady state oscillation in 6.3 msec. The oxygen feed line had an oscillatory pressure of 25 psi peak to peak at 7000 Hz superimposed on a 1600 Hz, 50 psi peak to peak oscillation. The fuel line oscillated at 7500 Hz and 15 psi peak to peak once again on a 1600 Hz, 20 psi peak to peak signal.

Test 11 was designed to test the effect on stability of preconditioning both propellants at nominal mixture ratio and chamber pressure conditions. This test produced a 10 KHz steady state oscillation at 5 psi peak to peak with a 70 psi bomb induced spike decaying in 4.6 msec. The propellant lines both had 8000 Hz oscillations at 15 psi peak to peak. This was superimposed on a 1600 Hz 30 psi peak to peak oscillation in the oxygen line.

Test 12 was a reverse of tests 6 through 10 in that the hydrogen was at ambient conditions and the oxygen was preconditioned. It can be seen that from Table 7 that in the tests where only one propellant is preconditioned the intermanifold heat transfer is sufficient to significantly reduce the temperature of the ambient propellant. In most cases this did not amount to much, however, in this case the ambient hydrogen was reduced from approximately 530^{o}R to 400^{o}R in the hydrogen manifold. The high frequency instruments showed results very similar to Test 11 with a 9500 Hz, 5 psi oscillation in the chamber. The bomb caused a 55 psi spike which decayed in 5.3 msec. The propellant line high frequency oscillations were 8000 Hz and 15 psi in Test 11.

VI Test Results (cont.)

The data from chamber thermocouples were evaluated with the intention of possibly obtaining some information on combustion efficiency as a function of axial distance. This proved fruitless, however, perhaps due to the fact that the thermocouple closest to the injector was 3.35 in. from the face. Most likely, the largest transients in combustion intensity were upstream of this point.

b. Stability Correlations

All twelve tests in this test program were similar from a combustion stability standpoint. All were spontaneously unstable with very low level instabilities (one to five percent of chamber pressure) and all recovered from the bomb detonation to the steady state condition in less than 10 msec. Due to the fact that there was no demarkation point where the engine changed from a stable to an unstable operating condition, there appears to be only two possible methods of evaluating combustion stability as a function of mixture ratio and propellant temperatures from this data; the amplitude of the steady state oscillations and the recovery time from the bomb induced pressure spike. Even at that, the use of the recovery time can at best only indicate trends since every test did regain the steady state position within 10 msec. It is conceivable that data from other tests with sizeable instabilities could alter any trends noted from these recovery times.

Attempts to correlate the data in regards to the amplitude of the spontaneous steady state instabilities all proved unsuccessful. The plot of recovery time versus mixture ratio in Figure 48 shows a definite trend toward increasing recovery time with increasing mixture ratio. This conclusion is even more evident when plotting recovery time versus mixture ratio for selected tests at relatively constant fuel temperatures as seen in Figures 49 and 50. This trend is in opposition to that expressed by kinetics models such as Goede, Ref. 8, but once again must be tempered by the fact that no instabilities greater than five percent of chamber pressure were noted in the data. Nevertheless, the data herein leads to the conclusion that recovery time from a pressure perturbation increases with increasing mixture ratio.

VI Test Results (cont.)

2. Low Pressure

a. Test Results

A total of 40 tests were completed during this phase of the program. Twenty-seven of these tests were valid. The remainder failed to ignite or achieve sufficient chamber pressure. The data obtained from the successful tests is shown in Table 8. The apparent negative pressure drop on the oxygen feed system side remains unexplained except for a possibility that the recorded pressure was in a low pressure area immediately downstream of the oxygen flow venturi.

The first series of tests included Tests 4 through 15. The purpose of this series of tests was to evaluate the effect of the resonator in the fuel feed system. The length of the resonator was changed throughout the test series from zero to 54 in. by adding 6 in. increments between tests. The intention of this approach was to attempt to locate a frequency whose wave length would react with the resonator in such a way so as to effect the chamber oscillation.

Tests 4, 5, 6 and 7 were fired with resonator lengths of 0 in., 6 in., 12 in., and 18 in. respectively. The high frequency instrumentation in the chamber indicated a oscillation of approximately 6000 Hz at 1 - 2 psi peak to peak with some lower frequency component. This low frequency component was too irregular to be accurately determined in Tests 4 and 5 however it appeared more clearly on Tests 6 and 7 as a frequency of 1400 - 1500 Hz with an amplitude of 2 - 3 psi peak to peak. For all of these tests the Kistler in the end of the resonator was indicating no pressure oscillations of measurable amplitude and thus no apparent interaction between the feed system and the chamber.

Test 10 was conducted with a 24 in. resonator. Both the Kistler in the chamber and the resonator indicated oscillations of 1500 Hz with peak to peak amplitudes of 2 - 3 psi in the chamber and approximately 1 psi in the resonator. In order to evaluate the phasing of the 1500

VI Test Results (cont.)

resonator the data was 180° out of phase throughout the majority of the test.

The tests of resonator lengths from 0 in. to 18 in. Tests 25 through 28, were similar to the previous tests in this series. Once again there were 1500 Hz oscillations at 1 - 2 psi peak to peak in the chamber and 6000 - 6700 Hz oscillations at 2 - 3 psi superimposed on 1500 Hz oscillations 1 psi in the resonator. The previous testing with these resonators sizes, tests 4 through 7 indicated no oscillatory pressure in the resonator whatsoever and only a 6000 Hz signal apparent in the chamber. The increased pressure drop in these cases may be contributing to the differences in reaction, however, the mechanism of this contribution is not readily apparent.

The last two series of tests utilized only resonator lengths of 0, 6, 12 and 18 in. These series were abbreviated due to a lack of test stand availability and funds. The first of these series, Tests 29 through 35, was a repeat of Tests 4 through 7 with a slight hardware modification. The fuel inlet manifold is designed to be supplied through three inlets. The three fuel feed lines as shown in Figures 31 and 33 are of varying lengths. The two longest tubes are each approximately 9.5 in. long and the remaining inlet is approximately 8.5 in. in length. It was felt that if a pressure wave generated in the chamber were progressing up the fuel feed system that the difference in lengths of these feed lines would cause interference to occur since the wave would reach the intersection of the three lines at slightly different times. The chamber is shown in Figure 51 with the short tube disconnected and a Kistler put in its place.

It was believed at the time of the testing that Test 30 had been a successful test with a 6 in. resonator; however, it was subsequently determined that in fact there had been no ignition. Therefore, only three valid tests were conducted in this series. The only significant result from this test series was the fact that there was no appearance of oscillations in the 6000 Hz range. All high frequency instruments indicated

VI Test Results (cont.)

H_z signals from the chamber and resonator the records were run through a 2 KHz low pass filters. The oscillations in Test 10 were 180^o out of phase throughout the test. Tests 1 through 15 utilized resonators from 30 in. to 54 in. long. The high frequency data from the chamber indicate a consitent appearance of the 1500 Hz oscillation. The resonator data however shows the appearance of high frequency oscillation (5000 - 6700 Hz) in addition to the 1500 Hz. All of these tests seemed to have a shifting phase relationship between the two instruments throughout any one test.

The next series of tests was designed to increase the pressure drop on the fuel feed system and repeat the previous series using incremental resonator lengths from 0 to 54 in. The four 0.5 in. dia. holes in the fuel manifold spacer were reduced to 0.2 in. by means of a collar welded to the manifold spacer. The pressure drop on the fuel side increased from 7 to 24 percent with the exception of the test with the 24 in. resonator. For some unexplained reason the pressure drop decreased 6 percent from the previous test with this resonator.

The results of this series of Tests 16 through 28 do not vary significantly from tests in the first series. The tests conducted with resonators ranging from 30 in. to 54 in. compared directly with the results of the previous series with these conditions (Tests 11 through 15). The chamber indicated an oscillatory pressure at approximately 1500 Hz at 1 to 3 psi peak to peak and the resonator data showed a 6500 - 6900 Hz at 1 to 2 psi peak to peak oscillation superimposed on the 1500 Hz oscillation. Again the phasing of these two sets of data was random with the exception of Test 23. This test used a 36 in. resonator and the phase relationship between the two instruments appeared to be constant at 0^o.

The pressure oscillations observed on Test 21 were similar to those above except that once again as before with the 24 in.

VI Test Results (cont.)

pressure oscillations in the 1450-1500 Hz range at 1 - 3 psi peak to peak. This series was the first to incorporate the use of a Kistler in the oxygen feed system. While the data showed the presence of the 1500 Hz oscillation there was a 350 Hz oscillation at 2-3 psi peak to peak also apparent.

The final series of tests, 37 through 40, was an attempt to evaluate oxidizer feed system effects on the chamber oscillations. Past testing with this hardware had demonstrated success in eliminating chamber oscillations by including an orifice in the oxygen feed line and thus "stiffening" the system. In this series of tests an orifice was inserted in the line downstream of the oxygen pressure tap. The Kistlers in the chamber and fuel feed system indicated no apparent change over the previous test series, i.e., there were 1450 - 1500 Hz oscillations at 1 - 2 psi peak to peak. The Kistler in the oxygen feed system was apparently faulty or there was a ppor connection and no data was recovered from this instrument. The steady state pressure transducer in the oxygen line indicated, as in Tests 31 through 35, a 1500 Hz oscillation superimposed on a 350 Hz oscillation.

b. Stability Correlations

The testing of the uni-element test hardware at conditions comparable to the scheduled low pressure (15 psia) Auxilliary Propulsion System of the Space Shuttle have produced no significant data from which to draw a conclusive result other than the fact that this injector design appears quite susceptible to chamber-feed system coupled pressure oscillations. Attempts to establish a passive damping mechanism in the fuel feed line were unsuccessful in these tests. This was possibly due in part to the distance of the resonator from the injector face and to particularities in the feed system geometry.

Previous testing of this hardware had success in damping chamber pressure oscillations by increasing oxidizer feed system pressure

VI Test Results (cont.)

drop. Efforts to duplicate those results here were in vain. The data from this test program does not indicate conclusively which feed system, if in fact it is only one, is the driving mechanism.

VII ANALYTICAL MODEL DEVELOPMENT

A. Sensitive Time Lag High Mach Number Analysis

1. Introduction

The sensitive time lag theory has been used to formulate analyses of transverse and logitudinal modes of combustion instability. These analyses have been incorporated into a single computer program as presented in Ref. 8.

Much effort was expended during the development of the program to include an analysis that would be valid at high Mach numbers. However, the high Mach number analysis turned out to be quite complex and was never satisfactorily completed in the originally intended form. The analysis was then simplified, but not to the extent of neglecting the effects of Mach number, by assuming that combustion was concentrated at some arbitrary distance from the injector face. The original transverse mode analysis in the computer program was valid only for the fundamental transverse mode even if the high Mach number terms were neglected whereas combined transverse - longitudinal modes could not be calculated by the program. The modified analysis can be used for any mode of oscillation, though the assumption of concentrated combustion becomes more restricting for the combined modes since the oscillatory axial pressure profile is not uniform for combined modes. The computer program given in Ref. 8 has been modified to reflect the changes in the analysis and appears in Ref. 16.

2. Analysis

The analysis begins by writing the conservation equations that are valid for a concentrated combustion zone. The conservation equations are written for the gas only because only the gas can be considered as a continuum. The burning of droplets appears as the generation of additional mass. The continuity requirement, therefore, is that the rate of mass input to the control volume plus the rate of generation of mass in the control volume must equal the flow rate of mass leaving the control volume plus the rate of accumulation of mass in the control volume. If the

volume is considered to be of zero thickness in the limit, the mass accumulation term can be neglected. This same approach can be used for the conservation of momentum and energy as well. The conservation equations then become:

$$\rho_+^* v_+^* + \dot{m}_b^* = \rho_-^* v_-^*$$

$$p_+^* - p_-^* = \rho_-^* v_-^{*2} - \rho_+^* v_+^{*2} - \dot{m}_b^* v_L^*$$

$$\rho_+^* v_+^* \left(h_+^* g^* + \frac{v_+^{*2}}{2}\right) + \dot{m}_b^* \left(h_L^* g^* + \frac{v_L^{*2}}{2}\right) = \rho_-^* v_-^* \left(h_-^* g^* + \frac{v_-^{*2}}{2}\right)$$

where + and - indicate respectively the upstream and downstream of the combustion front and * indicates that the variable is dimensional. The term $\dot{m}_b^*$ is the mass burning rate which will be discussed in more detail later.

It is convenient to nondimensionalize all variables in the equations because it makes most of the coefficients of the perturbation equation of order 1. When this is not done, terms such as density and enthalpy with very different orders of magnitude will cause difficulties in the calculations. The equations are nondimensionalized by dividing the continuity equation by $\bar{\rho}_o^* \bar{C}_o^*$, the momentum equation by $\bar{\rho}_o^* \bar{C}_o^{*2}$, and the energy equation by $\bar{\rho}_o^* \bar{C}_o^{*3}$. The bar indicates these variables do not vary with time. The new nondimensional variables are then defined as:

$$h = \frac{h^* (\gamma - 1)}{\gamma R_o^* \bar{T}_o^*}$$

$$v = \frac{v^*}{\bar{C}_o^*}$$

$$\rho = \frac{\rho^*}{\bar{\rho}_o^*}$$

$$p = \frac{p^*}{\bar{p}_o^*}$$

$$\dot{m}_b = \frac{\dot{m}_b^*}{\bar{\rho}_o^* \bar{C}_o^*}$$

where the subscript o indicates the stagnation properties of the combustion gas.

Each variable can be separated into a perturbation variable plus a mean variable. The perturbation variables are time-dependent while the mean variables are not. The conservation equations can then be separated into perturbation equations and mean equations. From the standpoint of combustion stability we are interested only in the perturbation equations, though the mean equations will be used later to relate coefficients in the perturbation equations. The nondimensional perturbation conservation equations can now be written as:

$$v' + \dot{m}_b' = \rho_-' \bar{v}_- + \bar{\rho}_- v_-' \tag{1}$$

$$\frac{p_+' - p_-'}{\gamma} = \bar{v}_-^2 \rho_-' + 2 \bar{\rho}_- \bar{v}_- v_-' - \dot{m}_b' \bar{v}_L \tag{2}$$

$$\rho_+ h_+ v_+' + \dot{m}_b' \left(\bar{h}_L + (\gamma-1) \frac{\bar{v}_L^2}{2}\right) = (\gamma-1) \left(\frac{\bar{v}^3}{2} \rho_-' + \bar{\rho}_- \frac{\bar{v}^2}{2} v_-' + \bar{\rho}_- \bar{v}_-^2 v_-'\right) + \bar{h}_- \bar{v}_- \rho_-'$$

$$+ \bar{h}_- \bar{\rho}_- v_-' + \bar{\rho}_- \bar{v}_- h_-' \tag{3}$$

In these equations it has been assumed that the mass flow of liquid drops is uniform, $\bar{\rho}_+ = 1$, and that the mean gas velocity before the combustion front, $\bar{v}_+$, is zero. The occasional extra occurrences of γ and $\gamma - 1$ are the result of the method of defining the nondimensional variables.

In addition to the conservation equations, an equation of state is required to relate density to pressure. The perturbation part of this equation is:

$$p'_- = \rho'_- + T'_- , \qquad (4$$

where $T' = \dfrac{T^*}{\bar{T}_o^*}$

when enthalpy is related to temperature by the relation $h^* = C_p^* T^*$, the resulting perturbation equation becomes:

$$h' = T'$$

Upstream of the combustion front the mean velocity has been assumed to be zero. If, in addition, the interaction between the gas and drops is neglected, the dynamics of the region upstream of the combustion front is governed by the Helmholtz equation:

$$\nabla^{*2} p^{*'} + \frac{\omega^{*2}}{C^{*2}} p^{*'} = 0$$

Also, velocity can be related to pressure by the first order equation of motion:

$$j\omega^* v^{*'} = \frac{1}{\rho^*} \frac{\partial p^{*'}}{\partial x^*}$$

Nondimensionalizing these equations we get:

$$\nabla^2 p' + \omega^2 p' = 0$$

and $$j\omega v' = -\frac{1}{\gamma} \frac{\partial p'}{\partial x}$$

where $\omega = \frac{\omega^* r_c^*}{C_o^*}$, $x = \frac{x^*}{r_c^*}$ and $\nabla^2 = \nabla^{*2} r_c^{*2}$

Then solving the Helmholtz equation for a cylinder of radius r_c^*, the following equations result.

$$p_+' = A \cos\left[(\omega^2 - S_{\nu\eta}^2)^{1/2} x\right] J_\nu (S_{\nu\eta} r) \sin \nu\theta \qquad (6$$

$$v_+' = -\frac{jA}{\omega\gamma}(\omega^2 - S_{\nu\eta}^2)^{1/2} \sin\left[(\omega^2 - S_{\nu\eta}^2)^{1/2} x\right] J_\nu (S_{\nu\eta} r) \sin \nu\theta \qquad (7$$

The variable x is the nondimensional distance between the injector and the combustion front.

Downstream of the combustion front an admittance equation relating v', p' and s' can be used, where s' is the nondimensional perturbation entropy, $\frac{s'^*}{C_p^*}$.

$$\gamma v_-' + \frac{S_{\nu\eta}}{\omega} E p_-' + C s_-' = 0$$

This equation is obtained from the nozzle admittance relation in Ref. 14. The nozzle analysis has no restriction on Mach number, thus by extending the admittance calculation from the nozzle entrance to the combustion front, we eliminate the necessity of writing and then solving the acoustic equation with a finite Mach number. This simplifies the analysis considerably and reduces the possibility of errors. The only remaining equation required is one relating s_-' to other variables. This comes from the thermodynamic relation:

$$T\,ds = dU + pdV$$

where U is the internal energy and V is volume.

In our scheme of variables this becomes:

$$\bar{T}_- s'_- = h'_- - \frac{\gamma-1}{\gamma}\frac{p'_-}{\bar{p}_-} \qquad (9$$

The mass burning rate can be written in terms of the sensitive time lag τ and an interaction index, n, as:

$$\dot{m}'_b = \bar{\rho}_- \bar{v}_- \frac{p'_-}{\bar{p}_-} n\,(1-e^{-i\omega\tau}) \qquad \text{where } p' = \frac{p'_+ + p'_-}{2} \qquad (10$$

It is possible to combine this last equation with Equations 1 through 9 to obtain a characteristic equation

$$H = n\,(1-e^{-i\omega\tau})$$

where H is a complex function of frequency and τ and n are real functions of frequency.

3. Method of Computation

The characteristic equation can be formed by writing equations 1 thru 9 in matrix form as follows:

$$\begin{bmatrix} 1,1 & 1,2 & \cdots \\ & & \\ \cdots & 8,9 & 9,9 \end{bmatrix} \begin{bmatrix} 1 \\ \vdots \\ 9 \end{bmatrix} + \dot{m}_b' \begin{bmatrix} 1 \\ \vdots \\ 9 \end{bmatrix} = 0$$

where the first pair of brackets indicates a square matrix and the others are column matrices. When this matrix equation is multiplied by the inverse of the square matrix, two of the equations represented relate $\dot{m}_b'$, p_+' and p_-'. The characteristic equation can be written from these and Equation 10. The size of the matrix can be reduced by eliminating some variables merely by substitution. From Equations 6 and 7, the constant A can be eliminated, giving:

$$\frac{v_+'}{p_+'} = Y = -\frac{i}{\omega\gamma} \tan \left(\omega^2 - S_{\nu\eta}{}^2\right)^{1/2} \times \left(\omega^2 - S_{\nu\eta}{}^2\right)^{1/2}$$

Equations 1 through 9 can then be written:

$$Y p_+' - \bar{v}_- \rho_-' - \bar{\rho}_- v_-' + \dot{m}_b' = 0 \qquad (11$$

$$\frac{p_+'}{\gamma} - \frac{p_-'}{\gamma} - \bar{v}_-^2 \rho_-' - 2 \bar{\rho}_- \bar{v}_- v_-' + \bar{v}_L \dot{m}_b' = 0 \qquad (12$$

$$Y \bar{\rho}_+ \bar{h}_+ p_+' - (\gamma - 1)\left(\frac{\bar{v}_-^3}{2} \rho_-' + \frac{\bar{\rho}_- \bar{v}_-^2}{2} v_-' + \bar{\rho}_- \bar{v}_-^2 v_-'\right) \qquad (13$$

$$- \bar{h}_- \bar{v}_- \rho_-' - \bar{h}_- \bar{\rho}_- v_-' - \bar{\rho}_- \bar{v}_- h_-' + \dot{m}_b' \left(\bar{h}_L + (\gamma-1)\frac{\bar{v}_L^2}{2}\right) = 0$$

$$p_-' - \rho_-' - h_-' = 0 \tag{14}$$

$$\bar{T}_- s_-' - h_-' + \frac{\gamma-1}{\gamma} \frac{p_-'}{\bar{\rho}_-} = 0 \tag{15}$$

$$\gamma v_-' + \frac{S_{\nu\eta}}{\omega} E p_-' + C \gamma s_-' = 0 \tag{16}$$

If the first column matrix is written:

$$\begin{bmatrix} p_-' \\ \rho_-' \\ v_-' \\ p_+' \\ h_-' \\ s_-' \end{bmatrix}$$

the square matrix can be written:

$$\begin{bmatrix} a_{11} & a_{12} & a_{13} & a_{14} & a_{15} & a_{16} \\ a_{21} & & & & & \\ a_{31} & & & & & \\ a_{41} & & & & & \\ a_{51} & & & & & \\ a_{61} & & & & & \end{bmatrix} = \mathbb{A}$$

where

$$a_{14} = Y \qquad a_{41} = 1$$

$$a_{12} = -\bar{v}_- \qquad a_{42} = -1$$

$$a_{13} = -\bar{\rho}_- \qquad a_{45} = -1$$

$$a_{21} = -\frac{1}{\gamma} \qquad a_{51} = \frac{\gamma-1}{\gamma\,\bar{\rho}_-}$$

$$a_{22} = -\bar{v}_-^2 \qquad a_{55} = -1$$

$$a_{23} = -\bar{\rho}_-\,\bar{v}_- \qquad a_{56} = \bar{T}_-$$

$$a_{24} = +\frac{1}{\gamma} \qquad a_{61} = \frac{S_{\nu\eta}\,E}{\omega}$$

$$a_{32} = -(\gamma-1)\,\frac{\bar{v}_-^3}{2} - \bar{h}_-\,\bar{v}_- \qquad a_{63} = \gamma$$

$$a_{33} = -(\gamma-1)\,\frac{3}{2}\,\bar{\rho}_-\,\bar{v}_-^2 - \bar{h}_-\,\bar{\rho}_- \qquad a_{66} = C\gamma$$

$$a_{34} = Y\,\bar{\rho}_+\,\bar{h}_+$$

$$a_{35} = -\bar{\rho}_-\,\bar{v}_-$$

and all other a's are zero.

If the second column matrix is:

$$\begin{bmatrix} b_1 \\ b_2 \\ b_3 \\ b_4 \\ b_5 \\ b_6 \end{bmatrix}$$

then

$$b_1 = 1,\ b_2 = \bar{v}_L,\ b_3 = \bar{h}_L + (\gamma-1)\frac{\bar{v}_L^2}{2},\ b_4 = 0,\ b_5 = 0,\ b_6 = 0$$

The a's and b's must be evaluated from the following input parameters:

$$S_{\nu\eta},\ \omega^*,\ x^*,\ E(\omega),\ C(\omega),\ \bar{v}_-,\ \bar{v}_L^*,\ \bar{C}_o^*,\ r_c,\ \bar{w}^*,\ \gamma,\ \bar{p}_o^*$$

as well as the conditions:

$$\bar{p}_+ = 1,\ \bar{\rho}_+ = 1,\ \bar{h}_+ = 1,\ \bar{h}_L = 1$$

The following equations can be used to determine other variables:

$$\bar{v}_L = \frac{\bar{v}_L^*}{\bar{C}_o^*} \qquad gR_oT_o = \frac{\bar{c}_o^{*2}}{\gamma} \qquad \bar{\rho}_o^* = \frac{\bar{p}_o^*}{gR_o^*\bar{T}_o^*}$$

$$\bar{\rho}_- = \frac{\bar{w}^*}{\bar{\rho}_o^*\ \pi r_c^{*2}\ \bar{C}_o^*\ \bar{v}_-} \qquad \bar{p}_- = 1 - \gamma(\bar{\rho}_-\ \bar{v}_-^2 - \bar{\rho}_-\ \bar{v}_-\ \bar{v}_L),$$

$$\bar{h}_- = 1 + \frac{\bar{v}_L^2}{2} - \frac{\bar{v}_-^2}{2} \qquad \omega = \frac{\omega^*\ r_c^*}{\bar{C}_o^*} \qquad x = \frac{x^*}{r_c^*} \qquad \bar{T}_- = \bar{h}_-$$

All coefficients involving Y, E, and C will be complex.

After the matrix equation is multiplied by the inverse of A, it represents a series of equations relating each perturbation variable to $\dot{m}_b'$. The first and fourth of these relate p_-' and p_+' to m_b'. A characteristic

equation is formed by combining these equations with equation 10:

$$\dot{m}_b' = \bar{\rho}_- \bar{v}_- \frac{p_+' + p_-'}{2\bar{p}_-} \quad n\,(1-e^{-i\omega\tau})$$

$$p_+' = K_1 m_b'$$

$$p_-' = K_2 m_b'$$

$$\left.\begin{aligned} \frac{2\bar{p}_-}{\bar{\rho}_- \bar{v}_- (K_1 + K_2)} &= H_r + iH_i \\ H_r + i\,H_i &= n\,(1-e^{-i\omega\tau}) \end{aligned}\right\} \text{Characteristic equation}$$

$$\left.\begin{aligned} n &= \frac{H_r^2 + H_i^2}{2H_r} \\ \tau &= \tan^{-1}\left(\frac{H_i}{n-H_r}\right) \end{aligned}\right\} \text{Solution for n and t}$$

This process will be performed for several values of ω. Tables of E_r, E_i, C_r, C_i versus ω will be input.

Definition of Terms

a	elements of square matrix
A	intermediate constant
$\mathbb{A}$	square matrix
b	elements of second column matrix
C	speed of sound
C_p	specific heat at constant pressure
g	gravitational constant
h	enthalpy
H	chamber admittance
j	$\sqrt{-1}$
J_ν	Bessel function of the first kine of order ν
K_1	intermediate constant in characteristic equation
K_2	intermediate constant in characteristic equation
$\dot{m}_b$	mass burning rate
n	interaction index
p	pressure
r_e	radius of cylindrical chamber
r	radius
R	gas constant
s	entropy
$S_{\nu m}$	Mode number for a transverse mode of a cylindrical chamber
T	temperature
U	internal energy
v	velocity
V	volume
X	non-dimensional distance between injector and combustion front
Y	Acoustic admittance
C	combined nozzle admittance coefficient
E	nozzle admittance coefficient

Greek Letters

γ	ratio of specific heats
θ	coordinate in the tangential direction
ρ	density of chamber gases
τ	sensitive time lag
ω	frequency

Superscripts

-	denotes variable does not vary with time
'	denotes variable does vary with time
*	indicates that variable is dimensional

Subscripts

+	denotes variable is evaluated upstream of combustion front
-	denotes variable is evaluated downstream of combustion front
L	liquid
O	denotes variable is evaluated at stagnation conditions
r	real part of complex variable
i	imaginary part of complex variable

B. Gas Tapoff Cycle Analysis

1. Introduction

This analysis deals with a feed system coupled one-dimensional stability problem for a gas tapoff cycle using gaseous hydrogen and oxygen. The tapoff cycle considers that a portion of the combustion product gases are "tapped off" for use elsewhere. The computer program generated as a result of this analysis can be run with or without the tapoff cycle included. It includes the wave motion and heat motion (entropy wave) in the chamber. The burning process is treated as a process of temperature, molecular weight and specific heat change. A very general expression relating injection rate to burning rate is used. This computer program appears as an appendix to Ref. 16.

The many equations obtained are solved using matrices. The matrix operations however are used only on the equations involving real variables. The complex arithmetic used on the complex equations has been built into the program so that the program can be used on a variety of computers.

The final result of the analysis is a system characteristic equation. Stability of the system can be determined using the Nyquist criteria Ref. 11.

2. Technical Description

The feed system coupled stability problem at low frequencies can be analyzed conveniently by dividing the problem into two parts; the feed system and the chamber. Each part can be analyzed separately and then combined to determine the system stability. Method of analyzing the feed system is well developed, Ref. 11, but the traditional method of analyzing the chamber is quite primitive. The traditional method, Ref. 12 and 13, considers the volume of propellant injected into the chamber to be negligible and the burning to be a process of gas generation. In other words the volume of unburned propellant is assumed negligible compared to the volume of

burned gases. This is a good assumption for liquid propellants burning at low chamber pressures. But when the propellants are gaseous, especially gaseous hydrogen, this assumption is not good. Actually unburned gases flow into the chamber and when burning occurs gas properties (such as molecular weight, temperature and specific heat) change. The same weight flow of gas exists before and after burning.

This analysis looks only at the chamber analysis but has provision for adding the feed system effects. For simplicity the combustion is assumed to occur at one discrete plane. This is justified since the combustion does occur over a length that is small compared to the wave length of the oscillation. After combustion the gas goes through the sonic exhaust nozzle. The dynamics of a sonic exhaust nozzle have been well analyzed in Reference 14. The results of that analysis will be used here. In addition to the propellant feed lines an additional feature must be accounted for in the gas tapoff cycle, the dynamics of the tapoff duct. To analyze the combustion front the following relationships must be used:

Conservation of mass

$$\dot{w}_t + \dot{w}_x + \dot{w}_f = \dot{w}_p$$

Conservation of Momentum

$$P_f = P_x$$

$$P_x = P_p$$

Conservation of energy

$$\dot{w}_x h_x + \dot{w}_f h_f + \dot{w}_t h_t = \dot{w}_p h_p$$

Definition of enthalpy for a chemical system

$$h_x = hO_x + \int_{T_R}^{T_x} CP_x \, dT$$

$$h_f = hO_f + \int_{T_R}^{T_f} CP_f \, dT$$

$$h_p = hO_p + \int_{T_R}^{T_p} CP_p \, dT$$

$$hO_p = Y_{H_2} \; hO_{H_2} + Y_{H_2O} \; hO_{H_2O}$$

Definition of the product specific heat in terms of its composition

$$CP_p = Y_{H_2} \; CP_{H_2} + Y_{H_2O} \; CP_{H_2O}$$

Definition of the mass fraction of species in the products

$$Y_{H_2O} = \frac{9}{8} \frac{\dot{w}_x}{\dot{w}_p}$$

$$Y_{H_2} = 1 - Y_{H_2O}$$

Equation of state

$$P = R\rho T$$

$$R = \frac{\mathcal{R}_g}{MW}$$

Definition of the molecular weight of the products

$$MW_p = X_{H_2} \; MW_{H_2} + X_{H_2O} \; MW_{H_2O}$$

Definition of the mole fraction of species in products

$$X_{H_2} = \frac{\dfrac{Y_{H_2}}{MW_{H_2}}}{\dfrac{Y_{H_2}}{MW_{H_2}} + \dfrac{Y_{H_2O}}{MW_{H_2O}}}$$

$$X_{H_2O} = 1 - X_{H_2}$$

The analysis of the sonic exhaust nozzle results in a relationship between perturbations in pressure, velocity and entropy:

$$\gamma_p \, v_p' + \alpha \, p'_p + \beta \, S_p' = 0$$

The entropy can be related to other properties through the thermodynamics equation

$$T \, ds = dh - \frac{1}{g\rho} \, dp$$

The injection rates are related to the feed line dynamics by the following equations:

$$\frac{w'_x}{p'_x} = \frac{e^{-i\omega\tau_x}}{Z_x}$$

$$\frac{w'_f}{p'_f} = \frac{e^{-i\omega\tau_f}}{Z_f}$$

$$\frac{w'_t}{P'_x} = \frac{1}{Z_t}$$

The final equation which completely characterizes the system stability can be written as

$$\frac{F\, e^{-i\omega\tau_x}}{Z_x} + \frac{G\, e^{-i\omega\tau_f}}{Z_f} + \frac{H}{Z_t} + 1 = 0$$

The problem then amounts to the determination of F, G and H from the previous equations. To do this, all variables must be written as a mean value plus a perturbation value which varies with time. Each equation can then be divided into a mean equation and a perturbation equation. There are 27 perturbation equations which must be solved simultaneously. This is done with the help of matrices. Since 22 of the equations contain only real coefficients they will be solved using matrices as follows:

$$[AA][BB] + [CC]\,\dot{w}_x' + [DD]\,\dot{w}_f' + [EE]\,\dot{w}_t' + [FF]\,P'_p + [GG]\,S'_p = [0]$$

The matrix $[AA]$ is a 22 x 22 matrix and the others are column matrices. All the coefficients of these matrices are real. The remaining 5 equations involve complex variables and are solved simultaneously to obtain the final equation.

There are some important assumptions that are implied by the basic equations presented. First in the momentum and energy equations, the gas momentum and kinetic energy terms have been dropped. This assumes that the Mach number is small compared to unity. Also, in developing the perturbation equations, products of perturbations are neglected which means that only small amplitude oscillations can be treated (small compared to the mean variables). In defining the properties of the products only hydrogen and water are assumed to be in the products which infers that the engine must be running fuel rich. The analysis is limited to an engine using gaseous oxygen and gaseous hydrogen.

3. DEFINITION OF TERMS

AA	22 x 22 real matrix
BB	column matrix multiplying AA
CC	column matrix multiplying $\dot{w}_x'$
CP	specific heat at constant pressure
DD	column matrix multiplying $\dot{w}_f'$
e	base of the natural logarithm
EE	column matrix multiplying $\dot{w}_t'$
F	coefficient in characteristic equation
FF	column matrix multiplying P_p'
g	acceleration of gravity
G	coefficient in characteristic equation
GG	column matrix multiplying S_p'
h	enthalpy
hO	enthalpy of element at reference temperature of $77^{\circ}F$
H	coefficient in characteristic equation
i	$\sqrt{-1}$
MW	molecular weight
P	pressure
ℜ	universal constant
R	gas constant
S	entropy
T	temperature
v	velocity
$\dot{w}$	weight flow rate
X	mole fraction

Y	mass fraction
Z	axial coordinate
α	nozzle admittance coefficient
β	nozzle admittance coefficient
γ	ratio of specific heats
ρ	density
τ	total time lag between injection and combustion
ω	frequency

Subscripts

x	oxidizer
f	fuel
t	tapoff
H_2	hydrogen
H_2O	water
p	products
o	stagnation conditions
R	reference

C. Staged Combustion Cycle Analysis

1. INTRODUCTION

This analysis uses the sensitive time lag theory in both combustors of a staged combustion cycle. It considers only longitudinal modes and no feed system effects are included. The primary and secondary combustors are coupled by including in the secondary analysis the flow oscillation generated in the primary combustor. As in other analyses using the sensitive time lag theory and n and τ curve for neutral stability is obtained (Ref. 8). Since a staged combustion cycle has two combustors there are two sets of n's and τ's, one set for the primary combustor and one set for the secondary combustor. In this analysis the n and τ for the primary are assumed known and the analysis solves for the n and τ of the secondary.

2. TECHNICAL DESCRIPTION

There are many possible variations in configuration of staged combustion cycles. The one analyzed here is shown ir Figure 52. Figure 52 also includes dimensions and variables used in the input to the program. The purpose of the primary combustor is to generate gases to drive the turbine which in turn drives the propellant feed pumps. In this analysis the turbine is simulated by a pressure drop which is assumed to be proportional to the square of the flow rate through the turbine. No effect of turbine speed change or vibration is included. The distance between the turbine inlet and the point where the primary gases are injected into the secondary chamber is assumed to be negligible. The flow coming from the turbine that is injected

into the secondary combustor is assumed to have a time delay τ_{fs} between injection and combustion. This time delay is a mean total time delay as distinguished from the sensitive time lags τ_s and τ_p. The chambers and nozzles are analyzed using one-dimensional acoustics with a finite but small Mach number.

Both chambers are analyzed acoustically the same way so the following development applies to both the primary and secondary combustors. The following equations are used in developing the model:

Conservation of mass.

$$\frac{\partial \rho}{\partial t} + \frac{\partial}{\partial Z} (\rho u) = 0 \qquad \text{Eq. 17}$$

Conservation of momentum.

$$\rho \frac{\partial u}{\partial t} + \rho u \frac{\partial u}{\partial Z} + \frac{\partial p}{\partial Z} = 0 \qquad \text{Eq. 18}$$

Conservation of energy.

$$\frac{\partial}{\partial t} (\rho e_o) + \frac{\partial}{\partial Z} (\rho u h_o) = 0 \qquad \text{Eq. 19}$$

where,

$$e_o = c_v T + \frac{u^2}{2} \qquad \text{Eq. 20}$$

$$h_o = c_p T + \frac{u^2}{2} \qquad \text{Eq. 21}$$

$$c_v = \frac{RT}{\gamma - 1} \qquad \text{Eq. 22}$$

$$c_p = \frac{\gamma RT}{\gamma - 1} \qquad \text{Eq. 23}$$

Ideal gas law.

$$p = \rho RT \qquad \text{Eq. 24}$$

The energy equation is simplified if the kinetic energy terms are neglected. These terms become important only when Mach number is near 1. With this assumption the energy equation becomes:

$$\frac{\partial p}{\partial t} + \gamma p \frac{\partial u}{\partial Z} + \gamma u \frac{\partial p}{\partial Z} = 0 \qquad \text{Eq. 25}$$

The above equations have built into them the assumption that the area of the chamber does not change with the distance Z. It has also assumed no combustion. The combustion will be assumed to occur at the injector face and will be included in the analysis as a boundary condition.

All the dependent variables in the above equations will be assumed to be composed of a mean part which does not vary with time and a perturbation part which does vary with time.

$$p = \bar{p} + p' e^{St}$$

$$\rho = \bar{\rho} + \rho' e^{St} \qquad \text{Eq. 26}$$

$$u = \bar{u} + u' e^{St}$$

The variable S is the Laplace variable and is in general complex. When these are substituted into the equations and products of perturbations are neglected (which implies that only small amplitude oscillations will be considered) the following equations result:

$$S\rho' + \bar{u} \frac{d\rho'}{dZ} + \bar{\rho} \frac{du'}{dZ} = 0 \qquad \text{Eq. 27}$$

$$\bar{\rho} S u' + \bar{\rho}\bar{u} \frac{du'}{dZ} + \frac{dp'}{dZ} = 0 \qquad \text{Eq. 28}$$

$$Sp + \gamma \bar{p} \frac{du'}{dZ} + \gamma \bar{u} \frac{dp'}{dZ} = 0 \qquad \text{Eq. 29}$$

In obtaining the above equations $\frac{d\bar{u}}{dZ}$, $\frac{d\bar{p}}{dZ}$, $\frac{d\bar{\rho}}{dZ}$ were all set equal to zero since the area is not changing and no combustion is occurring.

These three equations can be combined to give:

$$\frac{c^2}{S^2} \frac{d^2}{dZ^2}\left(\frac{p'}{\bar{p}}\right) - (1-\gamma M^2)\frac{p'}{\bar{p}} = \frac{\bar{u}}{S}(\gamma+1)\frac{d}{dZ}\left(\frac{p'}{\bar{p}}\right) \qquad \text{Eq. 30}$$

where M is the Mach number and c is the acoustic velocity, $c = \sqrt{\gamma g R T}$. If the Mach number is small enough γM^2 is negligible compared to 1. For an even smaller Mach number the right-hand side can be neglected. The governing equation then becomes the homogeneous Helmholtz equation:

$$\frac{d^2}{dZ^2}\left(\frac{p'}{\bar{p}}\right) - \frac{S^2}{c^2}\left(\frac{p'}{\bar{p}}\right) = 0 \qquad \text{Eq. 31}$$

From equations 27thru 30 velocity and density can be obtained in terms of pressure.

$$\frac{u'}{\bar{u}} = \frac{1}{\gamma}\frac{p'}{\bar{p}} - \frac{1}{\gamma}\frac{c^2}{S\bar{u}}\frac{d}{dZ}\left(\frac{p'}{\bar{p}}\right) \qquad \text{Eq. 32}$$

$$\frac{\rho'}{\bar{\rho}} = \frac{1}{\gamma}\frac{p'}{\bar{p}} \qquad \text{Eq. 33}$$

Equation 31 is a second order equation and requires two boundary conditions. At the nozzle entrance the velocity and density are related by the specific acoustic admittance.

$$\frac{u'/\bar{u}}{\rho'/\bar{\rho}} = \alpha \qquad \text{Eq. 34}$$

At the injector the burning rate and pressure are related by the sensitive time lag burning expression.

$$\frac{(\rho u)'}{\bar{\rho}\bar{u}} = \mathcal{P}\frac{p'}{\bar{p}} \qquad \text{where} \qquad \mathcal{P} = n\,(1-e^{-S\tau}) \qquad \text{Eq. 35}$$

The solution to equation 31 is:

$$\frac{p'}{\bar{p}} = c_1\, e^{\frac{SZ}{c}} + c_2\, e^{-\frac{SZ}{c}} \qquad \text{Eq. 36}$$

Combining equation 36 with the 2 boundary conditions, after considerable algebra, the following expression is obtained.

$$M\,(1-\gamma\mathcal{P}) = \frac{1 - B\exp\left(\frac{2SL}{c}\right)}{1 + B\exp\left(\frac{2SL}{c}\right)} \qquad \text{where } B = \frac{1+\alpha M}{1-\alpha M} \qquad \text{Eq. 37}$$

This expression applies without qualification to the primary combustor:

$$M_p\,(1-\gamma\mathcal{P}_p) = \frac{1 - B_p\exp\left(\frac{2SL_p}{c_p}\right)}{1 + B_p\exp\left(\frac{2SL_p}{c_p}\right)} \qquad \text{where } B_p = \frac{1+\alpha_p M_p}{1-\alpha_p M_p} \qquad \text{Eq. 38}$$

For the secondary combustor equation 37 must be modified slightly to include the flow injected from the turbine exit as well as the pressure sensitive combustion:

$$M_S\left[1-\gamma\,(G\,e^{-S\tau_{fs}} + \mathcal{P}_s)\right] = \frac{1 - B_s\exp\left(\frac{2SL_s}{c_s}\right)}{1 + B_s\exp\left(\frac{2SL_s}{c_s}\right)} \qquad \text{Eq. 39}$$

$$\text{where} \quad B_s = \frac{1+\alpha_s M_s}{1-\alpha_s M_s}$$

The factor $e^{-S\tau_{fs}}$ is the combustion time delay for the fuel entering the secondary. The term G is determined as follows: Define $\hat{G}_p = \frac{\dot{w}_{p'}}{p'_p}$. This can be related to α_p by:

$$\hat{G}_p = \frac{1}{\gamma} \frac{\bar{\dot{w}}_p}{\bar{P}_p} (1 + \alpha_p) \qquad \text{Eq. 40}$$

The admittance upstream of the turbine is related to the admittance downstream of the turbine by:

$$\frac{1}{\hat{G}_{fs}} = \frac{1}{\hat{G}_p} - \frac{2(\bar{P}_p - \bar{P}_s)}{\bar{\dot{w}}_p} \qquad \text{Eq. 41}$$

The G in equation 33 is non-dimensional. To convert $\hat{G}_{fs}$ to G divide by $\frac{\bar{\dot{w}}_s}{\bar{P}_s}$

$$G = \hat{G}_{fs} \frac{\bar{P}_s}{\bar{\dot{w}}_s} = \frac{\bar{P}_s}{\bar{\dot{w}}_s} \frac{\frac{\bar{\dot{w}}_p}{2(\bar{P}_p - \bar{P}_s)}}{\frac{1}{\hat{G}_p} \frac{\bar{\dot{w}}_p}{2(\bar{P}_p - \bar{P}_s)} - 1}$$

$$G = \frac{-R_s}{1+R_s} \frac{\bar{P}_s}{2(\bar{P}_p - \bar{P}_s)} \left[\frac{1}{1 - \left(\frac{\bar{P}_p}{2(\bar{P}_p - \bar{P}_s)} \right) \left(\frac{\gamma}{1+\alpha_p} \right)} \right] \qquad \text{Eq. 42}$$

where R_s is the mixture ratio of the secondary chamber.

Equations 38, 39 and 42 are the governing equations for the system. These equations can now be solved simultaneously for $\mathcal{P}_s$.

Equation 38 must first be solved for α_p

$$\alpha_p = \frac{\Omega}{M_p} \frac{(1+\beta) - 1+\beta}{(\Omega (1-\beta) - \beta - 1)}$$

where $\beta = \exp\left(\frac{2SL_p}{c_p}\right)$ and $\Omega = M_p (1 - \alpha \mathcal{P}_p)$

Equation 42 can then be used to get G.

$$G = -\left(\frac{R_s}{1+R_s}\right)\left(\frac{\bar{P}_s}{2(\bar{P}_p - \bar{P}_s)}\right)\left[\frac{1}{1-\left(\frac{\bar{P}_p}{2(\bar{P}_p-\bar{P}_s)}\right)\left(\frac{\gamma}{1+\alpha_p}\right)}\right]$$

Finally equation 39 can be used to solve for $\mathcal{P}_s$.

$$\mathcal{P}_s = \frac{\left[\frac{1 - B_s \exp\left(\frac{2SL_s}{c_s}\right)}{1 + B_s \exp\left(\frac{2SL_s}{c_s}\right)} - M_s\right]}{-\gamma M_s} - G\, e^{-S\tau_{fs}}$$

The n and τ come from the definition of $\mathcal{P}_s$.

$$\mathcal{P}_s = n_s (1 - e^{-S\tau_s})$$

Set $S = 0 + i\omega$ and solve for $n(\omega)$ and $\tau(\omega)$

3. DEFINITION OF TERMS

B	Intermediate term defined in equation 37
C_1--C_2	Constants in equation 36 to be determined by the boundary conditions
c_p	Specific heat at constant pressure
c_v	Specific heat at constant volume
e	Base of Natural Logarithms
e_o	Internal energy of stagnant combustion gases
G	Nondimensional weight flow admittance injected into secondary chamber
G_p	Dimensional weight flow admittance upstream of the primary exhaust nozzle
h_o	Enthalpy of stagnant combustion gases
L	Length of cylindrical portion of chamber
M	Mach number in cylindrical portion of chamber
n	Pressure interaction index measuring the amount of interaction between pressure oscillations and burning rate oscillations
p	Pressure
R	Universal gas constant
R_s	Mixture Ratio in secondary chamber
S	Laplace variable
t	Time
T	Temperature
u	Velocity of gas
$\dot{w}$	Weight flow rate
Z	Length dimension
α	Specific Acoustic admittance ($= -\frac{A\gamma}{M}$ where A is from Ref. 9)
γ	Ratio of specific heats
ρ	Gas density

τ_{fs}	Total time lag of the fuel injected into the secondary chamber in seconds
τ	Sensitive time lag in seconds
ω	dimensional frequency in radians per second
ρ	$n(1 - e^{-S\tau})$

Subscripts

p	Primary combustor
s	Secondary combustor

Superscripts

$\bar{}$	Mean value - does not vary with time
'	Perturbation value

REFERENCES

1 Stability Characterization of Advanced Injectors, Report No. 20672-P1F, Aerojet General Corporation, 25 October 1968

2 Design Guide for Stable H_2O_2 Combustors, Vol. II: Design Applications Contract NAS 8-20672, Aerojet Liquid Rocket Company, Report No. 20672-P2D, May 1970

3 Advanced Injector Concepts Investigation, Aerojet-General Corporation, Contract NAS 8-21052, Report 21052-2F, January 1970

4 J. P. Wanhainen, C. E. Feiler, C. J. Morgan, Effects of Chamber Pressure, Flow Per Element, and Contraction Ratio on Acoustic Mode Instabilities, NASA TND-4733, Lewis Research Center, Aug. 1968

5 An Experimental Investigation of Combustion Stability Characteristics at High Chamber Pressures, Final Report Contract NAS 8-11741, Aerojet-General Corporation, Report No. 11741/SA6-F, Aug. 1966

6 Dykema, O. W., An Engineering Approach to Combustion Stability, ICRPG 2nd Combustion Conference CPIA Publ. No. 105, May 1966

7 Goede, P. J., Small-Amplitude Combustion Oscillations in the Gas Rocket AFOSR Contracts T53-65, 66 Report No. TM-66-4, Jet Propulsion Center, Purdue University, dated June 1966

8 Stability Characterization of Advanced Injectors, Design Guide, Vol. 2 Operation of the Computer Program, Aerojet General Corporation, Report 20672-P2D, January 1970

9 Stability Characterization of Advanced Injectors, Aerojet-General Corporation, Report No. 20672-Q3, September 15, 1967.

10 Marks, Mechanical Engineer's Handbook, 6th Ed., McGraw-Hill Book Co., Inc., 1958

11 Apollo Service Module Engine Acoustic Impedance Characteristics of the AJ10-137 Injector , Report Number 3865-529, Aerojet-General Corp., Sacramento, Calif.

12 Summerfield, M., A Theory of Unstable Combustion in Liquid Propellant Rocket Systems , ARS Journal, Vol. 21, Sept. 1951, pp. 108-114.

13 Crocco, L., Cheng, S. I., Theory of Combustion Instability in Liquid Propellant Rocket Motors , AGARD Monograph No. (8), Butterworths Scientific Publications, Ltd., London, 1956.

14 Crocco, L., Sirignano, W. A., Behavior of Supercritical Nozzles Under Three-Dimensional Oscillatory Conditions , AGARDograph 117, North Atlantic Treaty Organization, 1967

15 General Reference Manual, UNIVAC 1108, Sperry-Rand Corp., 1966

16 Stability Characteristics of Advanced Injectors, Design Guide, Vol. 2, Revision A, Operation of the Computer Program, Aerojet Liquid Rocket Company, Report 20672-P3D, Feb. 1971

TABLE 1

STEADY-STATE OPERATIONS CONDITIONS
TRANSVERSE EXCITATION CHAMBER TESTS OF COAXIAL INJECTOR

Test No.	$\dot{w}_o$ (lb/sec)	$\dot{w}_f$ (lb/sec)	MR	P_c (psia)	PfJ (psia)	TfJf* (°R)	PoJ (psia)	ToJ (°R)	M_c	No. of Inj
1	3.08	0.80	3.85	150	335	200	265	200	0.11	5
2	3.92	1.1	3.56	215	475	125	345	200	0.11	5
3	2.18	2.03	1.07	155	885	210	365	200	0.11	5
4	16.02	5.34	3.00	930	2425	85	1755	190	0.11	5
5	2.46	0.20	12.3	190	300	150	300	220	0.11	2
6	2.36	0.34	6.94	210	369	240	315	200	0.11	2
7	4.55	1.00	4.55	505	1215	173	1090	190	0.11	2
8	9.20	1.58	5.82	855	1685	135	2085	190	0.11	2
9	8.22	3.55	2.31	975	2665	105	2170	185	0.11	2
10**	--	--	--	--	--	--	--	--	--	--
11	2.80	0.190	14.72	185	334	150	350	205	0.11	3
12	5.94	2.25	2.64	515	1403	140	1130	190	0.11	3
13	3.25	0.45	7.22	200	405	212	385	200	0.11	3
14	9.85	2.65	3.72	780	1805	100	2055	195	0.11	3
15	9.63	3.26	2.95	815	1165	100	2150	185	0.11	3
16	10.08	3.64	2.77	515	2425	125	2100	180	0.18	3
17	2.58	1.64	1.57	150	1165	170	525	190	0.18	3
18	16.9	3.2	5.3	770	1875	95	1840	170	0.132	4
19	10.4	3.7	2.8	580	2520	130	1430	180	0.132	4
20	13.0	4.1	3.2	715	2525	80	1695	182	0.132	4
21	16.8	3.2	5.3	745	1890	80	1850	175	0.132	4
22	14.9	4.2	3.6	760	2745	80	1885	175	0.132	4
23	9.6	1.8	5.3	435	1130	95	890	175	0.132	4
24	2.8	1.0	2.8	145	630	135	300	185	0.132	4

*Measured at the entrance of the fuel injection annulus.
**Abort due to low fuel flow.

TABLE 2

COAXIAL INJECTOR STABILITY RESULTS

Test No.	f (kHz)	f_s (kHz)	f/f_s	Decay Rate (db/sec x 10^3)	Chamber Configuration
1	———	No Pulse Data	———	———	5 Injectors
2	2.60	1.93	1.35	3.2	↓
3	1.80	1.72	1.05	8	
4	2.85	3.84	0.74	8	
5	5.10	1.85	2.75	4.0	2 Injectors
6	6.30	1.92	3.28	Poor pulse	
7	5.95	2.59	2.30	2.8 - 3.2	↓
8	5.80	3.68	1.57	4.0 - 5.0	
9	5.70	3.27	1.74	7.0 - 8.0	
10	———	Abort Test	———	———	3 Injectors
11	3.53	2.30	1.53	8	
12	4.10	2.58	1.59	7.0	
13	3.40	1.88	1.81	2.0 - 2.8	
14	3.80	3.70	1.03	7.0	
15	3.95	3.18	1.24	6.0	
16	4.00	2.17	1.84	6.0 - 8.0	
17	3.95	1.85	2.14	8	↓
18	3.00	4.10	0.73	2.4	4 Injectors
19	3.00	3.00	1.00	0.9	
20	2.95	3.96	0.75	4.0	
21	3.00	4.20	0.72	2.0 - 2.2	
22	2.95	4.04	0.73	1.1	
23	3.00	3.14	0.97	1.3	
24	3.75	1.58	2.37	2.7 - 3.6	↓

f - fundamental mode frequency
f_s - sensitive frequency

TABLE 3

TEST PLAN - HIPERTHIN INJECTOR TESTS

Test No.	Injector Face Width (in.)	P_c (psia)	$T_{(oxid)}$ (^oR)	$T_{(fuel)}$ (^oR)	MR	$\dot{w}_T$ (lb/sec)
1	4.0	100	375	375	5.0	0.258
2	4.0	800	↓	375	↓	2.06
3	4.0	800		550		2.06
4	3.0	100		375		0.193
5	3.0	800		375		1.55
6	3.0	800		550		1.55
7	2.0	100		375		0.13
8	2.0	800		375		1.03
9	2.0	800		550		1.03
10	8.0	100		375		0.52
11	8.0	800		375		4.13
12	8.0	800		550		4.13

TABLE 4

STEADY STATE TEST DATA - TRANSVERSE EXCITATION CHAMBER
HIPERTHIN INJECTOR

Test	Dura. Sec.	P_c psia	MR	$\dot{W}_T$ lb/sec	A_T in^2	C*	T_{ox} ^oR	T_{fuel} ^oR	P_{OJ} psia	P_{fJ} psia	$C^*_{theo.}$	Config. (2)
1	0.988	136.4	13.6	0.645	0.619	4210	407	410	176	321	-	B
2	1.038	98.5	5.12	0.260	0.619	7545	396	516	150	153	7840	B
3	1.037	100.1	5.37	0.270	0.619	7384	398	408	150	146	7760	B
4	1.049	95.7	5.02	0.190	0.469	7600	403	396	148	144	7860	C
5	1.035	75.25	4.69	0.179	0.469	6344	411	521	135	144	7950	C
6	0.486	698.0	4.61	1.385	0.469	7605	405	536	1018	1163	8100	C
7	0.486	688.6	5.09	1.400	0.469	7422	401	421	1014	1064	7980	C
8	0.518	763.8	4.90	1.941	0.619	7837	400	521	1062	1093	8040	B
9	0.500	731.2	4.84	1.859	0.619	7833	399	412	983	1001	8060	B
10	0.504	589.3	5.13	1.633	0.619	7189	400	529	873	873	7950	B
11	0.518	361.4	4.95	0.946	0.619	7608	397	420	499	505	7980	B
12	0.999	108.1	5.38	0.274	0.619	7857	372	490	159	148	7760	B
13	0.522	629.0	4.92	3.871	1.274	6660	415	521	1050	920	8010	A
14	0.519	696.5	4.60	3.969	1.274	7193	404	475	1082	1070	8110	A
15	0.520	663.0	4.86	3.908	1.274	6954	401	406	1051	999	8040	A
16	0.520	89.5	5.31	0.535	1.274	6857	387	416	151	134	7780	A
17	0.519	87.0	4.86	0.519	1.274	6871	390	488	147	139	7910	A
18	0.520	348.7	5.20	1.953	1.274	7319	400	433	552	495	7910	A
19	0.523	57.6	5.94	0.162	0.369	4221	412	541	165	137	7500	D
20	0.815	101.2	4.91	0.131	0.369	9172	396	537	154	153	7910	D
21	0.525	724.5	5.08	0.924	0.369	9309	420	544	1056	1076	7990	D

TABLE 4 (cont.)

Test	Dura. Sec.	P_c psia	MR	$\dot{W}_T$ lb/sec	A_T in^2	C*	T_{ox} ^oR	T_{fuel} ^oR	P_{OJ} psia	P_{fJ} psia	C^*_{theo}	Config. (2)
22	0.980	708.0	5.35	0.954	0.369	8811	396	544	1047	1220	7920	D
23	0.557	685.2	5.24	0.934	0.369	8710	401	548	1033	1139	7940	D
24	0.562	496.5	5.36	0.922	0.369	6393	394	546	890	636	7890	D
25	0.560	647.2	5.12	0.903	0.369	8509	390	420	942	963	7970	D
26	0.562	108.3	6.11	0.152	0.369	8459	424	441	181	153	7535	D
27	0.561	106.0	5.56	0.205	0.469	7802	407	543	172	159	7700	C
28	0.560	664.8	4.70	1.306	0.469	7681	404	555	980	1106	8090	C

(1) These data taken during steady state operation near FS-2.

(2) A - 4 injectors in one chamber - 8 inch wide face
B - 2 injectors in one chamber - 4 inch wide face
C - 1 injector for 3 inch wide face
D - 1 injector for 2 inch wide face

COMBUSTION STABILITY DATA - TRANSVERSE EXCITATION CHAMBER
HIPERTHIN INJECTOR

Test	Config. (3)	Time-sec. (1)	Freq. Hertz	Amplitude Psi - P-P (2)	P_c PSIA	MR	$\dot{W}_T$ lb/sec	Growth Rate db/cycle (2)	Decay Rate db/cycle (2)	REMARKS
13	A	-	-	-	-	-	-	-	-	One injector damaged during test: No valid data.
14	A	11	5040	-/38	14.3	4.78	4.01	-/1.588*	-	
	A	11	8000	-/70	14.3	4.78	4.01	-/1.0*	-	
	A	15	5040	-/38	14.5	4.77	4.00	-	-/1.19	
	A	15	8000	-/70	14.5	4.77	4.00	-	-/1.0*	
	A	505	5040	-/350	697	4.46	3.95	-/1.39	-	
	A	505	10080	-/350	697	4.46	3.95	-/.695	-	
	A	505	12800	-/350	697	4.46	3.95	-/.586	-	
	A	505	20000	190/160	697	4.46	3.95	.350/.400	-	
	A	517	5040	-/350	696	4.43	3.94	-	-/.104	
	A	517	10080	-/350	696	4.43	3.94	-	-/.052	
	A	517	12800	-/350	696	4.43	3.94	-	-/.041	
	A	517	20000	200/150	696	4.43	3.94	-	.073/.180	
	A	532	20000	100/30	695	4.40	3.94	.4*/.125	-	
	A	534	20000	100/30	695	4.39	3.93	-	.325/.125	
	A	541	20000	55/10	695	4.38	3.93	.300/.300	-	
	A	550	20000	50/25	693	4.37	3.94	-	.100/.100	
15	A	10	10080	60/50	14.8	5.08	3.90	.794*/.794*	-	
	A	26	10080	-/60	28.4	5.09	3.88	-	-/.794*	
	A	85	10080	400/250	527	4.71	3.61	.794*/.794*	-	
	A	85	20000	130/100	527	4.71	3.61	.125/.140	-	
	A	329	5040	-/40	654	4.97	3.92	-/.125	-	
	A	508	5040	-/10	663	4.82	3.91	-	-/.2	
	A	527	10080	400/300	665	4.82	3.91	-	.298/.497	
	A	527	20000	160/140	665	4.82	3.91	-	.073/.375	

TABLE 5 (cont.)

Test	Config. (3)	Time-sec. (1)	Freq. Hertz	Amplitude Psi - P-P (2)	P_c PSIA	MR	$\dot{W}_T$ lb/sec	Growth Rate db/cycle (2)	Decay Rate db/cycle (2)	REMARKS
16	A	-	-	-	-	-	-	-	-	Stable
17	A	508	10080	45/45	85.2	4.80	.514	.595/.595	-	Shutdown Spike
	A	522	10080	37/32	81.1	4.88	.521	-	.794*/.794*	
18	A	511	12800	13/13	348	5.10	1.93	.626*/.626*	-	Shutdown Spike
	A	517	12800	13/10	347	5.12	1.94	-	.390/.390	
1	B	--	--	--	--	--	--	--	--	Misranged transducer - no valid data.
2	B	6	6400	9/4	15.3	5.94	.308	.156/.562	-	
	B	13	6400	9/4	16.2	5.93	.307	-	.156/.059	
	B	14	16000	25/10	16.2	5.93	.307	.5*/.5*	-	
	B	734	16000	10/7	97.7	5.04	.256	-	.150/.091	
	B	742	16000	8/6	98.3	5.07	.256	5*/.438	-	
	B	982	16000	10/5	98.3	5.08	.257	-	.188/.169	
3	B	5	6400	5/4	15.2	6.41	.312	.703/.781	-	
	B	5	16000	25/20	15.2	6.41	.312	.438/.438	-	
	B	12	6400	13/-	16.0	6.40	.312	-	.196/-	
	B	12	16000	25/-	16.0	6.40	.312	-	.488/-	
	B	19	16000	16/-	16.9	6.40	.312	.125/-	-	
	B	892	16000	15/6	102	5.55	.279	-	.036/.050	
	B	952	6400	6/3	102	5.65	.284	-	.422/.281	
	B	960	12800	10/7	102	5.65	.284	.469/.625	-	
	B	973	12800	10/7	102	5.69	.286	-	.547/.469	
8	B	-	-	-	-	-	-	-	-	Stable
9	B	-	-	-	-	-	-	-	-	Stable
10	B	-	-	-	-	-	-	-	-	Stable

TABLE 5 (cont.)

Test	Config.(3)	Time-sec.(1)	Freq. Hertz	Amplitude Psi - P-P(2)	P_c PSIA	MR	$\dot{W}_T$ lb/sec	Growth Rate db/cycle(2)	Decay Rate db/cycle(2)	REMARKS
11	B	-	-	-	-	-	-	-	-	Stable
12	B	974	12800	8/8	108	5.45	.279	.547/.625*	-	Shutdown Spike
	B	980	12800	8/8	108	5.46	.279	-	.391/.313	
4	C	802	12800	10/10	97.5	5.11	.192	.469/.313	-	
	C	815	12800	10/-	97.4	5.07	.191	-	.625*/-	
	C	818	12800	10/15	97.4	5.08	.191	.266/.227	-	
	C	968	12800	8/11	93.4	4.92	.187	-	.625*/.547	
	C	978	16000	9/7	93.1	4.92	.187	.313/.250	-	
	C	995	16000	5/3	89.5	4.91	.187	-	.375/.469	
5	C	6	16000	20/10	19.2	6.04	.226	.313/.169	-	
	C	6	20000	60/35	19.2	6.04	.226	.200/.169	-	
	C	6	25600	12/17	19.2	6.04	.226	.313*/.025	-	
	C	45	25600	40/-	63.1	5.90	.221	.024/-		
	C	52	16000	6/4	66.1	5.91	.221	-	.034/.034	
	C	52	20000	50/30	66.1	5.91	.221	-	.033/.034	
	C	990	12800	6/-	70.4	4.54	.175	.250/-	-	
	C	990	16000	33/28	70.4	4.54	.175	.250/.2		
	C	990	20000	28/15	70.4	4.54	.175	.135/.2	-	
	C	997	20000	28/15	62.6	4.53	.175	-	.4*/.030	
	C	997	25600	15/15	62.6	4.53	.175	-	/313*/.313*	
	C	1036	12800	5/-	19.2	4.54	.175	-	.469/-	
	C	1036	16000	10/6	19.2	4.54	.175	-	.5*/.5*	
6	C	-	-	-	-	-	-	-	-	Stable
7	C	-	-	-	-	-	-	-	-	Stable
27	C	319	5040	15/6	106	5.68	.208	1.59*/1.59*	-	Bomb induced Spike

TABLE 5 (cont)

Test	Config. (3)	Time-sec. (1)	Freq. Hertz	Amplitude Psi - P-P (2)	P_c PSIA	MR	$\dot{W}_T$ lb/sec	Growth Rate db/cycle (2)	Decay Rate db/cycle (2)	REMARKS
27	C	323	5040	15/6	106	5.68	.208	-	1.59*/1.59*	
28	C	-	-	-	-	-	-	-	-	Stable
19	D	53	8000	100/10	25.0	6.32	.172	.156/.138	-	Data from the test is questionable.
	D	53	16000	40/10	25.0	6.32	.172	.156/.023	-	
	D	148	16000	50/-	55.4	6.15	.167	-	.313/-	
	D	153	8000	175/30	55.4	6.15	.167	.489/.450	-	
	D	153	16000	80/-	55.4	6.15	.167	.213/-	-	
	D	425	8000	300/30	57.5	5.80	.158	-	.072/.072	
	D	457	16000	100/25	57.7	5.80	.158	-	.775/.058	
20	D	-	-	-	-	-	-	-	-	Stable
21	D	-	-	-	-	-	-	-	-	Stable
22	D	-	-	-	-	-	-	-	-	Stable
23	D	-	-	-	-	-	-	-	-	Stable
24	D	342	12800	35/-	685	5.24	.933	.625*/-	-	Bomb induced Spike
	D	342	16000	200/150	685	5.24	.933	.468/.5*	-	
	D	348	12800	45/-	687	5.24	.933	-	.625*/	
	D	348	16000	200/150	687	5.24	.933	-	.5*/.5*	
25	D	-	-	-	-	-	-	-	-	Stable
26	D	338	16000	30/-	111	6.27	.156	.468/-	-	Bomb Induced Spike
	D	338	20000	30/-	111	6.27	.156	.4*/-	-	

TABLE 5 (cont.)

Test	Config. (3)	Time-sec. (1)	Freq. Hertz	Amplitude Psi - P-P (2)	P_c PSIA	MR	$\dot{W}_T$ lb/sec	Growth Rate db/cycle (2)	Decay Rate db/cycle (2)	REMARKS
26	D	342	16000	35/-	111	6.29	.157	-	.5*/-	
	D	342	20000	35/-	111	6.29	.157	-	.4*/-	

(1) Time After Ignition

(2) Values given as Pcl (or Pc3)/Pc-2

(3) A - 4 injectors in one chamber - 8 inch wide face

B - 2 injectors in one chamber - 4 inch wide face

C - 1 injector for 3 inch wide face

D - 1 injector for 2 inch wide face

* Maximum Limit of Data Reduction Equipment

TABLE 6

TEST PLAN -- 300 PSIA INJECTOR

Test Series 1 - Dynamic Stability at Nominal APS Conditions

Test No.	P_c psia	MR	T_{ox} °R	T_{fuel} °R
1	300	4.0	300	200
2	300	4.0	530	200
3	300	4.0	300	530
4	300	4.0	530	530

Test Series 2 - Dynamic Stability at Peripheral APS Conditions

Test No.	P_c psia	MR	T_{ox} °R	T_{fuel} °R
5	300	2.0	530	530
6	300	3.0	530	530
7	300	5.0	530	530
8	300	6.0	530	530
9	300	2.0	530	200
10	300	3.0	530	200
11	300	5.0	530	200
12	300	6.0	530	200

TABLE 7

STEADY STATE PRELIMINARY TEST DATA

Test No.	P_c psia	MR	$\dot{W}_T$ lb/sec	T_{ox} °R	T_{fuel} °R	C* ft/sec
1	295	2.07	6.94	520	540	7761
2	289	3.13	6.65	535	540	7957
3	291	4.24	6.90	535	550	7707
4	277	5.26	6.82	540	550	7438
5	264	6.16	6.68	530	555	7234
6	299	2.21	6.84	500	245	8006
7	289	3.08	6.60	500	245	7893
8	303	4.59	7.26	490	275	7506
9	292	4.11	6.80	480	250	7724
10	272	6.56	6.80	500	270	7115
11	244	3.77	5.44	380	310	8071
12	276	3.38	6.86	380	400	7363

TABLE 8

STEADY STATE TEST DATA

Uni-Element Coaxial Injector

Test No.	Resonator Length	MR	P_c Psia	W_T lb/sec	POJ Psia	PFJ psia	TOJ °R	TFJ °F
4	0"	2.63	17.50	.0571	17.00	19.26	521	541
5	6"	2.63	17.66	.0571	17.03	19.50	515	540
6	12"	2.63	17.72	.0571	17.15	19.57	519	539
7	18"	2.63	17.75	.0571	17.21	19.52	518	537
10	24"	2.63	17.42	.0571	17.12	19.56	510	530
11	30"	2.63	17.67	.0571	17.05	19.44	511	530
12	36"	2.63	17.49	.0571	16.94	19.30	509	510
13	42"	2.63	17.54	.0571	16.94	19.37	505	505
14	48"	2.63	17.59	.0571	16.99	19.35	508	508
15	54"	2.63	17.59	.0571	17.21	19.51	509	508
16	54"	2.65	17.60	.0581	17.01	19.66	518	518
17	48"	2.65	17.39	.0581	16.81	19.55	520	519
18	42"	2.65	17.47	.0581	16.95	19.60	520	519
21	24"	2.65	17.32	.0581	16.58	19.34	519	519
22	30"	2.65	17.28	.0581	16.80	19.48	519	519
23	36"	2.65	17.21	.0581	16.68	19.54	519	519
25	18"	2.65	17.46	.0581	16.97	19.63	519	518
26	12"	2.65	17.25	.0581	16.68	19.54	518	518
27	6"	2.65	17.43	.0581	16.95	19.57	518	518
28	0"	2.65	17.15	.0581	16.68	19.31	519	518
30	6"	2.75	8.79	.0579	6.96	12.31	542	-
31	12"	2.75	17.18	.0579	16.53	19.10	542	-
33	18"	2.75	16.86	.0579	16.40	18.78	542	-
35	0"	2.75	16.75	.0579	16.27	18.64	542	-
37	0"	2.75	17.32	.0579	16.51	19.25	541	-
38	6"	2.75	17.24	.0579	16.45	19.18	541	-
39	12"	2.75	16.82	.0579	16.37	18.73	542	-
40	18"	2.75	17.25	.0579	16.29	19.13	541	-

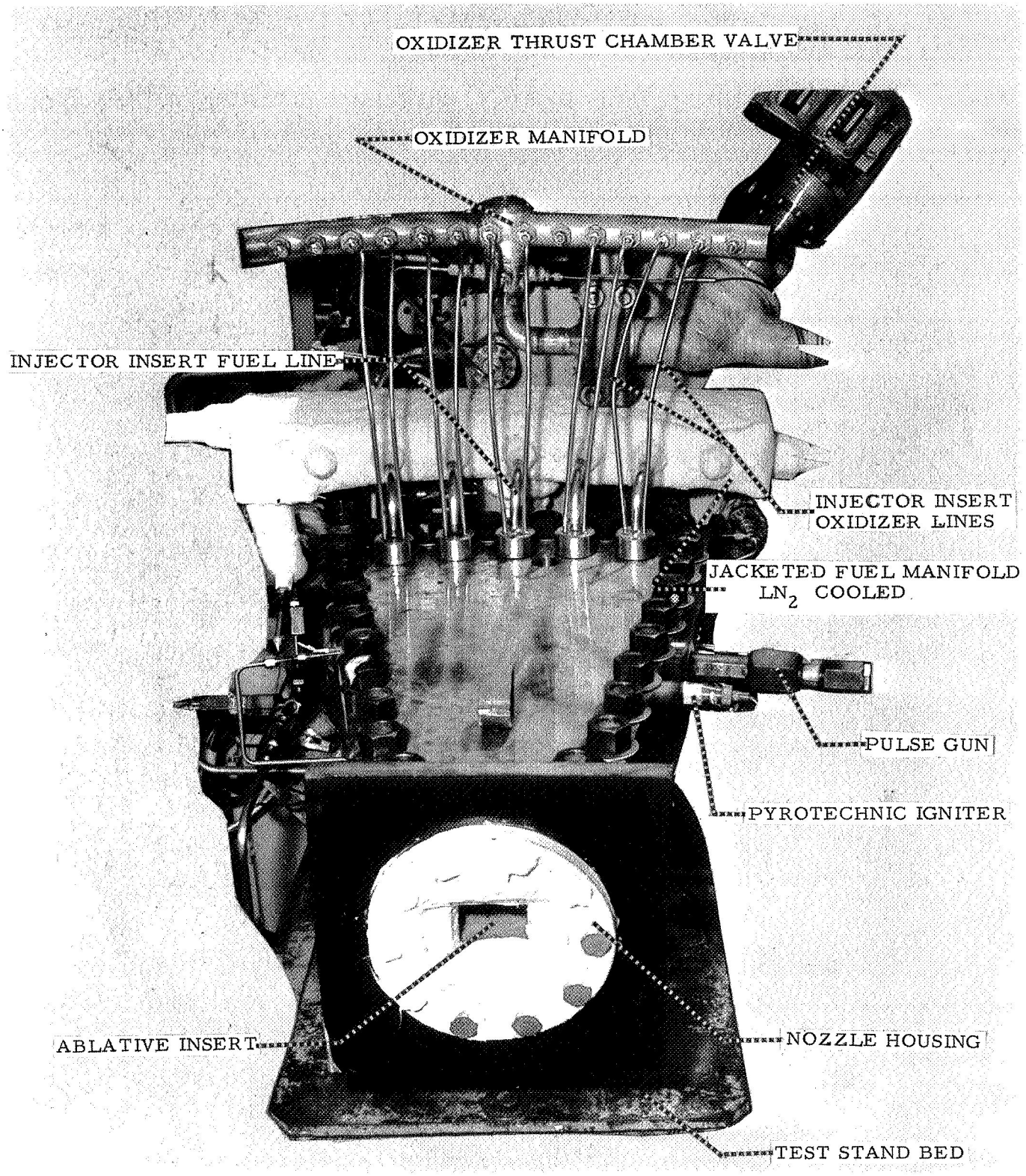

Transverse Excitation Chamber on Test Stand

Figure 1

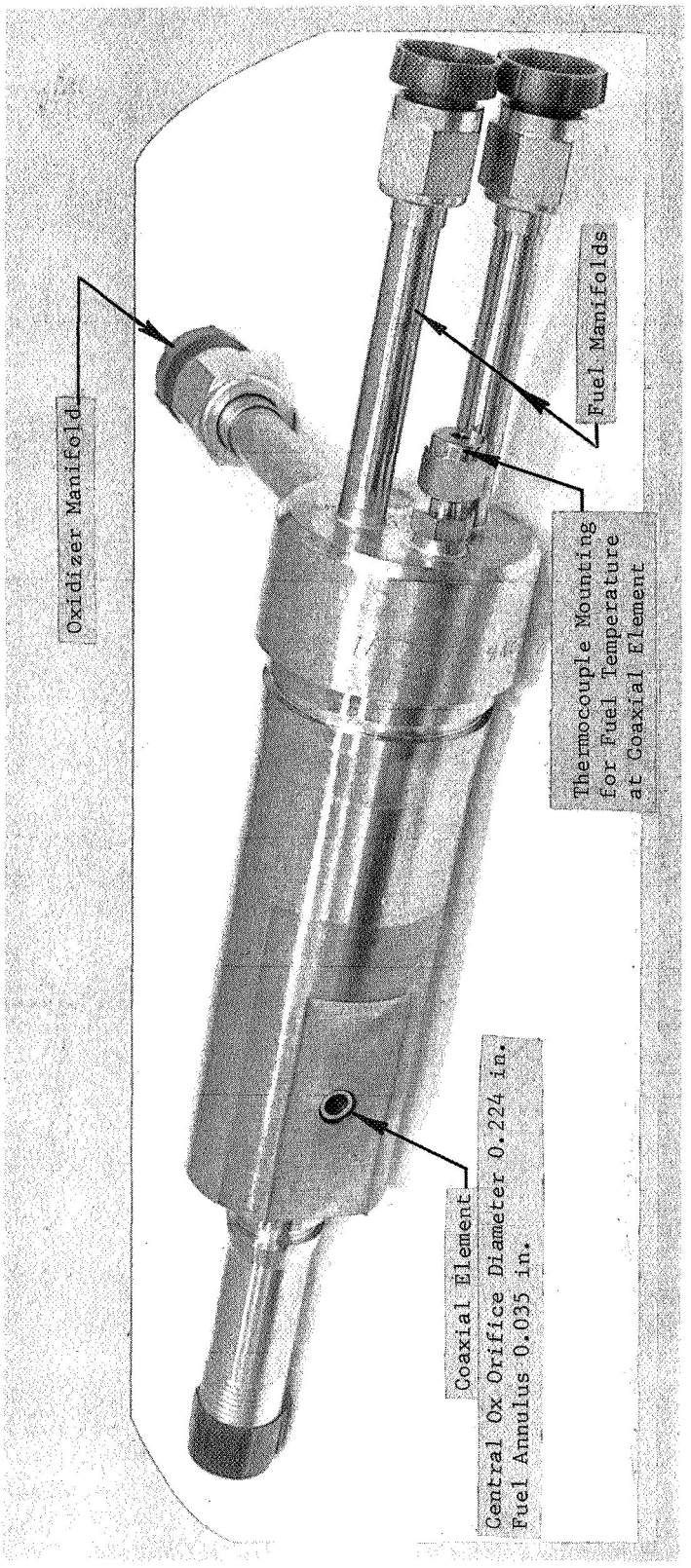

Coaxial Injector for Transverse Excitation Chamber

Figure 2

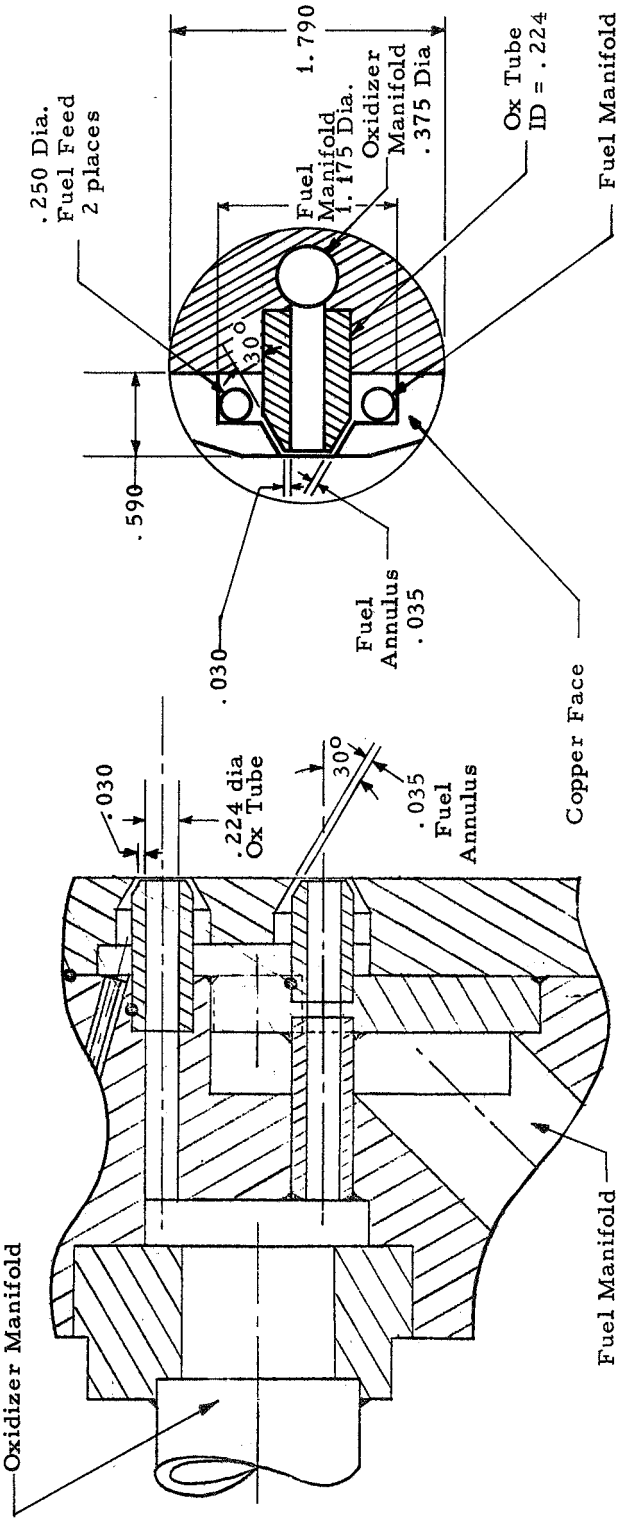

Coaxial Element for 54 Element Annular Injector. Phase 1

Coaxial Element for Excitation Chamber

Schematic of Coaxial Element

Figure 3

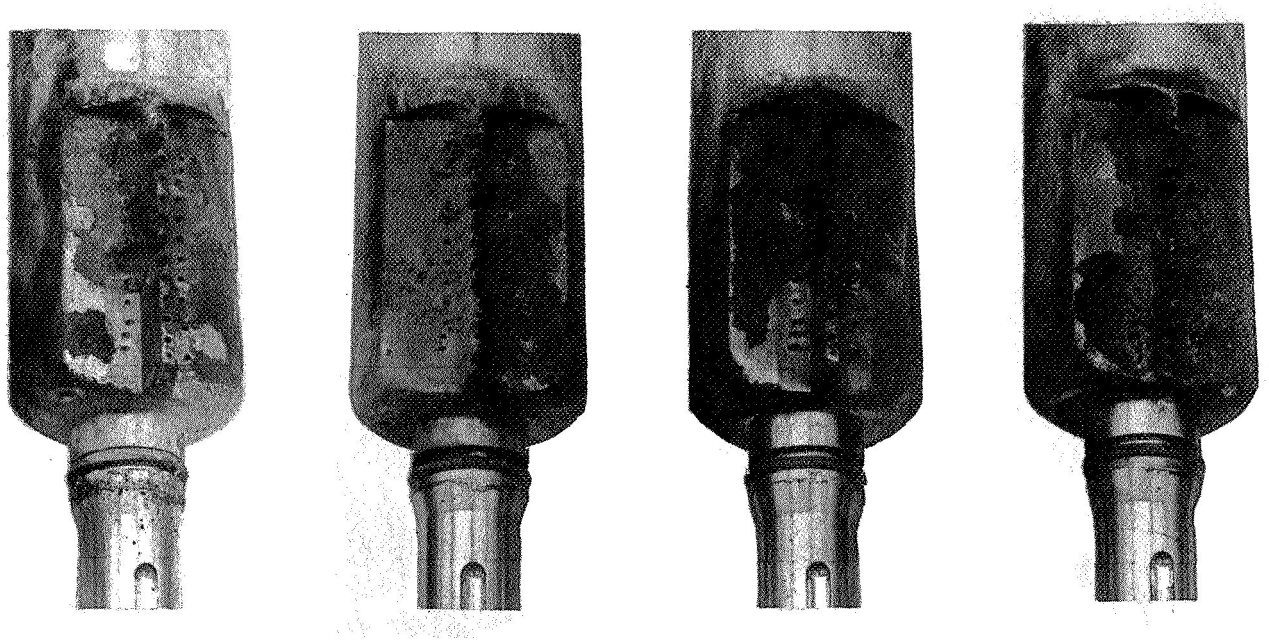

Figure 4a. Triplet Injector with Stainless Steel Face

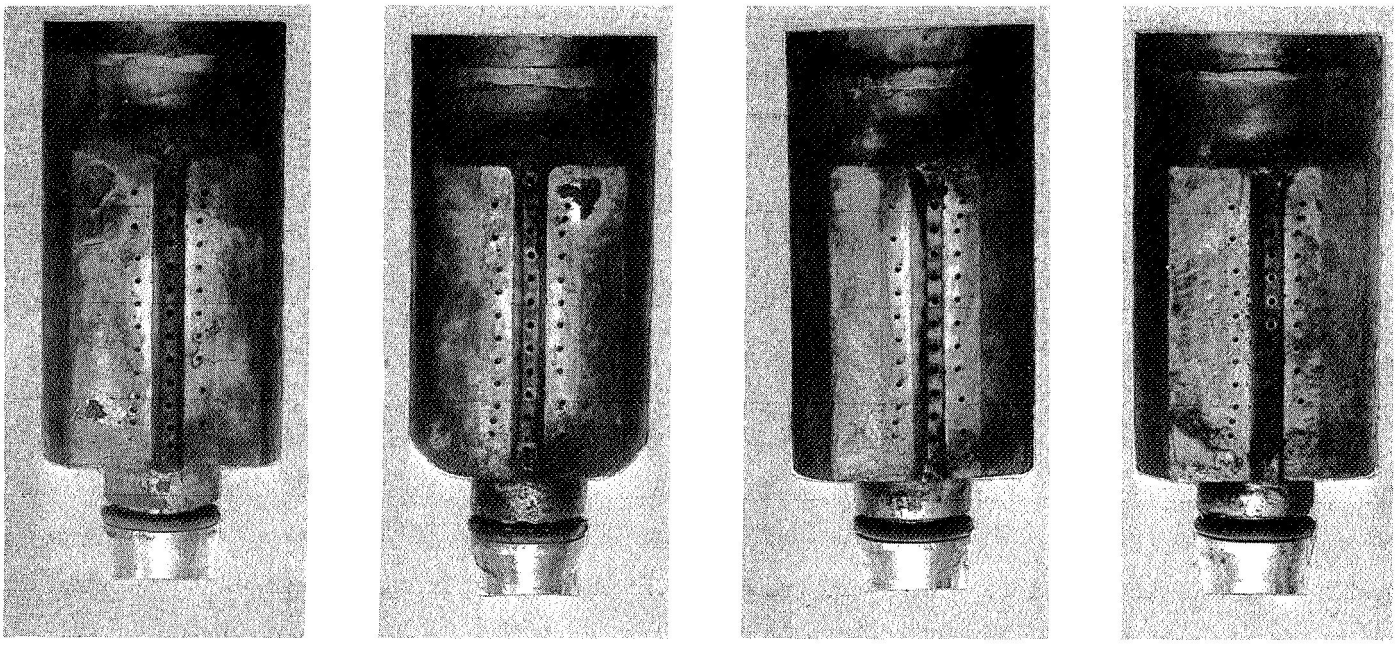

Figure 4b. Triplet Injector with All-Copper Face

Triplet Injectors - Stainless Steel and Copper Face Comparison

Figure 4

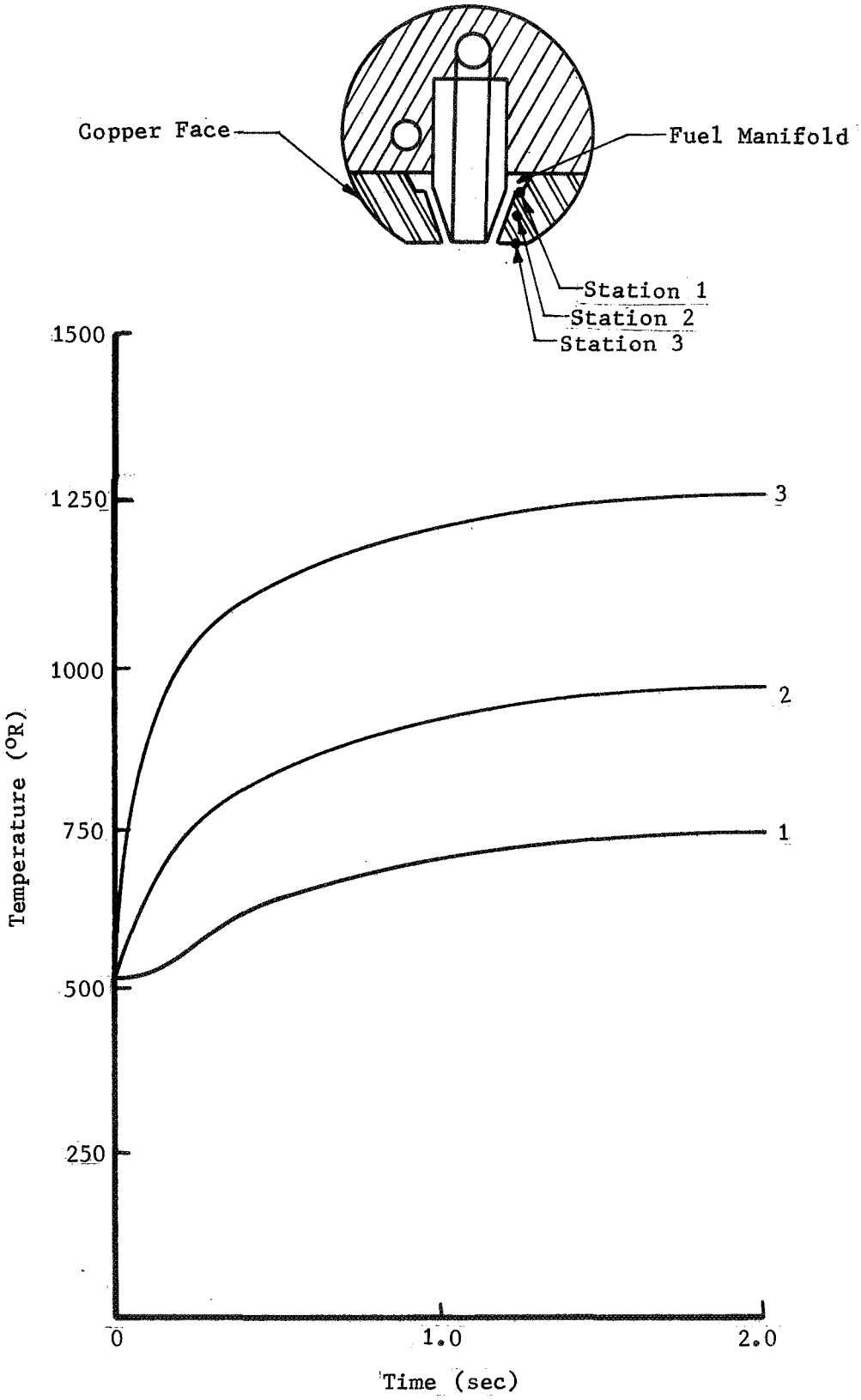

Predicted Transient Heating Through Coaxial Element

Figure 5

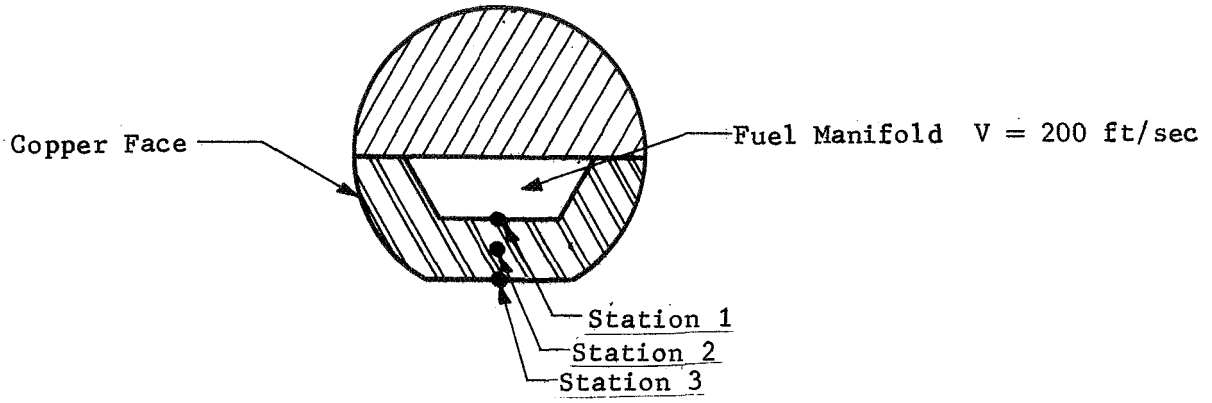

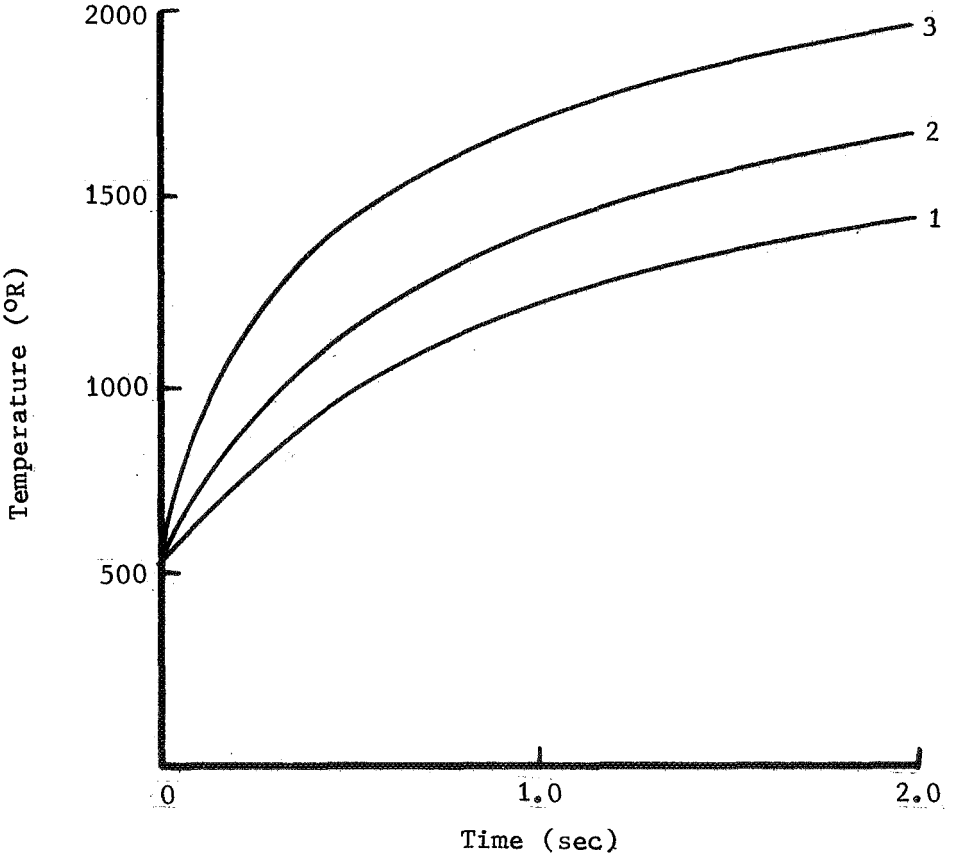

Predicted Transient Heating Through Coaxial Injector Body

Figure 6

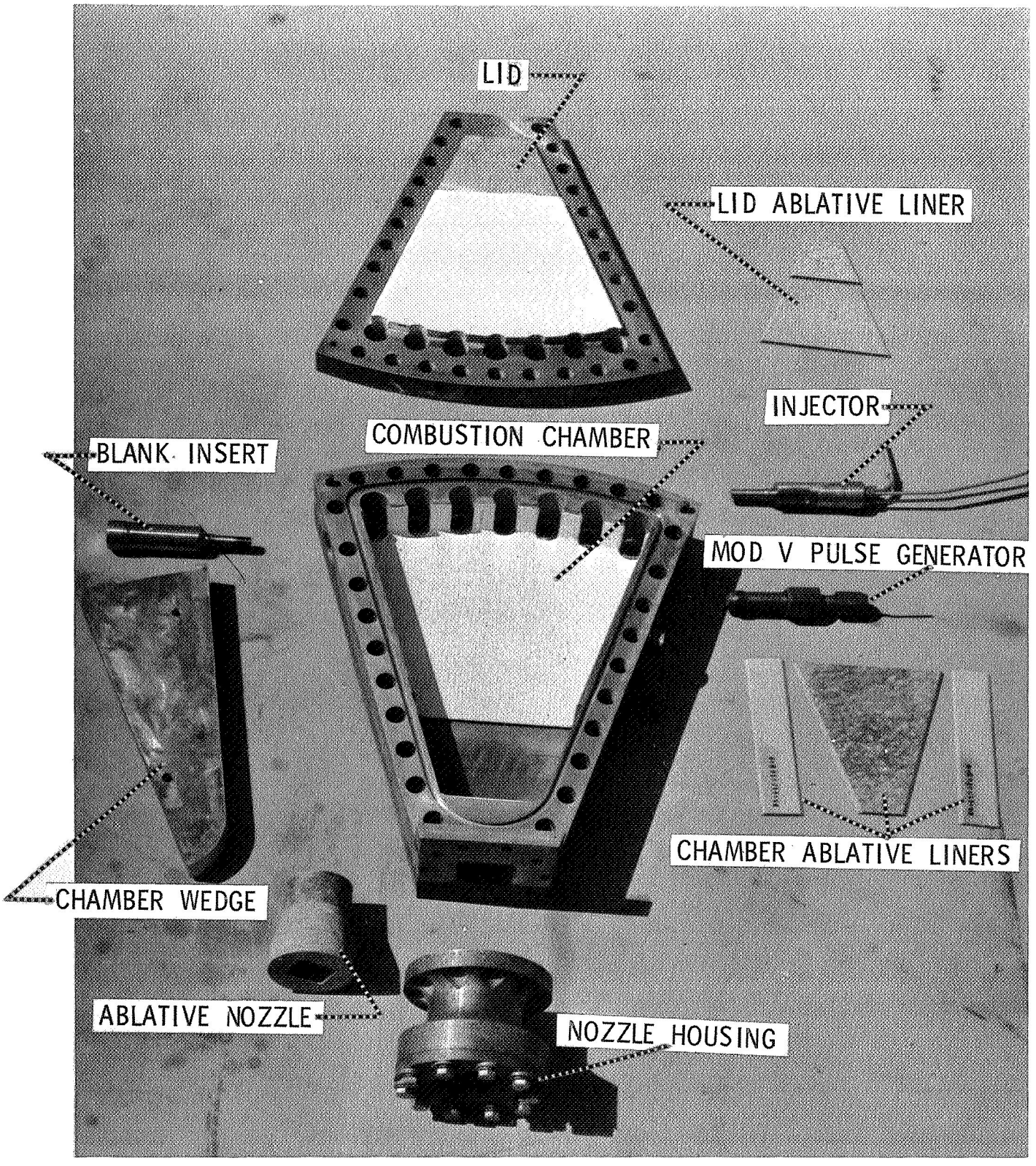

Seven Element Transverse Excitation Chamber and Components

Figure 7

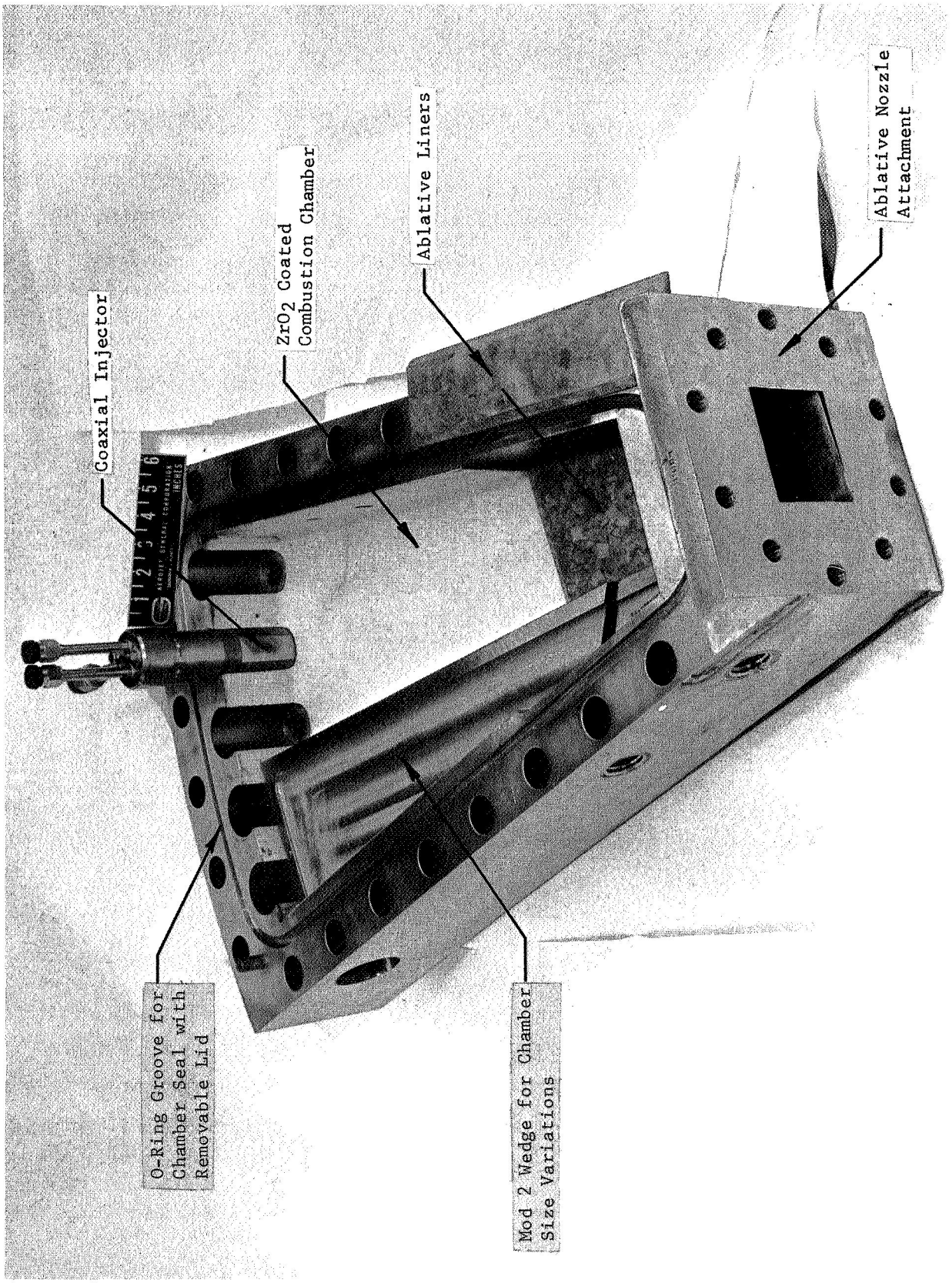

Five Element Transverse Excitation Chamber and Components

Figure 8

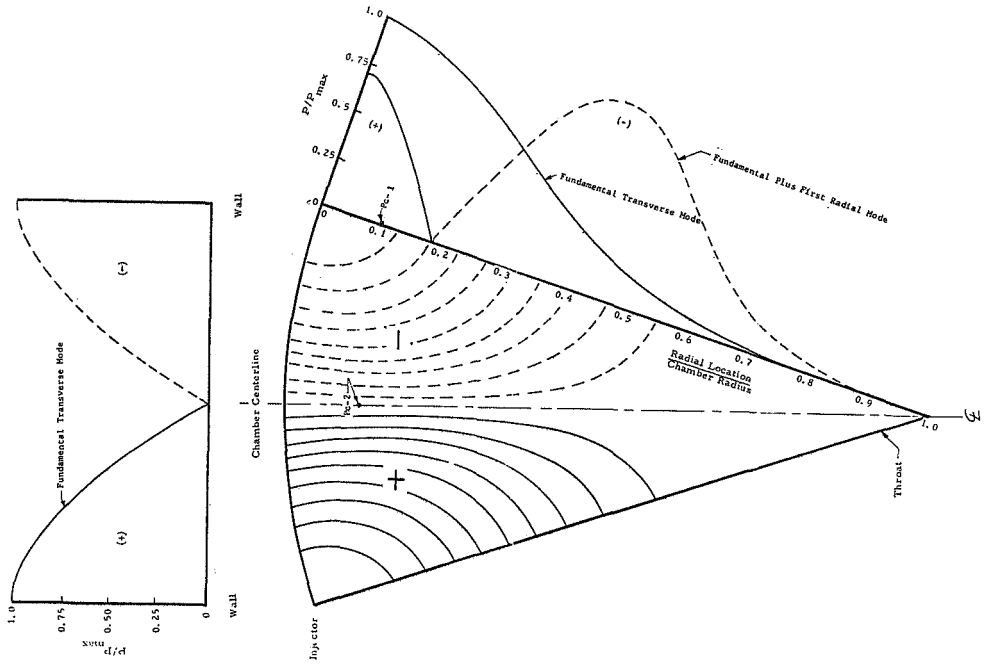

Figure 9a. Fundamental Transverse and Fundamental Plus First Radial Modes

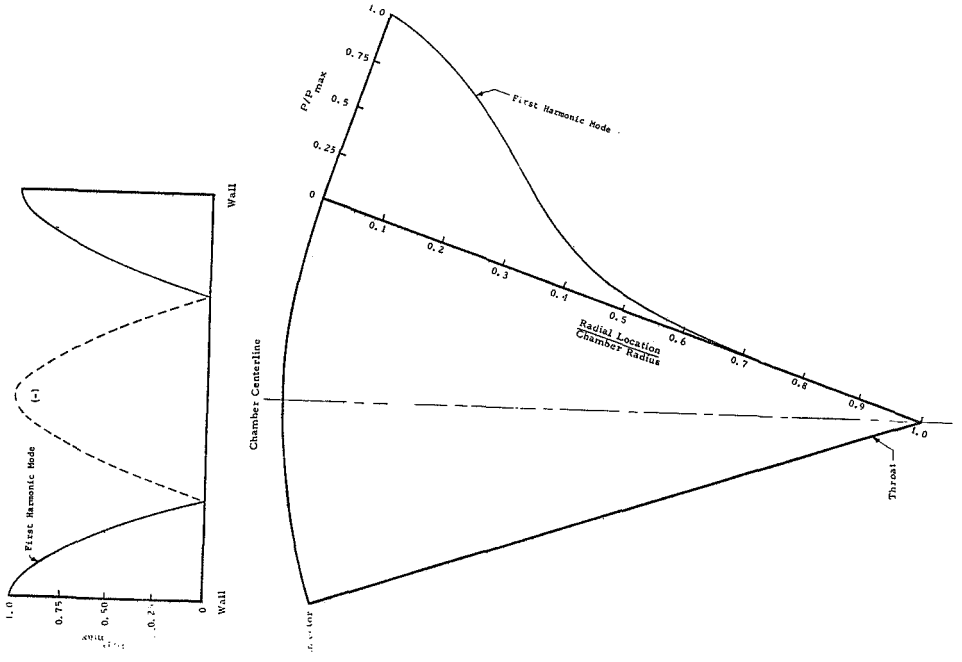

Figure 9b. First Harmonic Mode

Acoustic Pressure Profiles

Figure 9

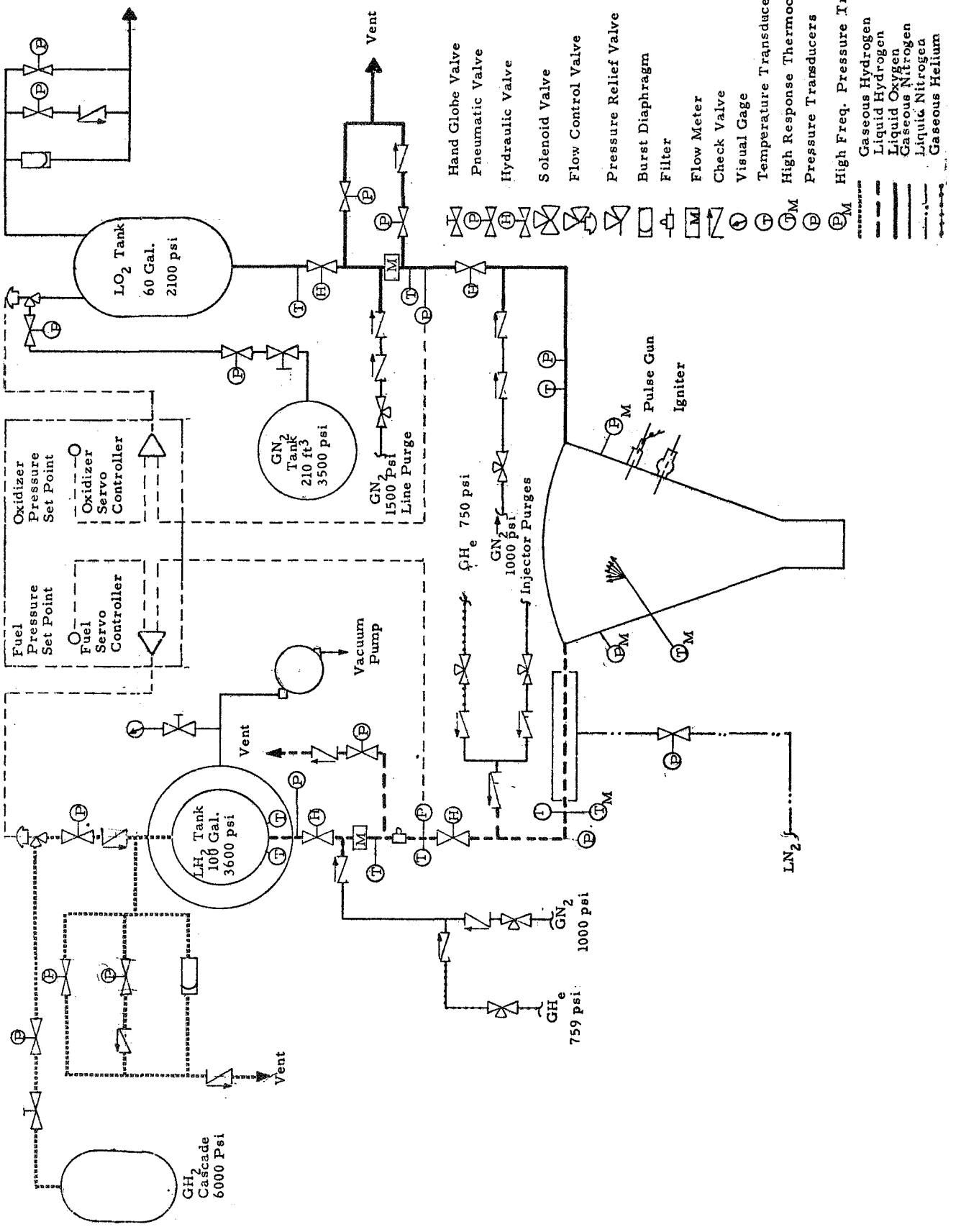

Test Stand J-1 Flow System Schematic

Figure 10

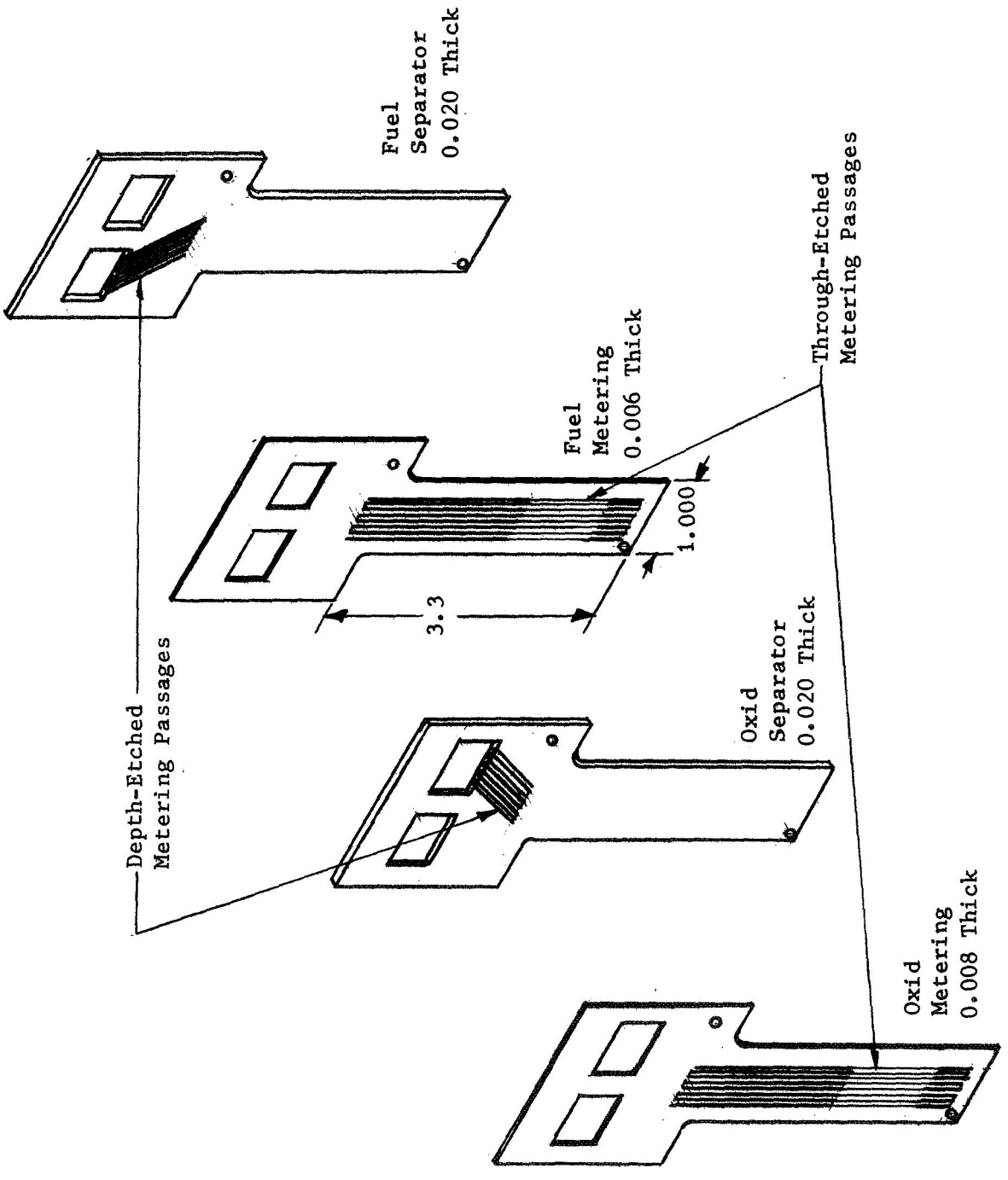

HIPERTHIN Platelet Assembly Schematic

Figure 11

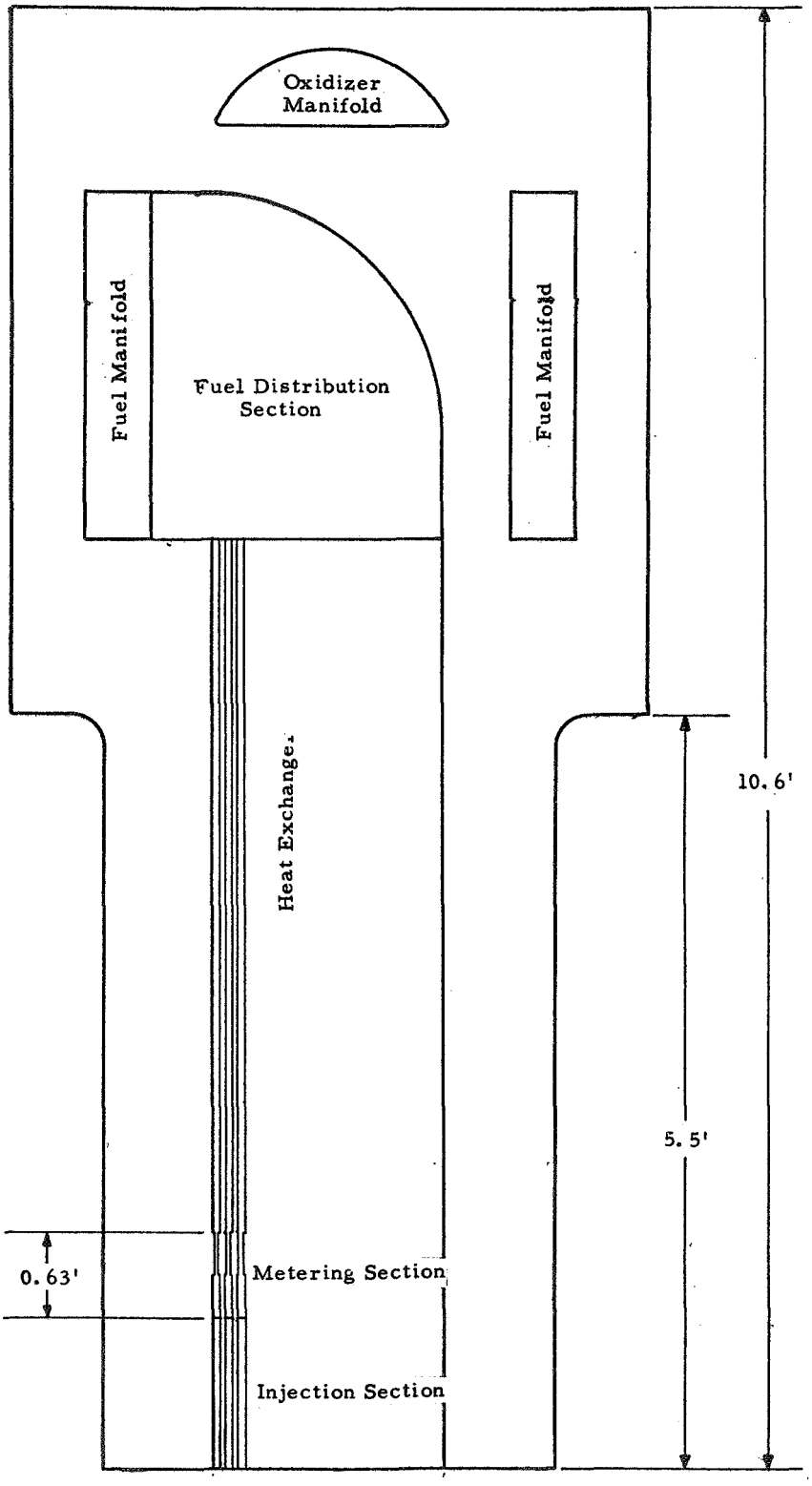

ADVANCED INJECTOR CONCEPTS

INVESTIGATION FUEL METERING PLATELET

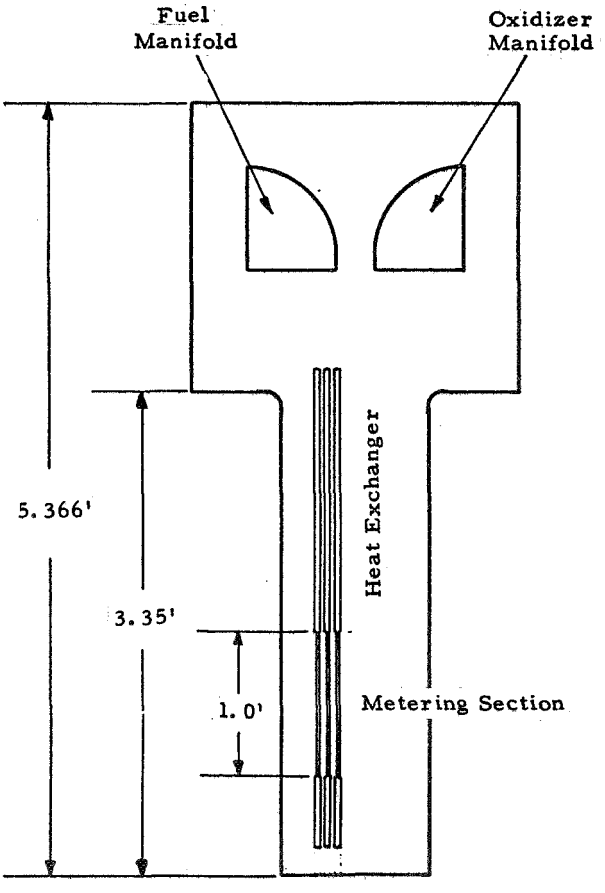

COMBUSTION STABILITY

EVALUATION PLATELET

Comparison of Platelets from Contracts NAS 8-21052 and NAS 8-20672

Figure 12

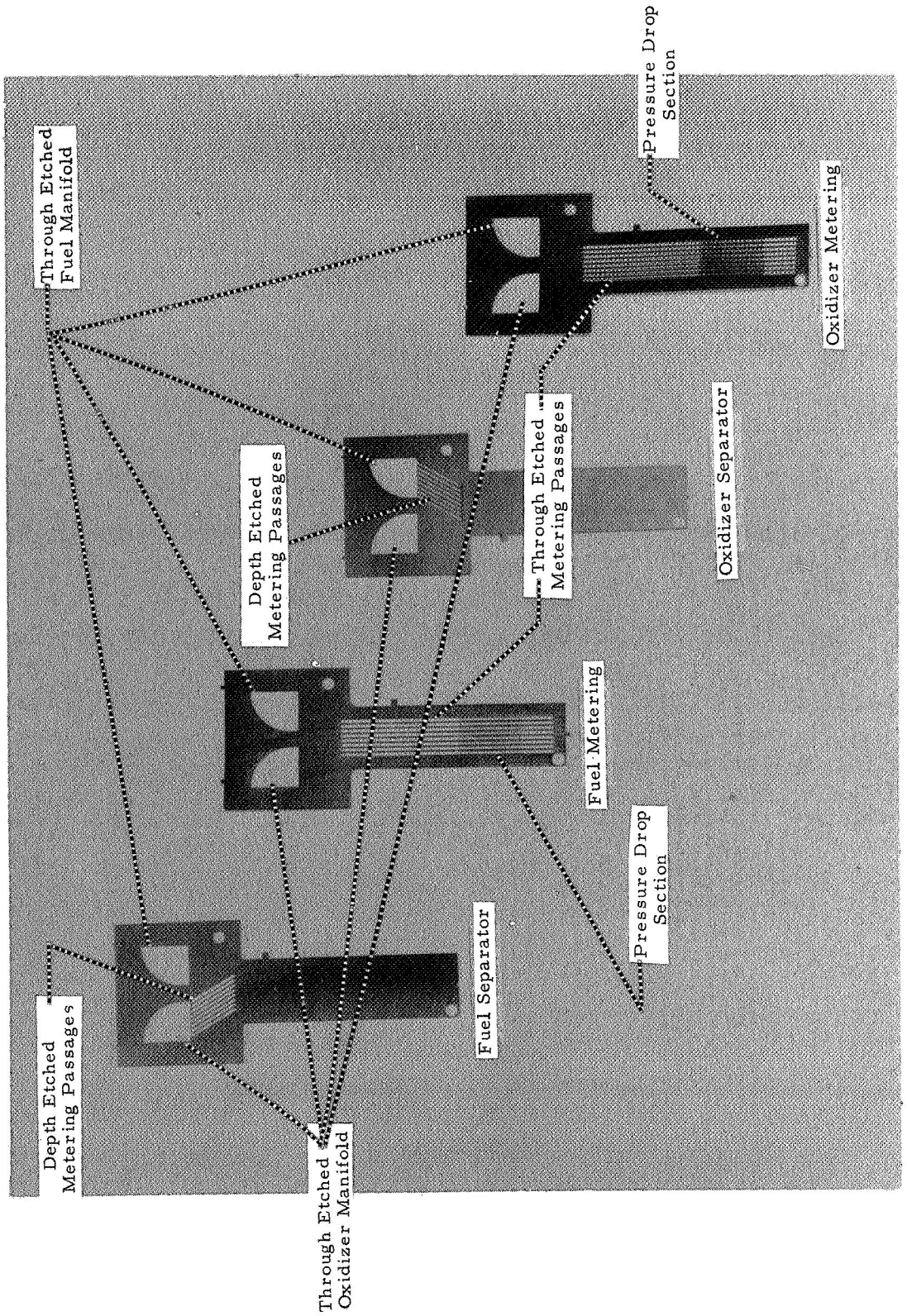

HIPERTHIN Injector Platelet Set

Figure 13

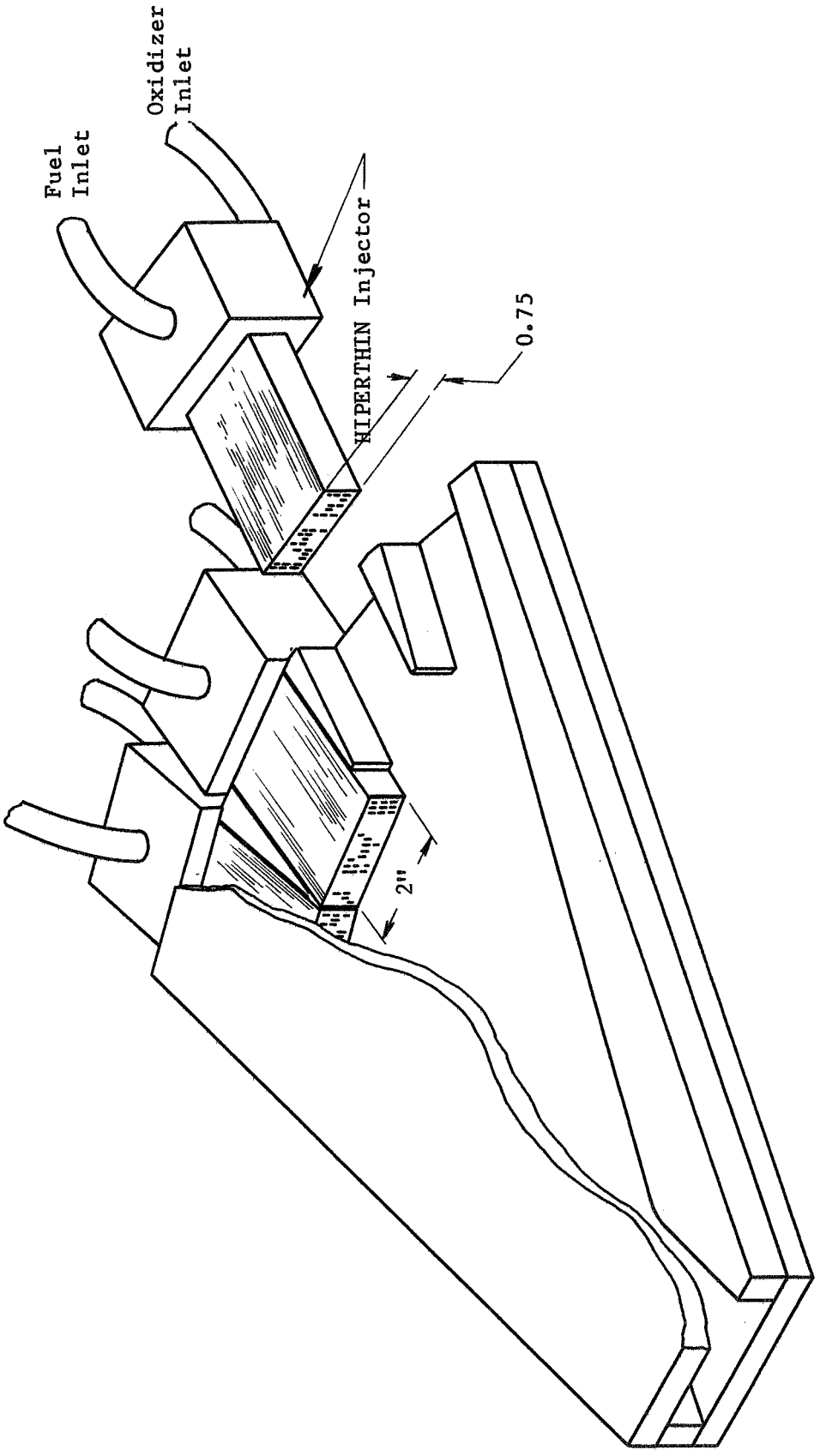

Heat Sink Excitation Chamber

Figure 14

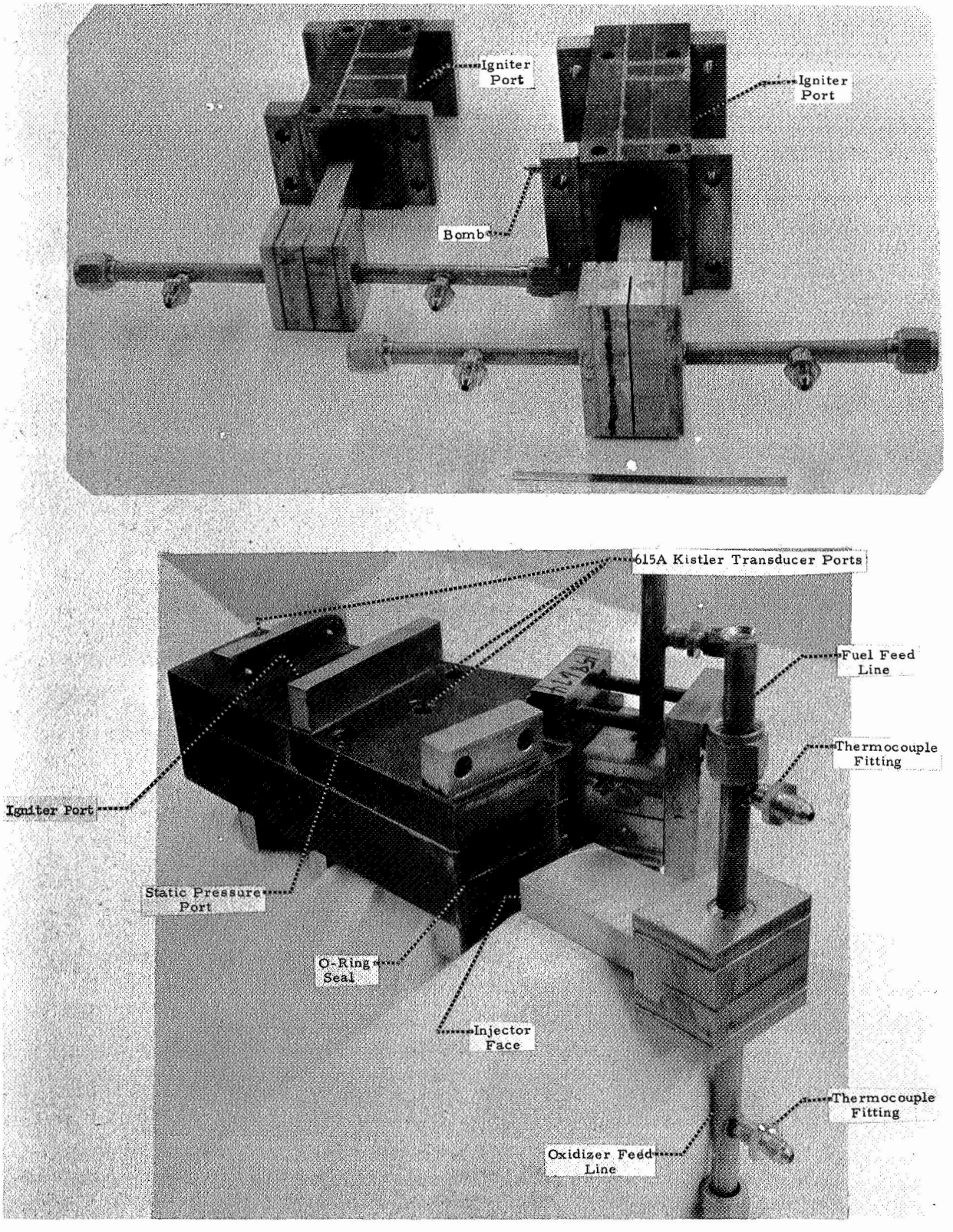

HIPERTHIN Injectors and Heat Sink Excitation Chambers

Figure 15

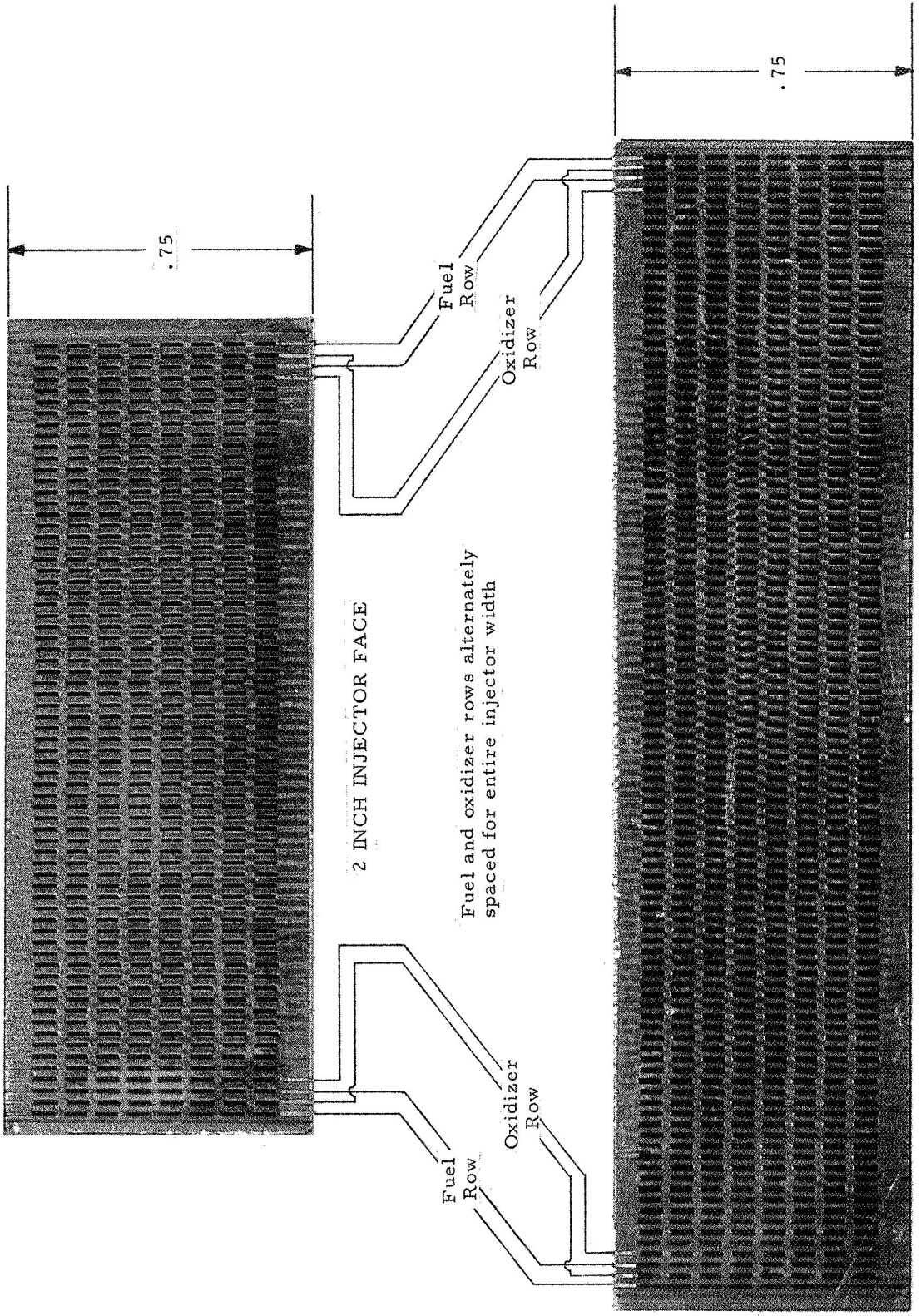

HIPERTHIN Injector Face

Figure 16

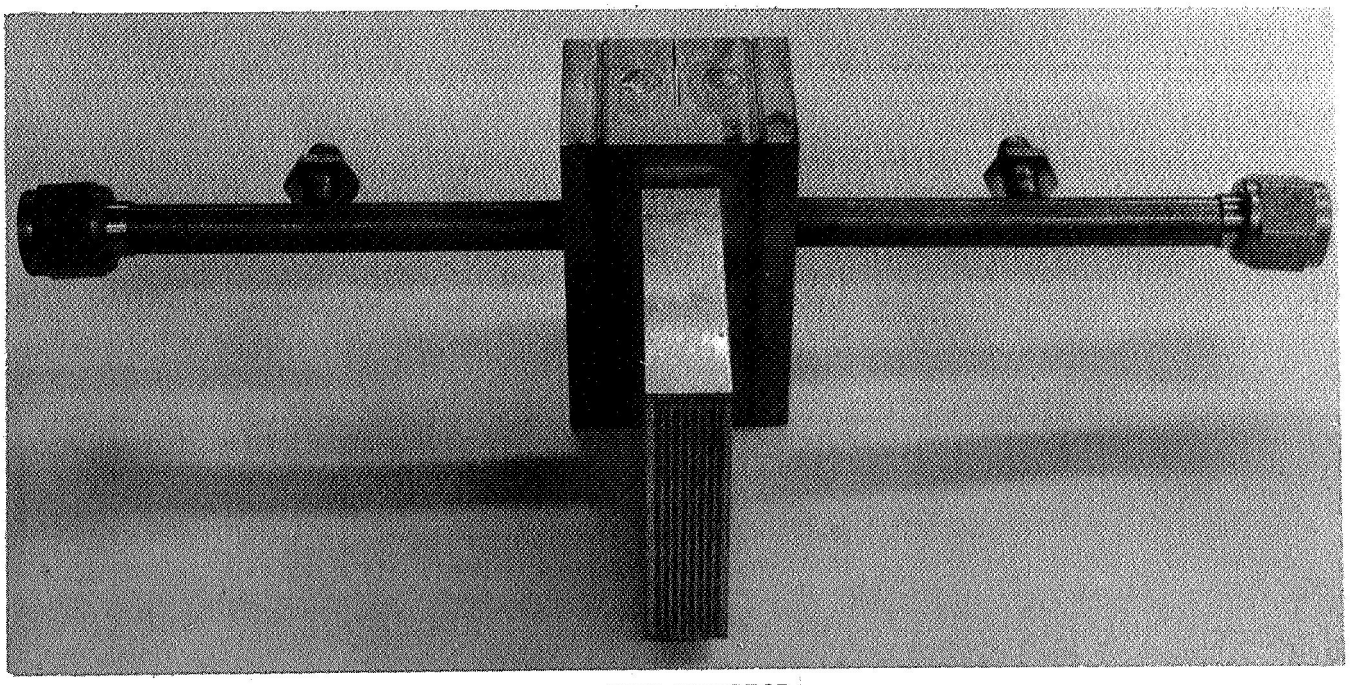

3 INCH INJECTOR

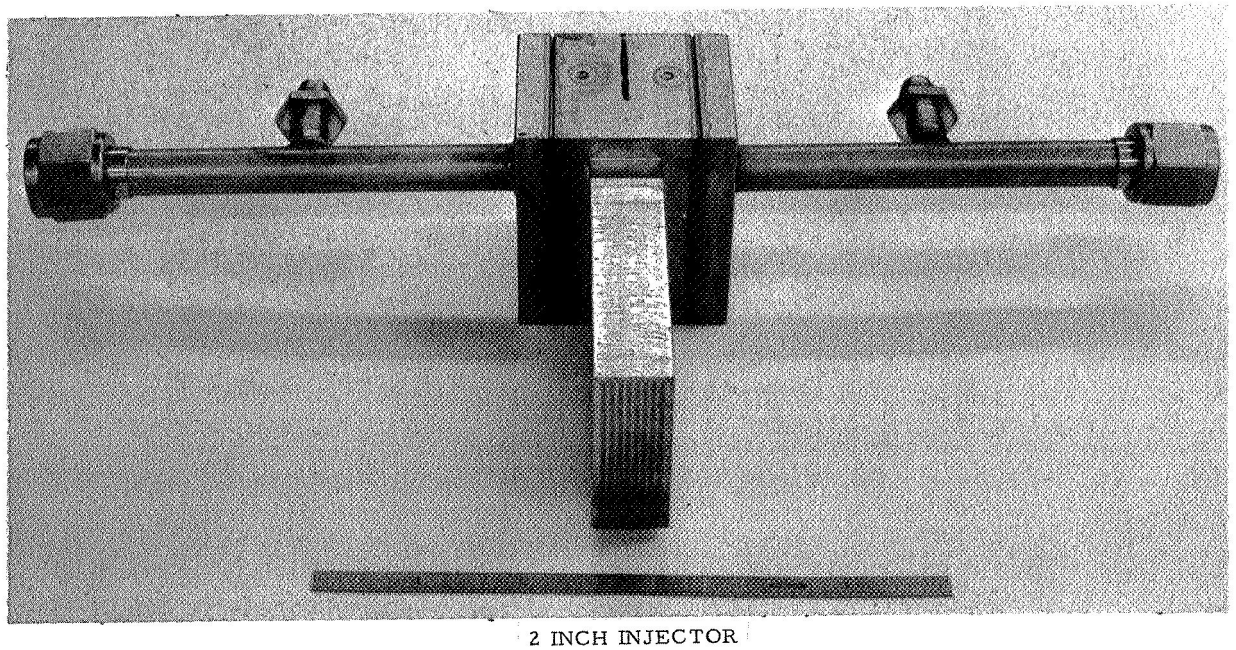

2 INCH INJECTOR

Completed HIPERTHIN Injectors

Figure 17

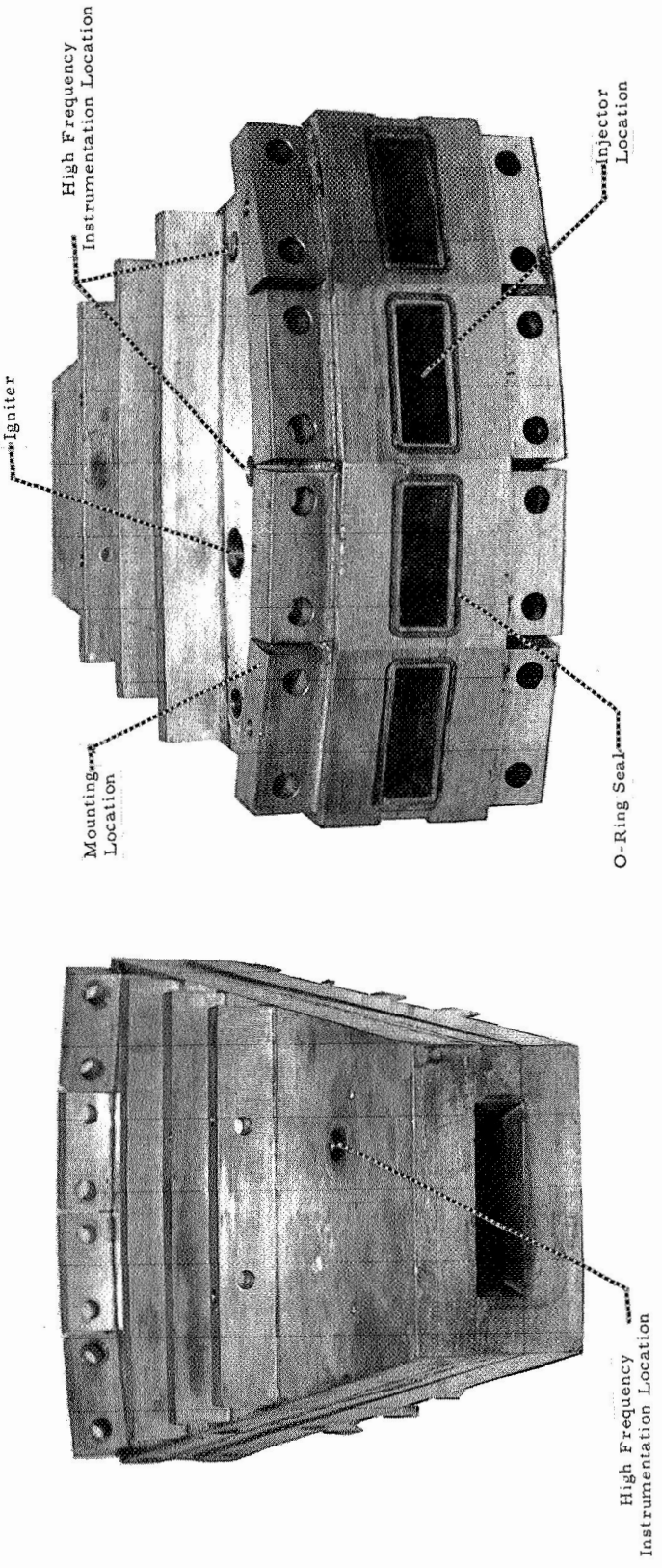

Four Injector Excitation Chambers

Figure 18

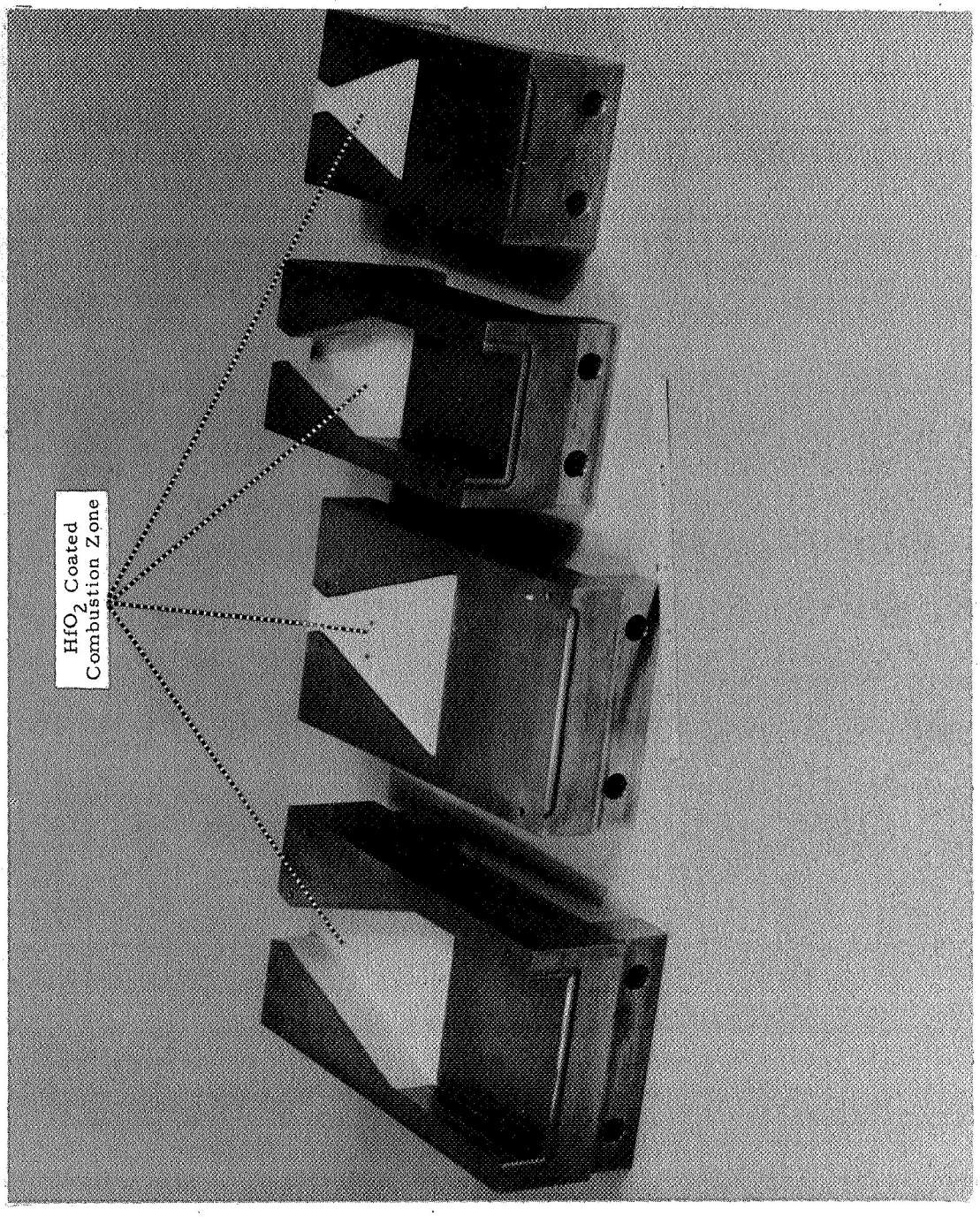

Single Injector Excitation Chambers with Hafnia (HfO_2) Thermal Coating

Figure 19

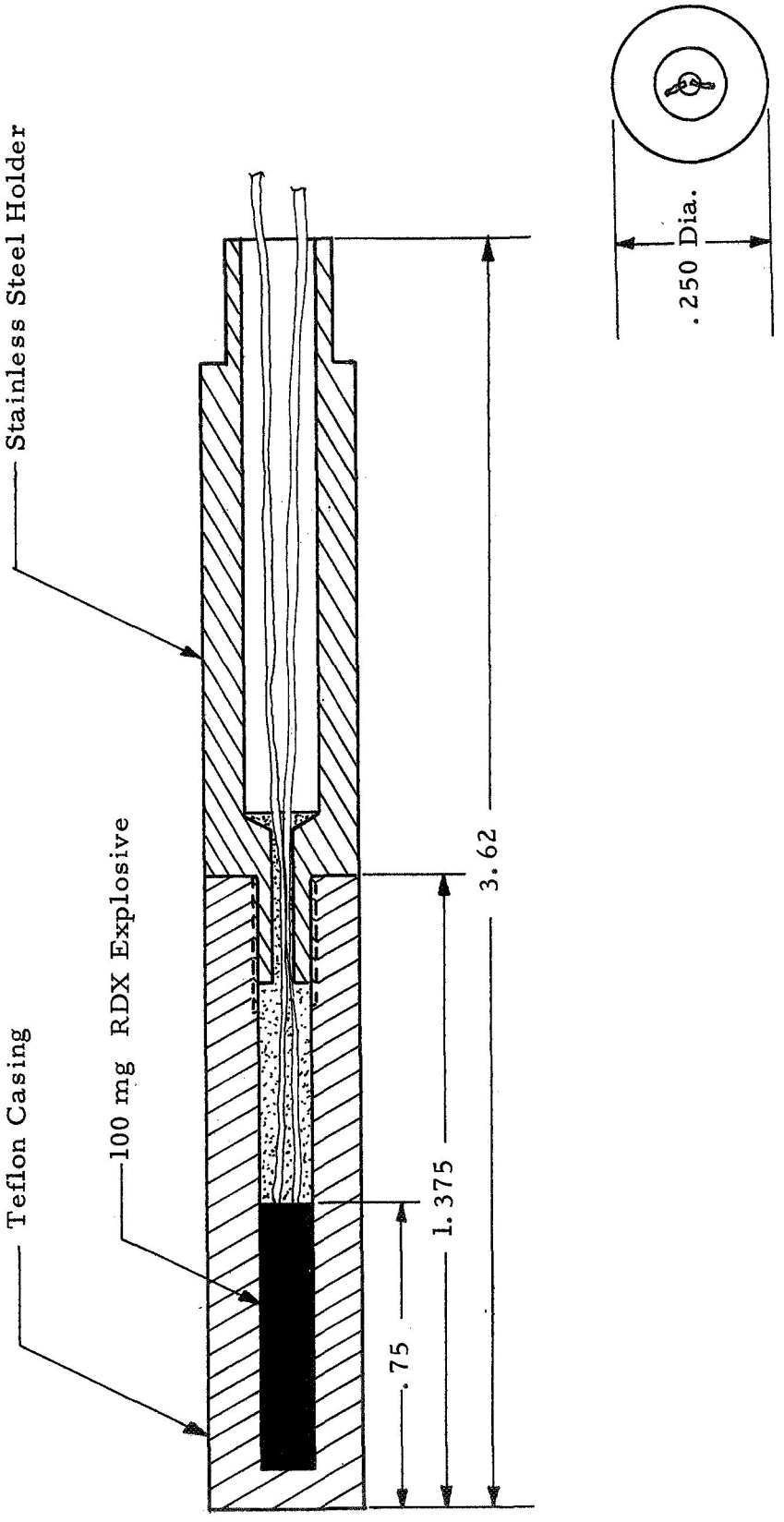

Nondirectional Bomb Used in Testing of HIPERTHIN Injectors

Figure 20

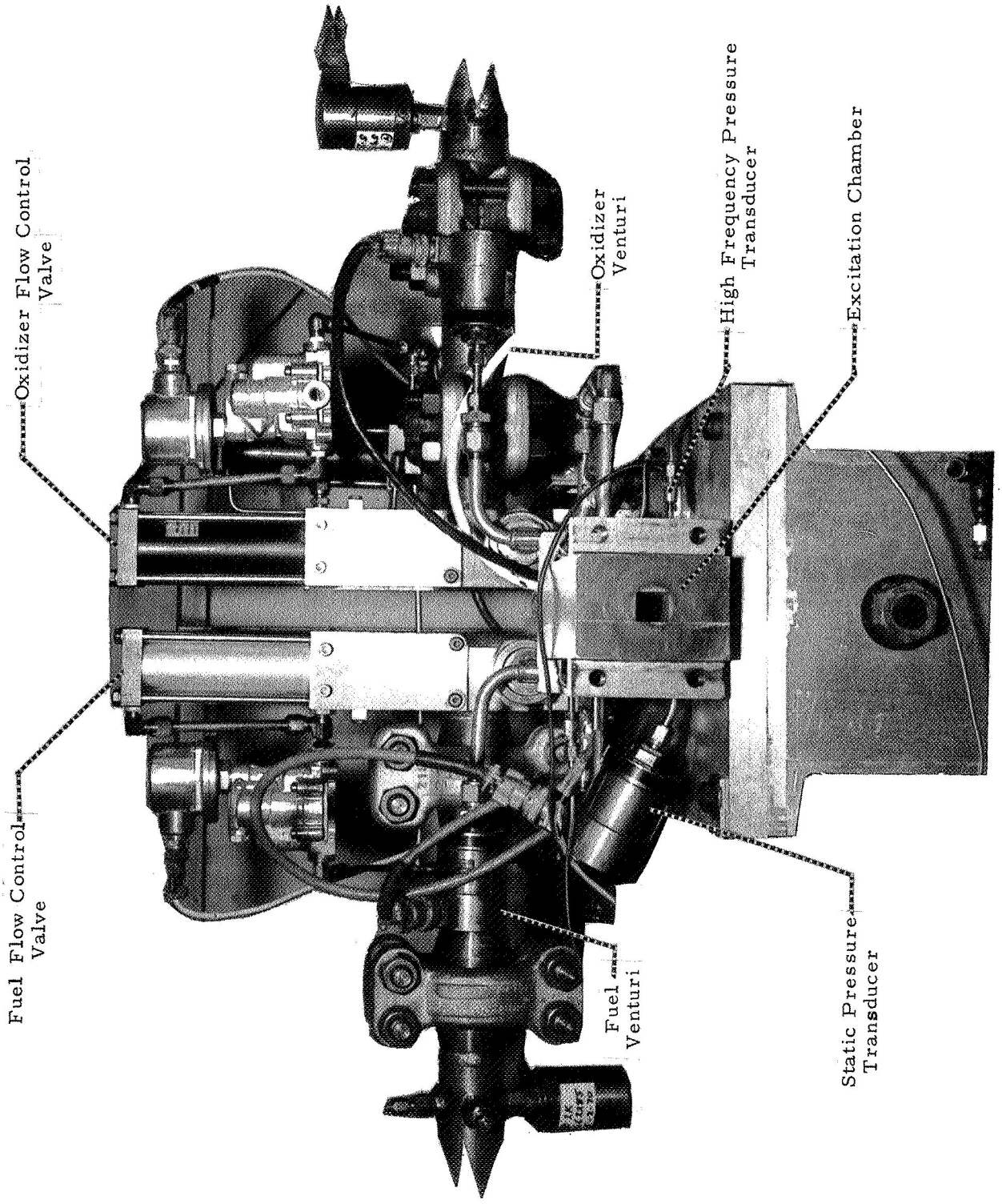

Excitation Chamber for HIPERTHIN Testing Installed on Test Stand A-7

Figure 21

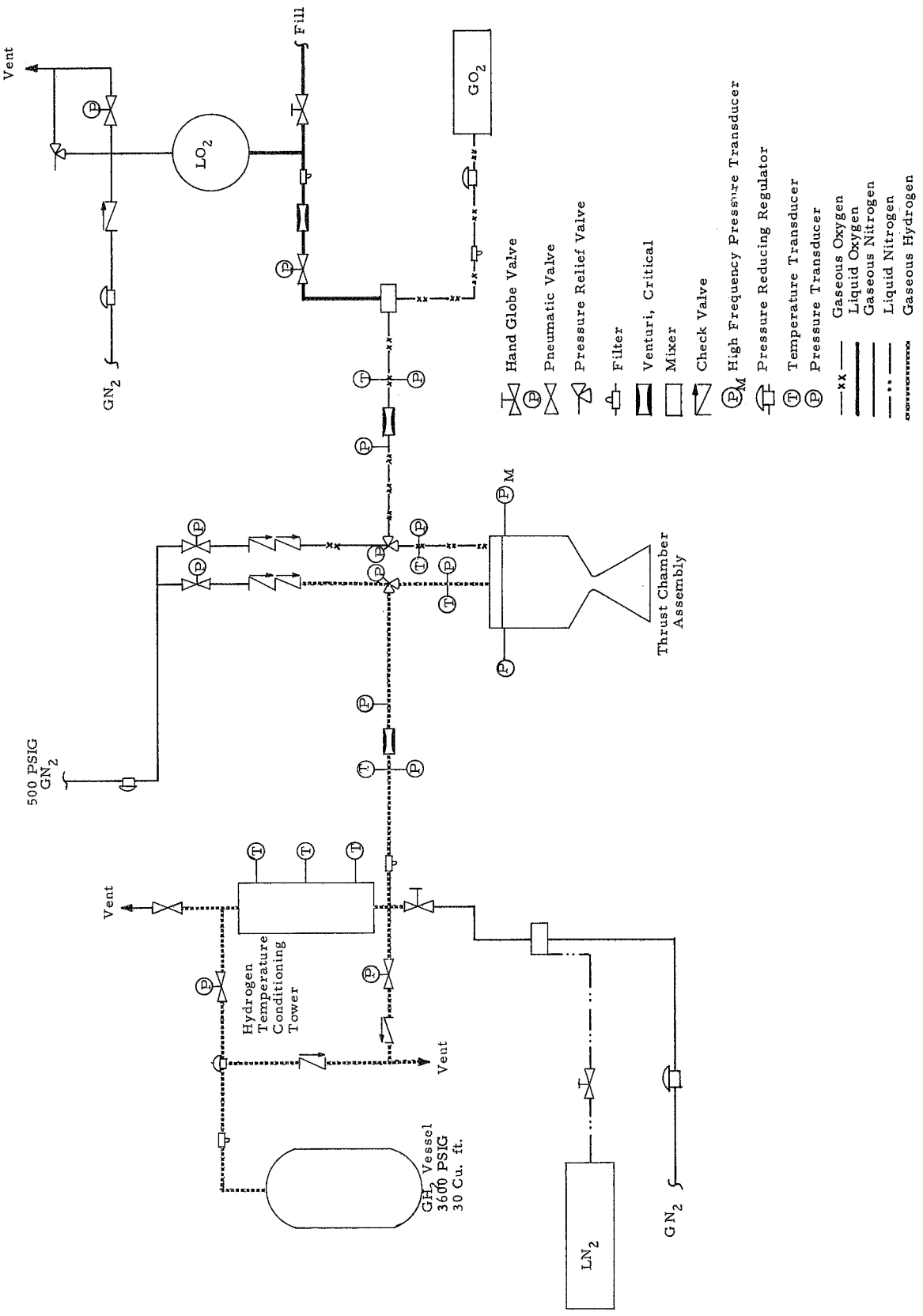

Bay 7 Schematic Flow Diagram

Figure 22

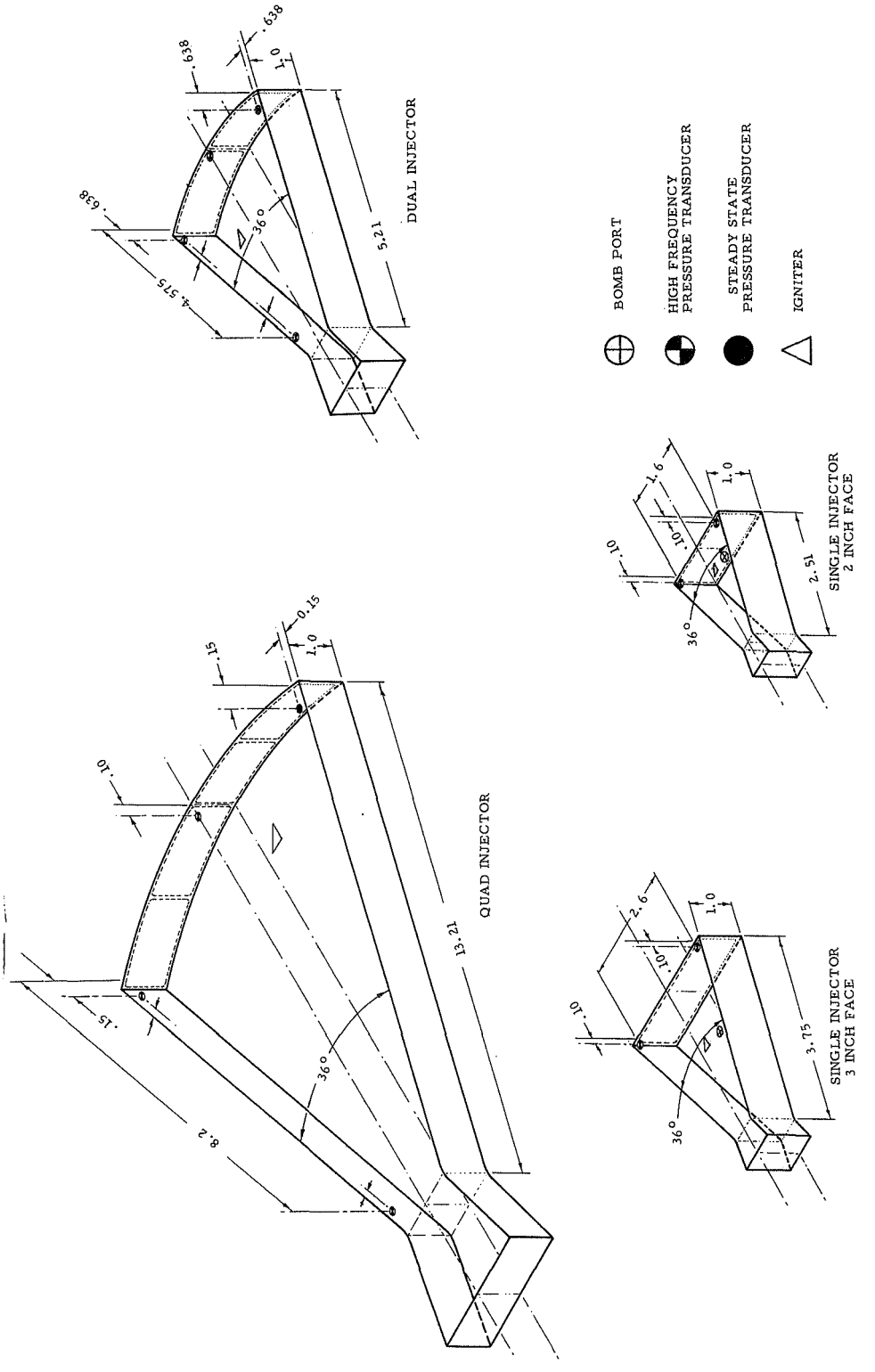

Transducer Location - HIPERTHIN Excitation Chambers

Figure 23

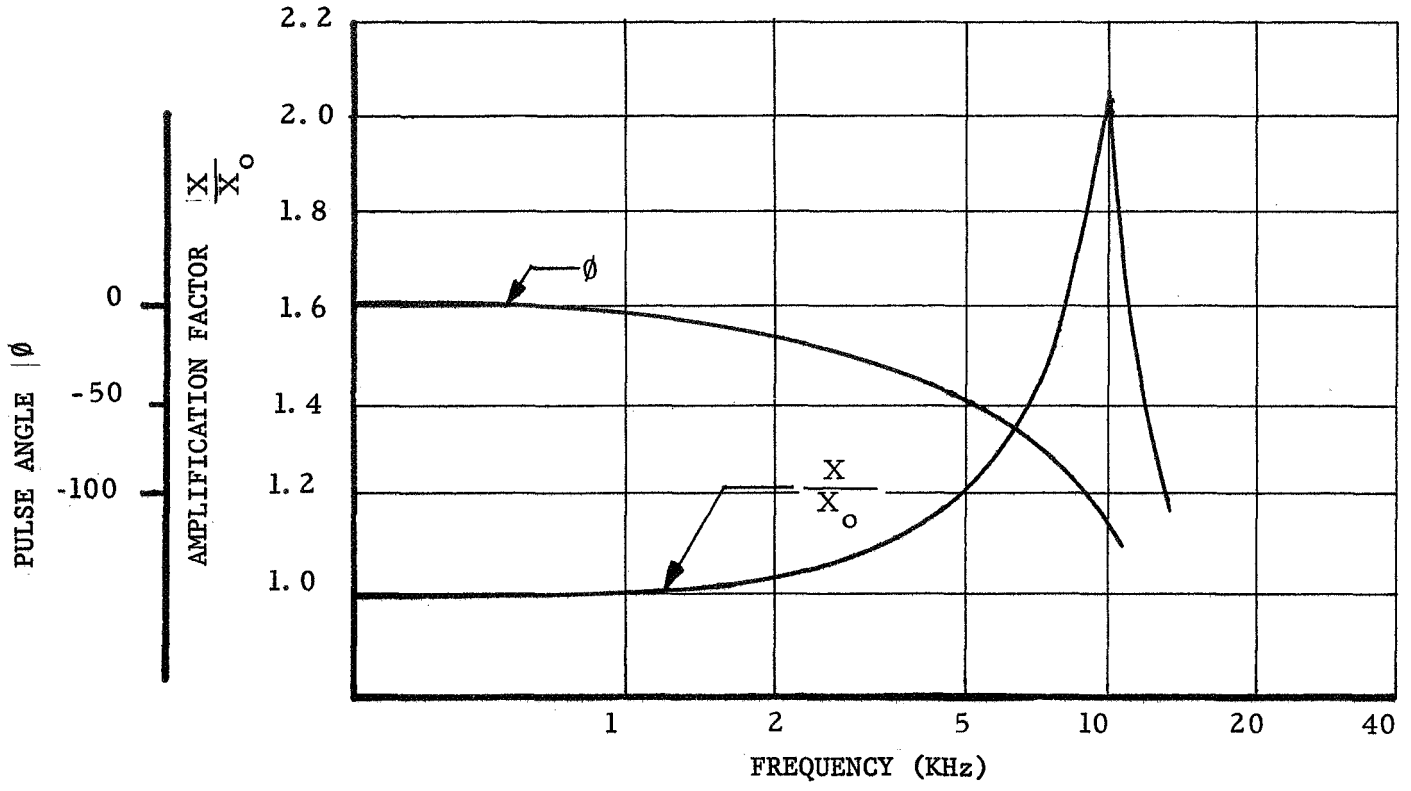

Figure 24b. Modified Kistler Model 615A Transducer

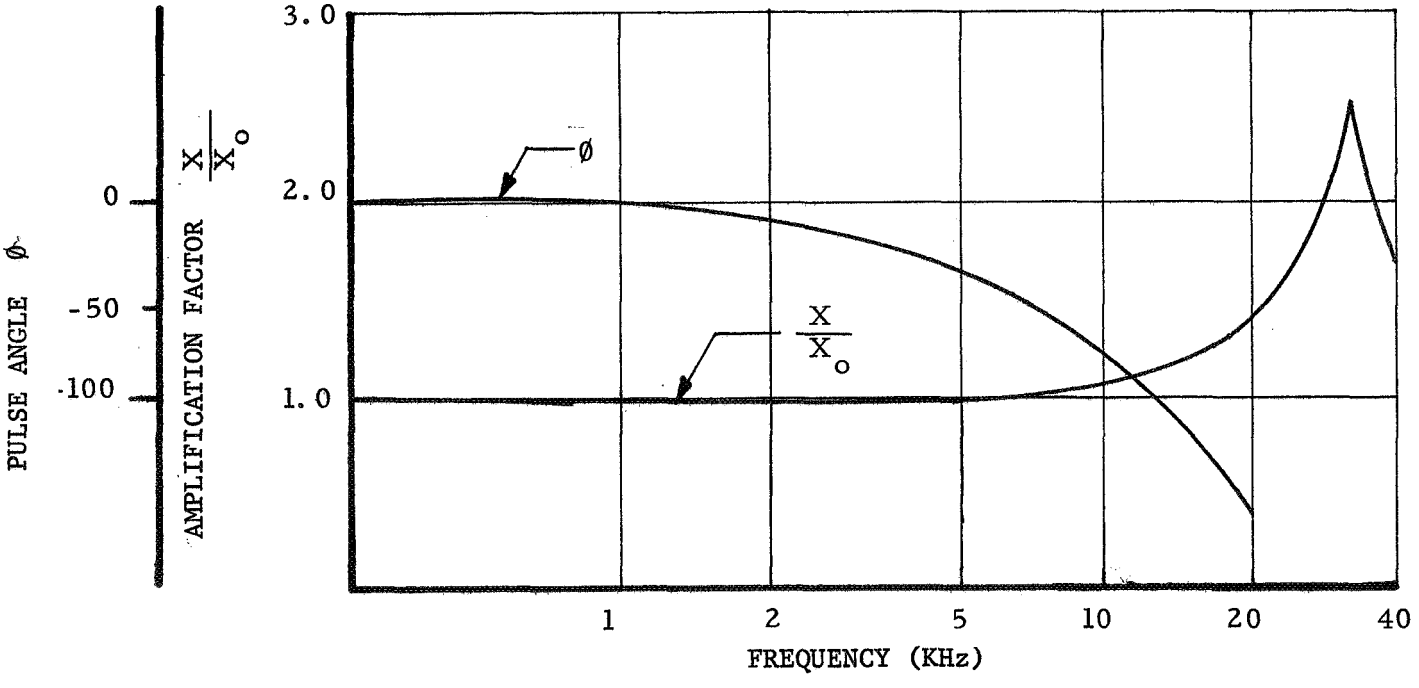

Figure 24a. Kistler Model 615A Transducer

Gain vs Frequency Characteristics - Kistler High Frequency Pressure Transducers

Figure 24

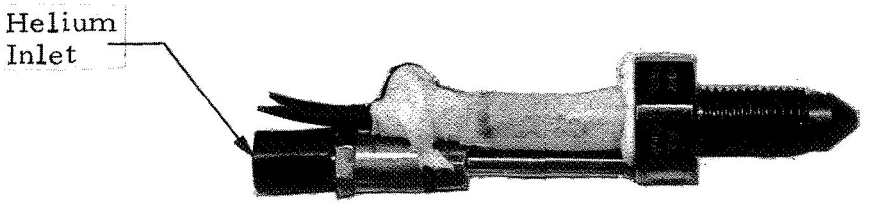

Kistler Model 615A Helium Bleed High Frequency Transducer

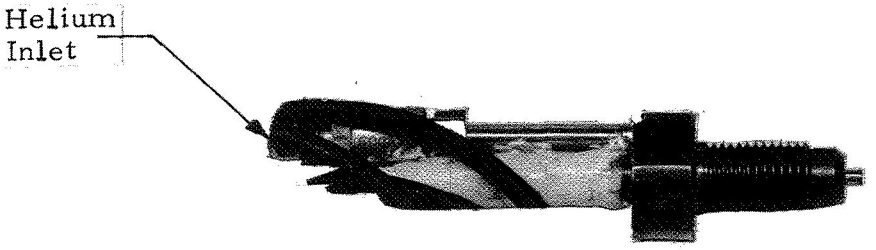

Kistler Model 615A Transducer Modified for Improved Frequency Response

Figure 25

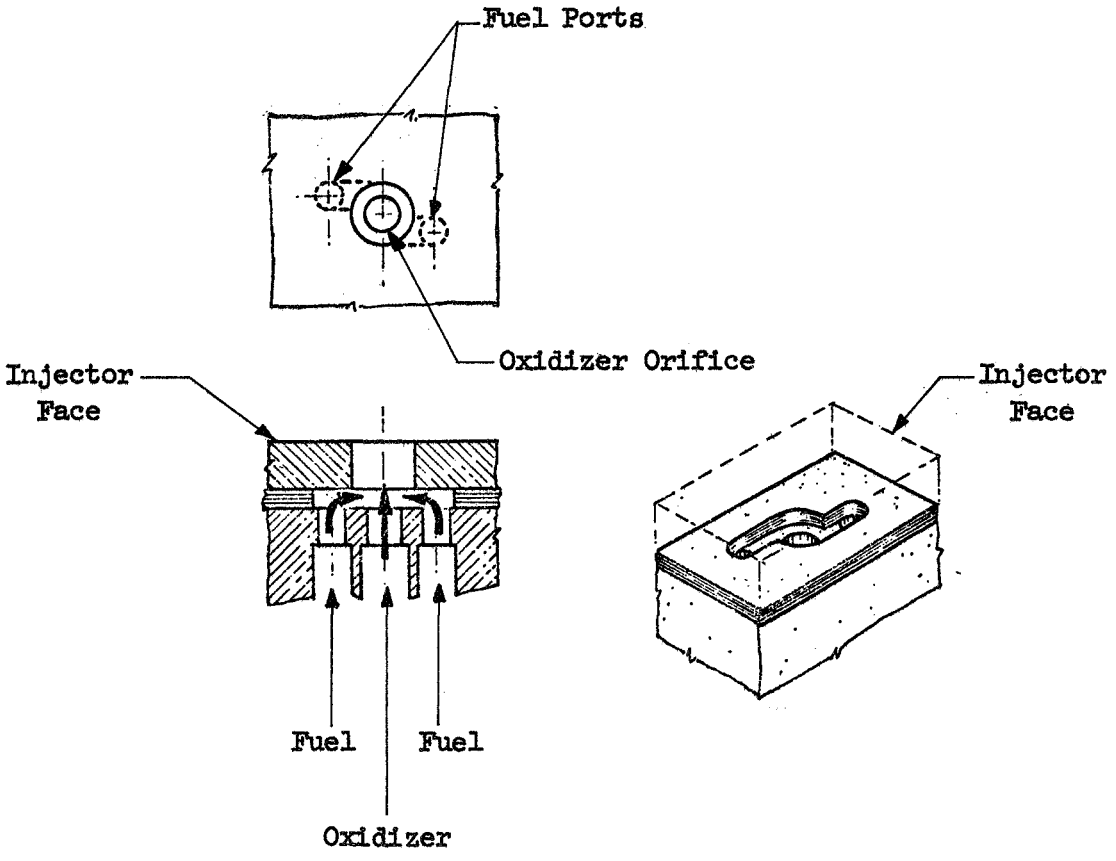

Schematic of Impinging Swirl Cup Coaxial Element

Figure 26

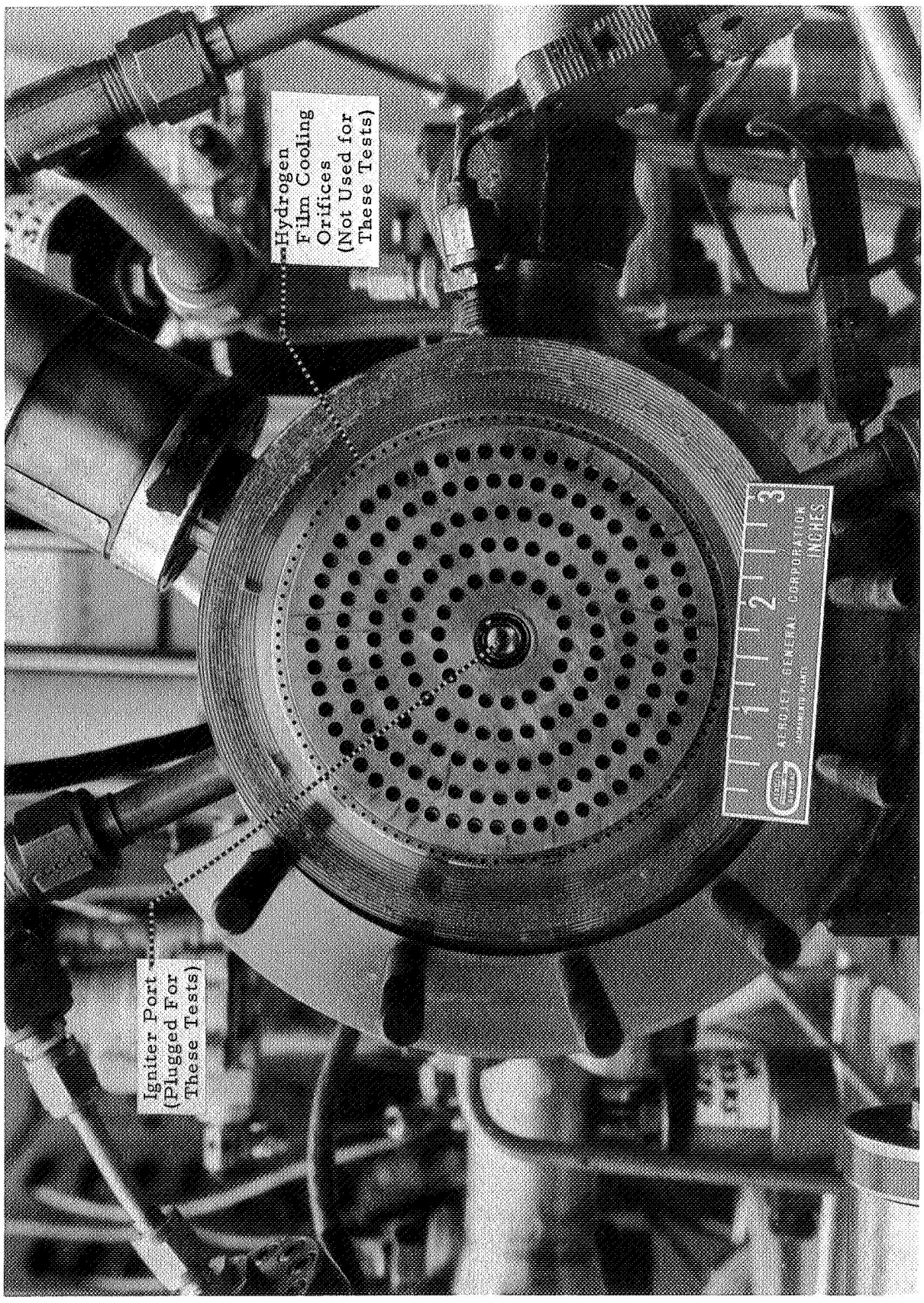

Impinging Swirl Cup Injector

Figure 27

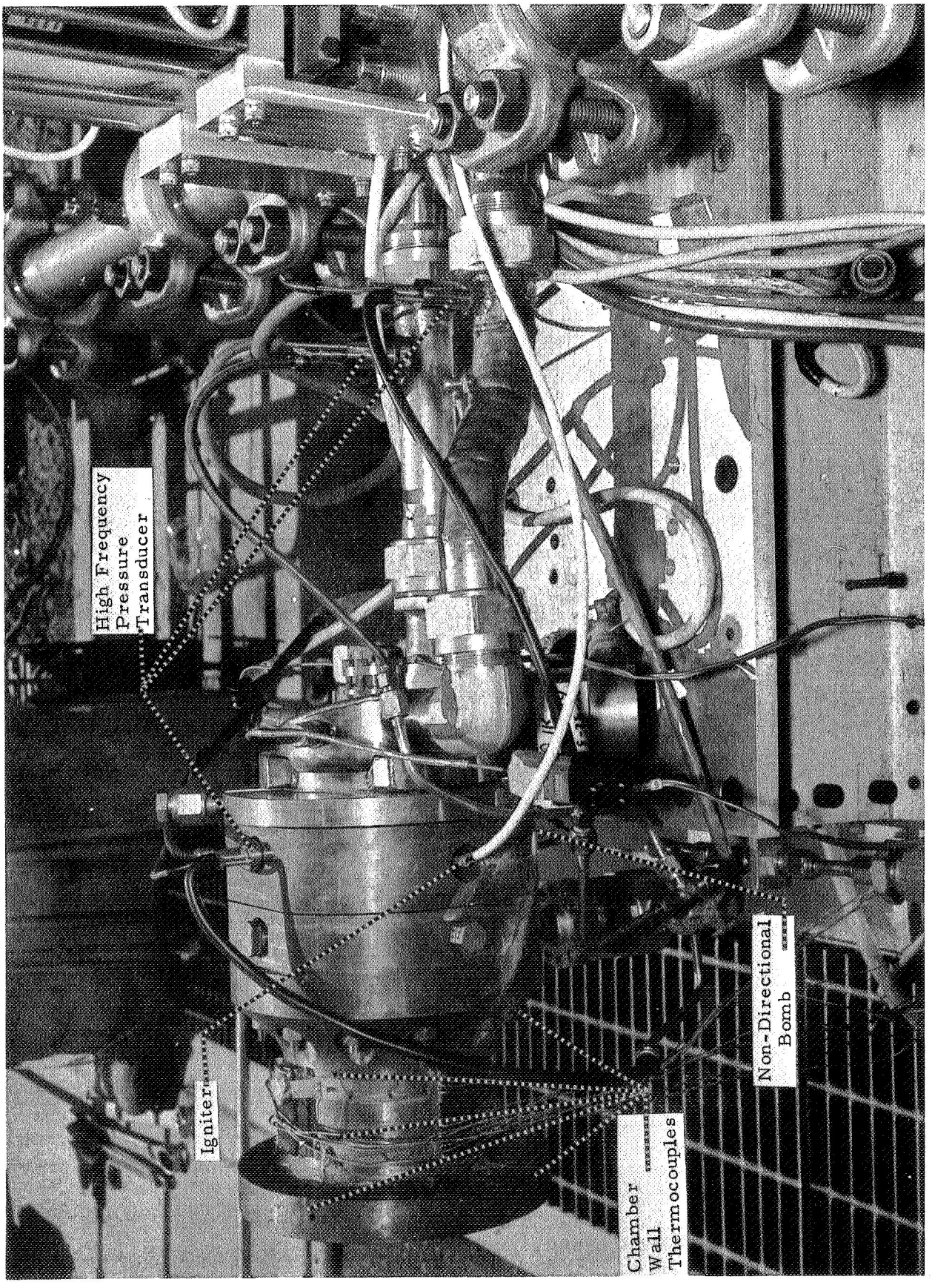

Figure 28

High Pressure Gas-Gas Hardware on Test Stand

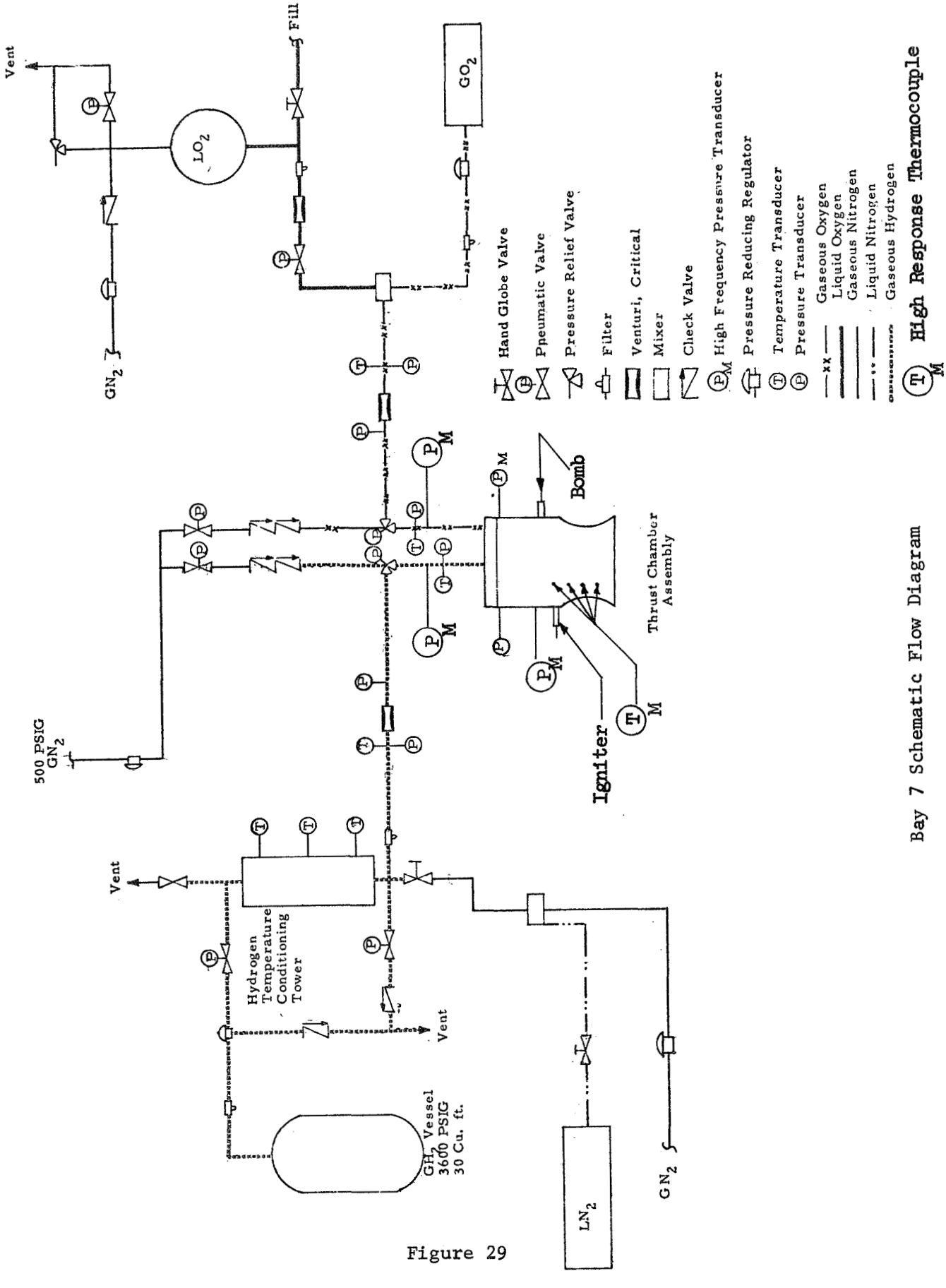

Bay 7 Schematic Flow Diagram

Figure 29

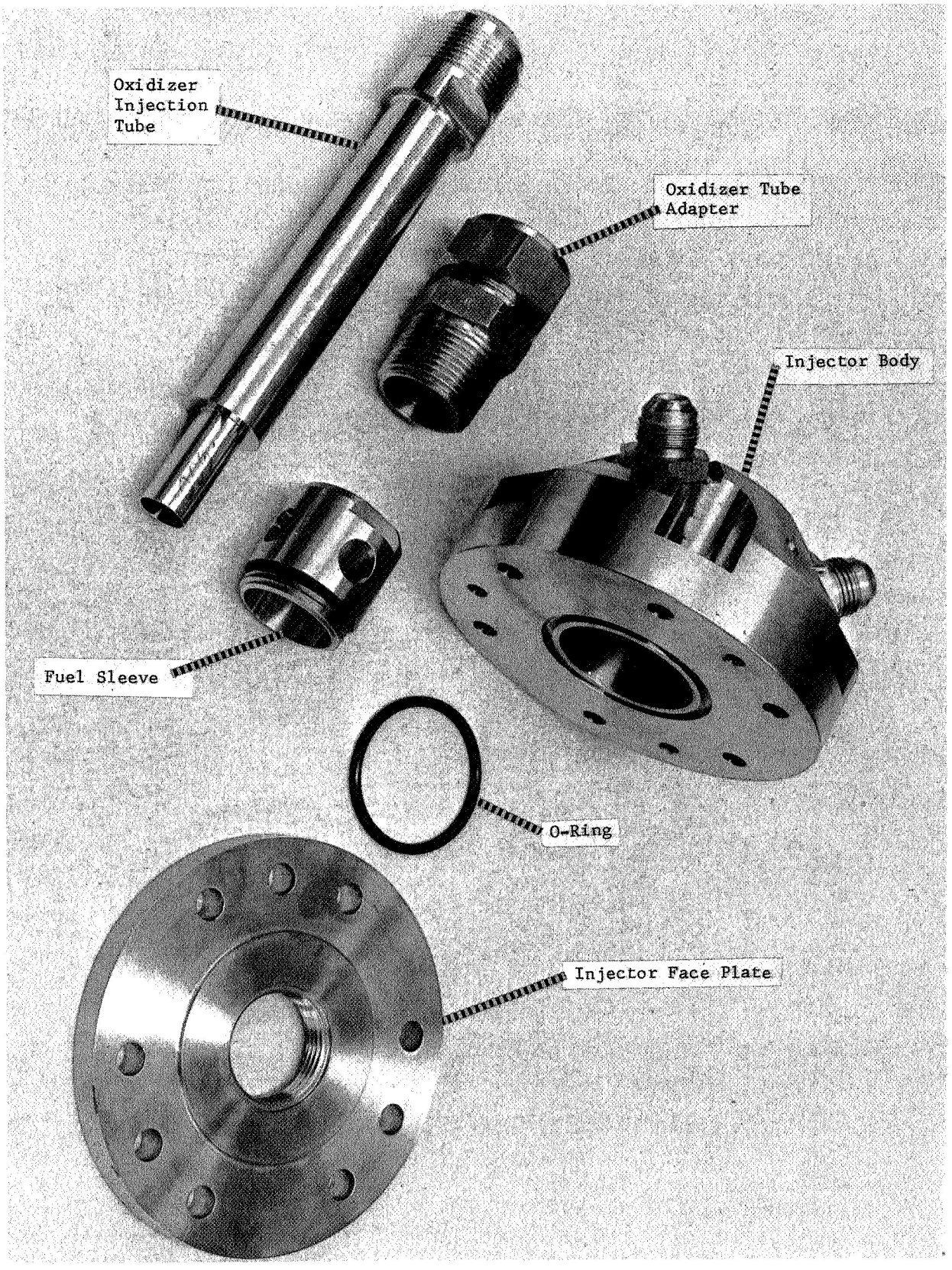

Low Pressure Gas-Gas Hardware

Figure 30

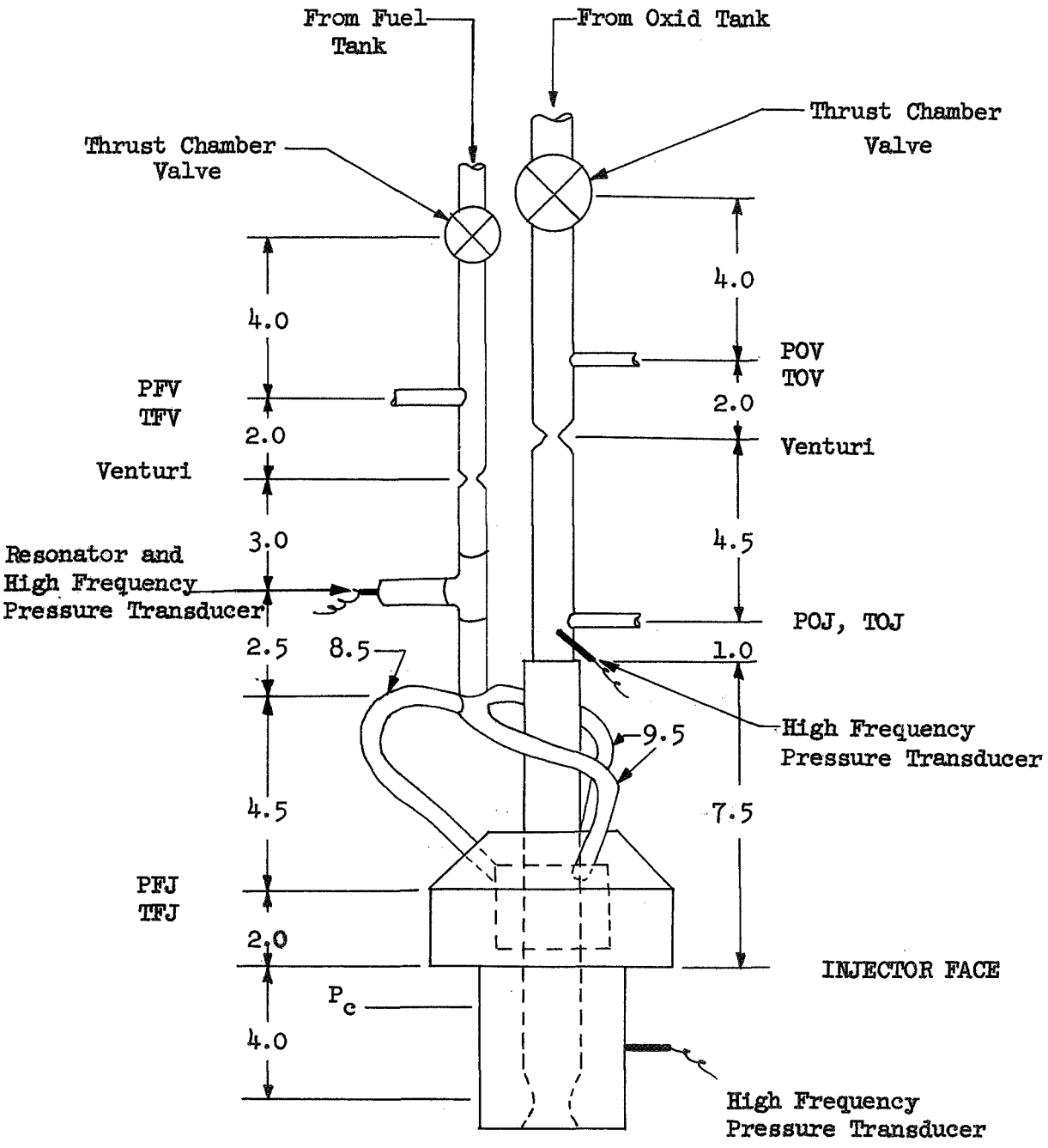

Low Pressure Gas-Gas Schematic

Figure 31

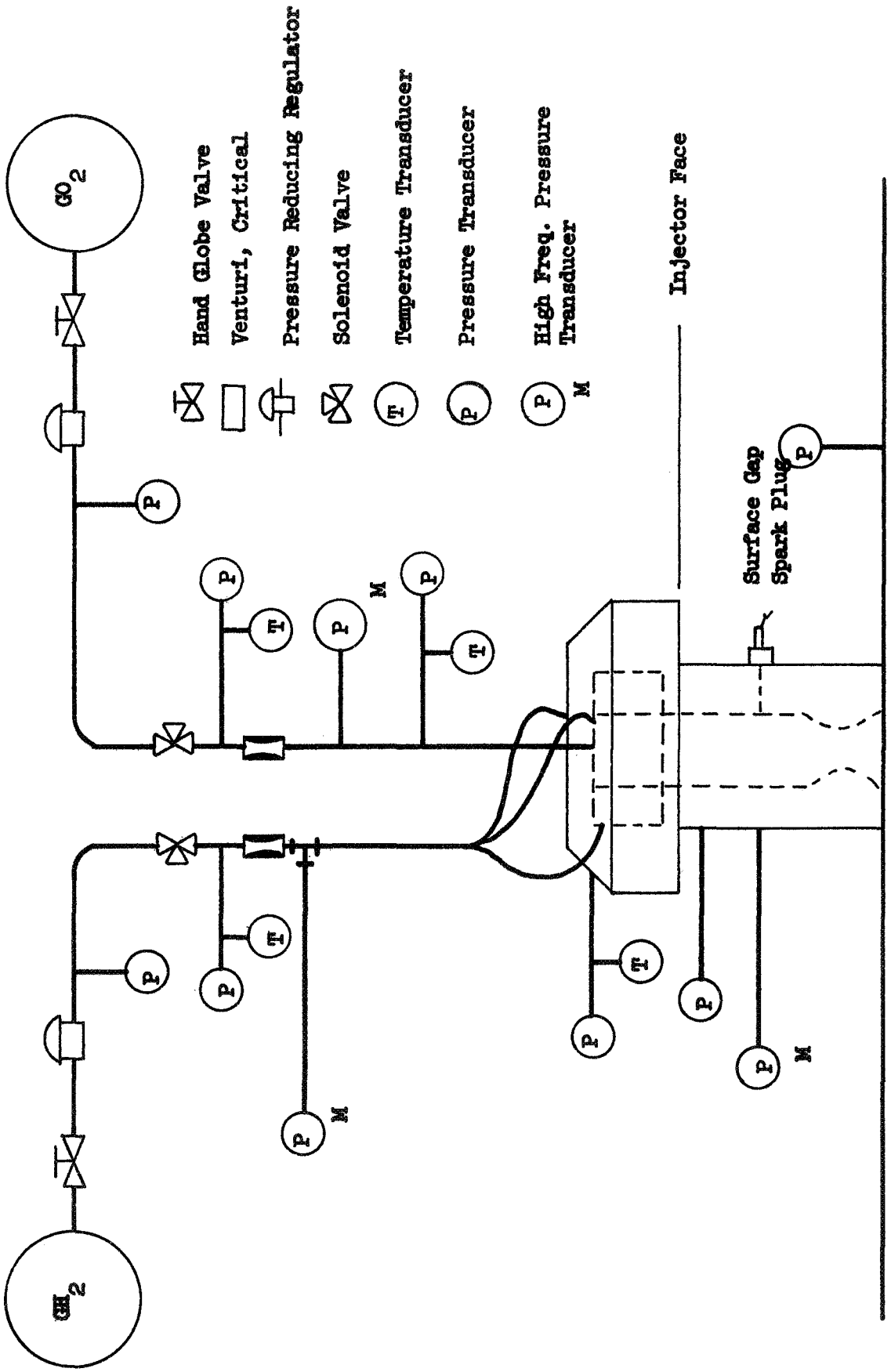

Bay 1 Flow Schematic

Figure 32

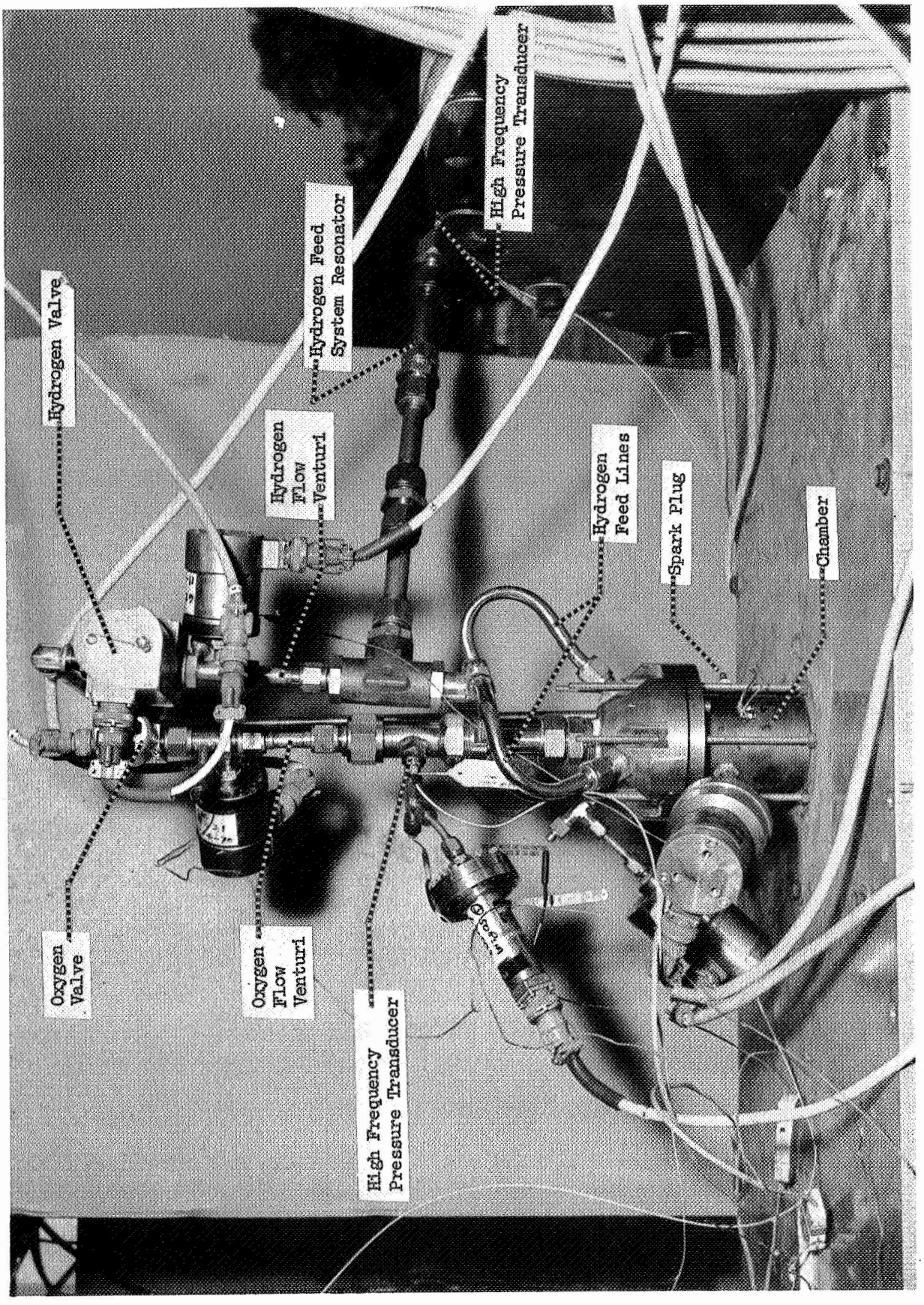

Low Pressure Gas-Gas Hardware on Test Stand

Figure 33

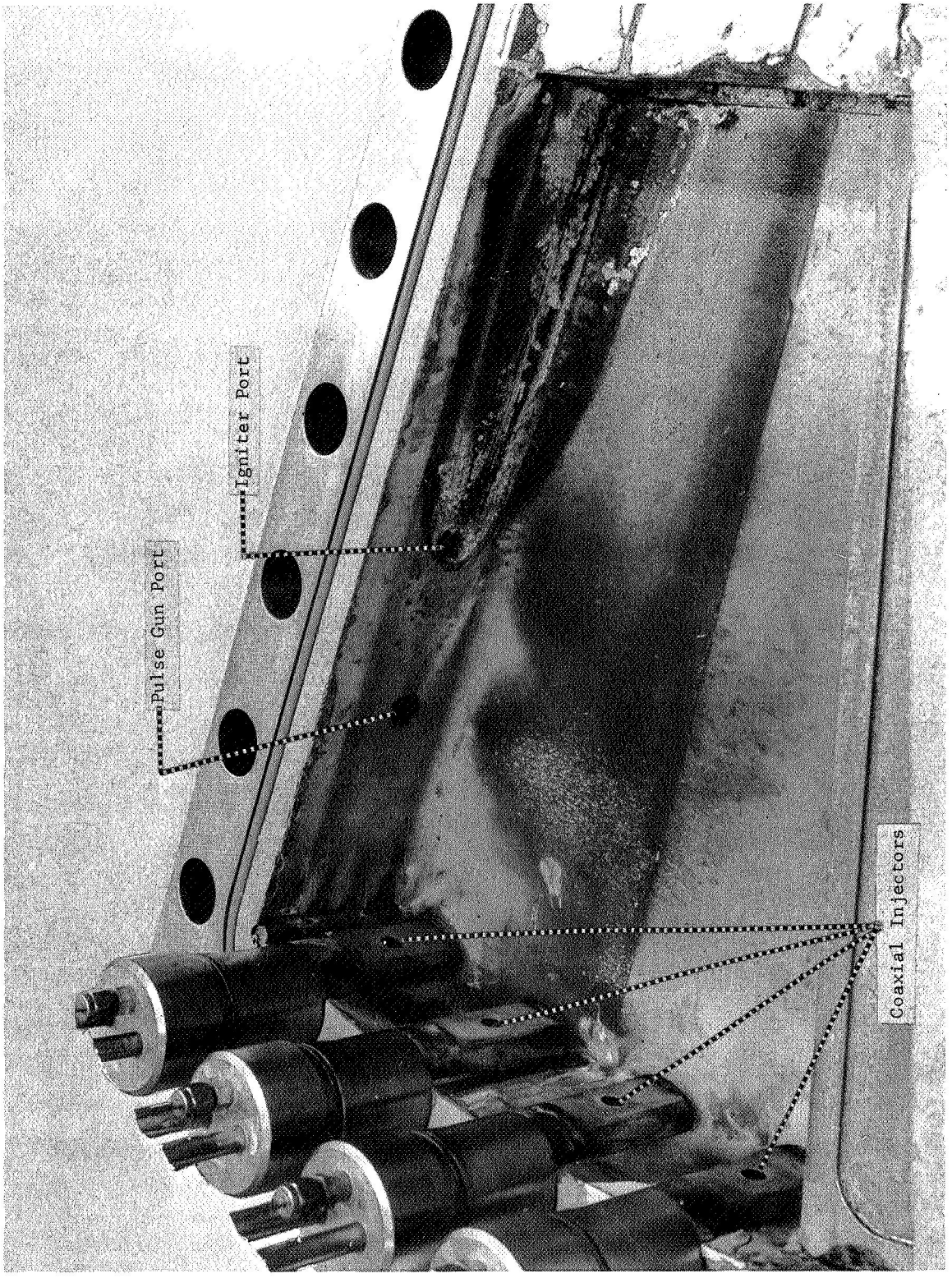

Transverse Excitation Chamber After Testing Coaxial Injectors

Figure 34

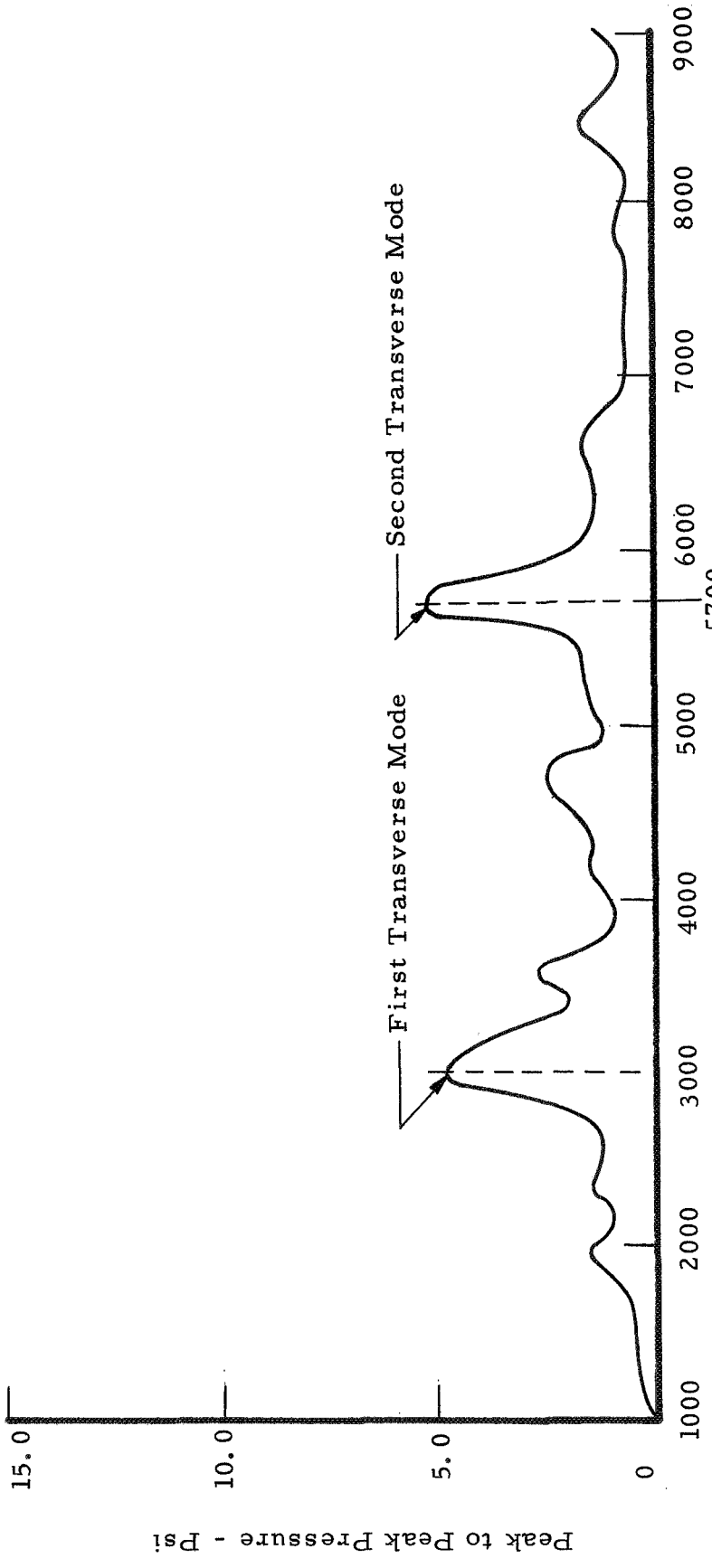

Spectral Plot at Peak-to-Peak Pressure Amplitudes vs Frequency - Test 23

Figure 35

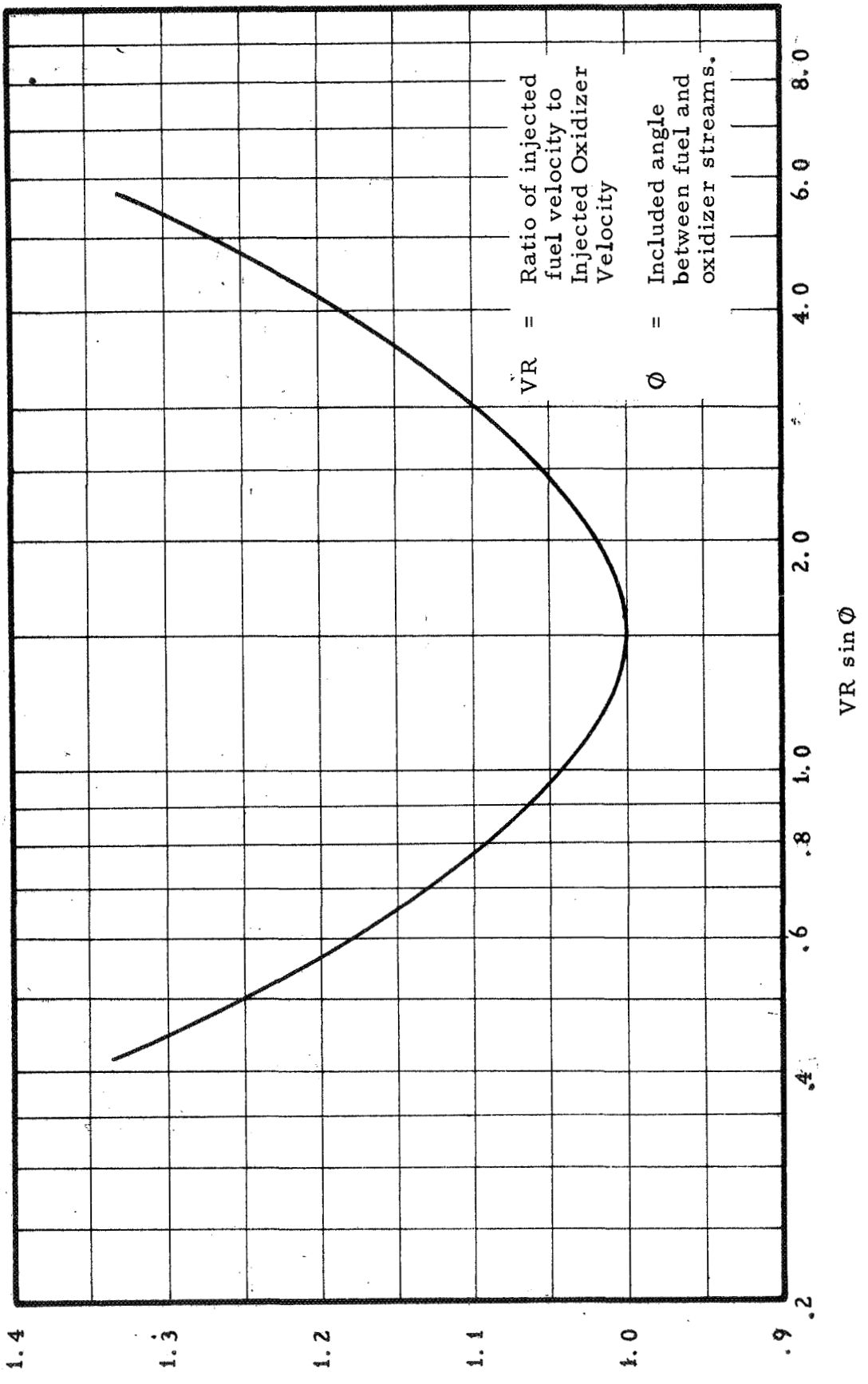

Function of VR sin Ø for Impinging Coaxial Elements

Figure 36

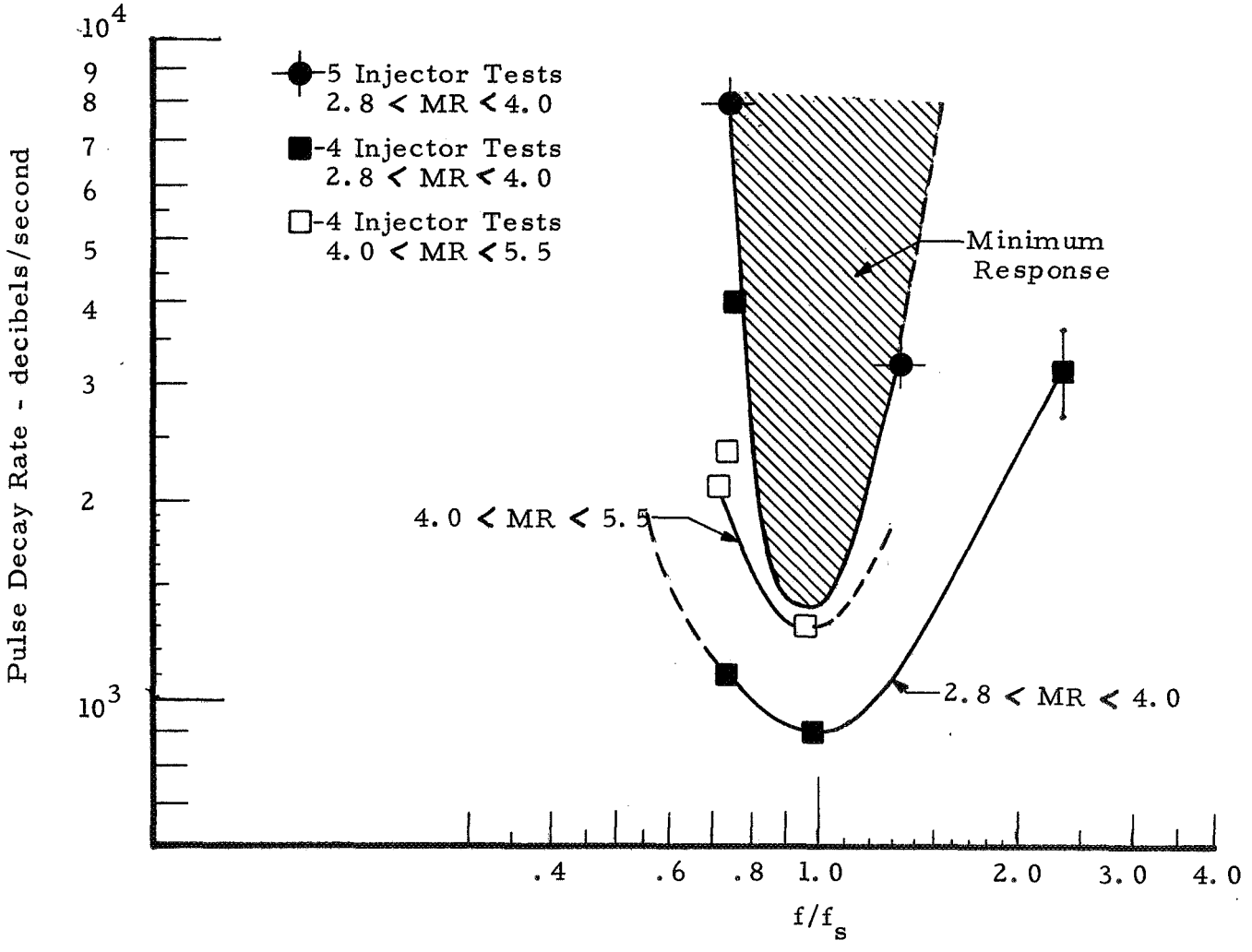

Coaxial Injector Correlations Using 4 and 5 Injector Tests Only

Figure 37

All data are within mixture ratio range of 2.5 to 7.0

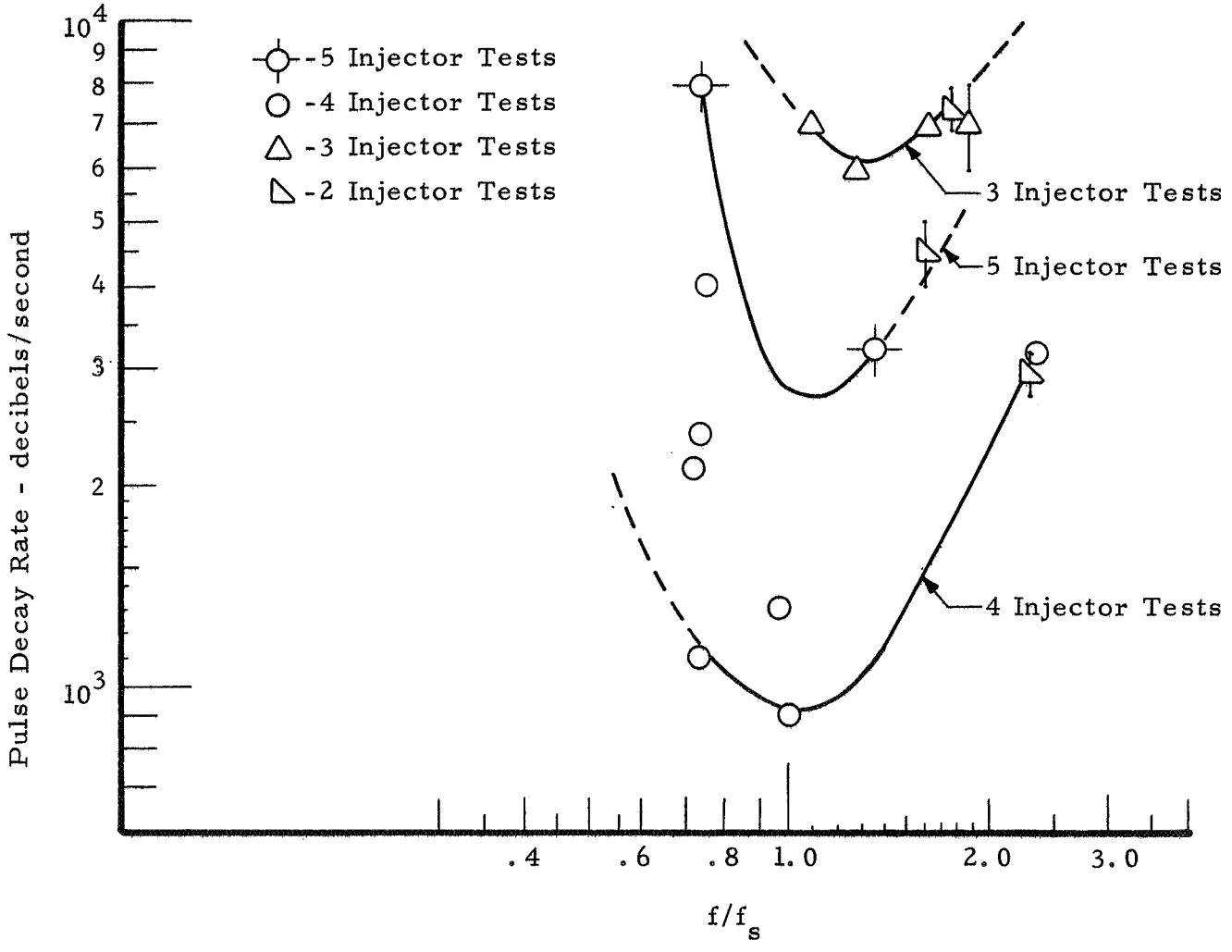

Coaxial Injector Correlations - All Tests

Figure 38

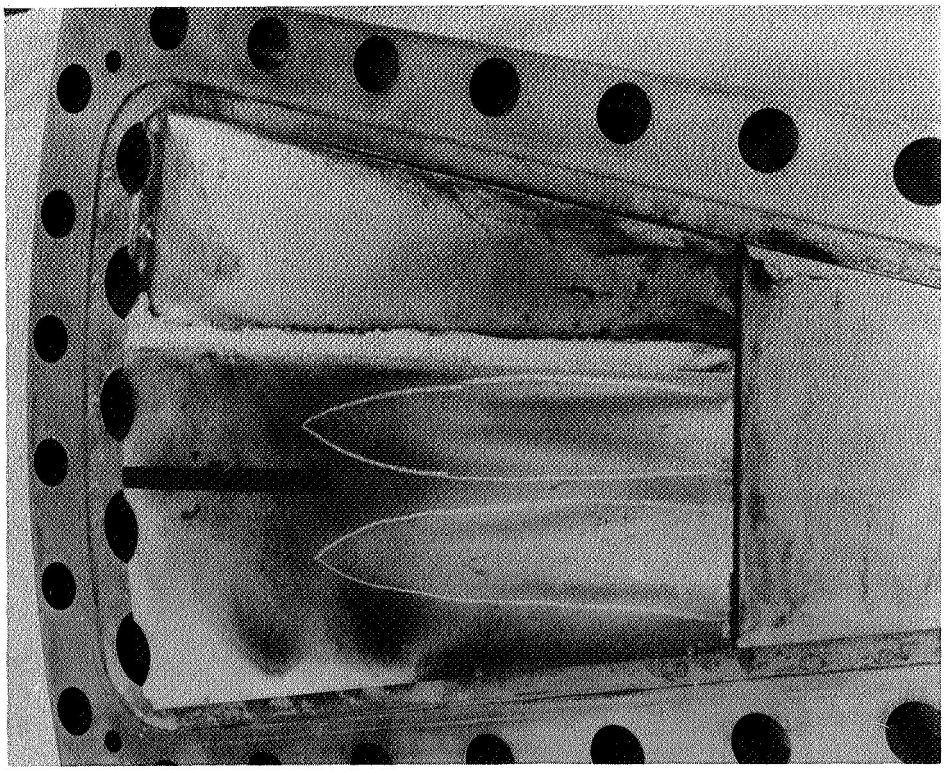

SN01

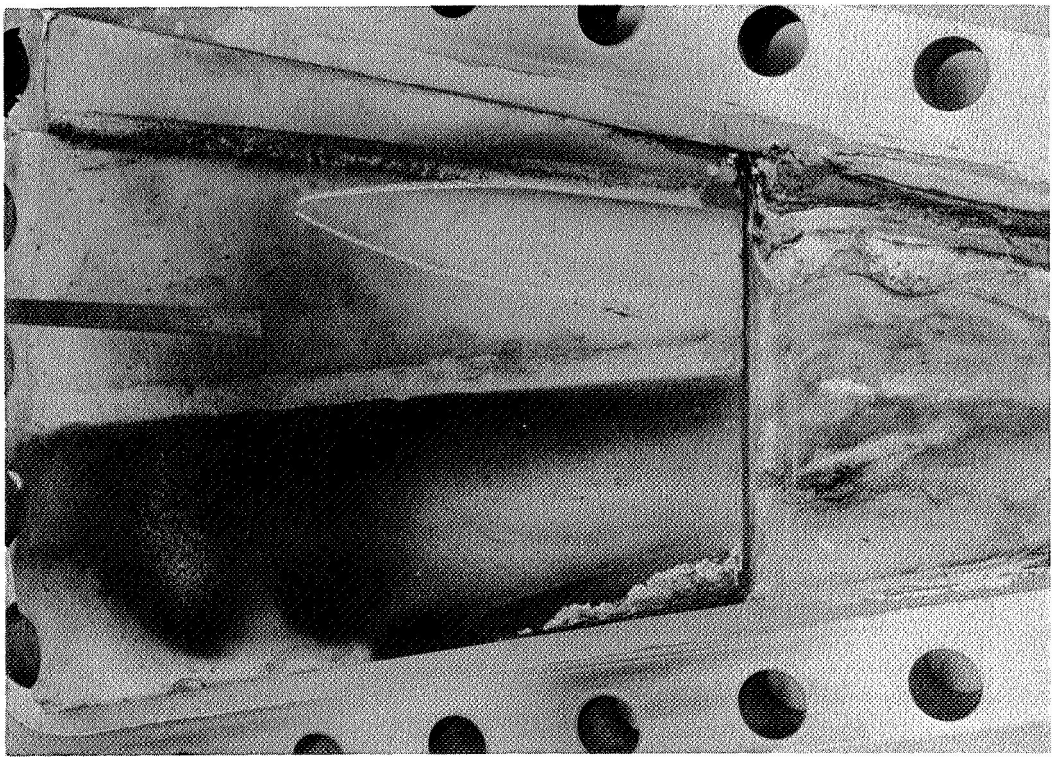

SN02

Transverse Excitation Chamber lids After 24 Coaxial Injector Tests

Figure 39

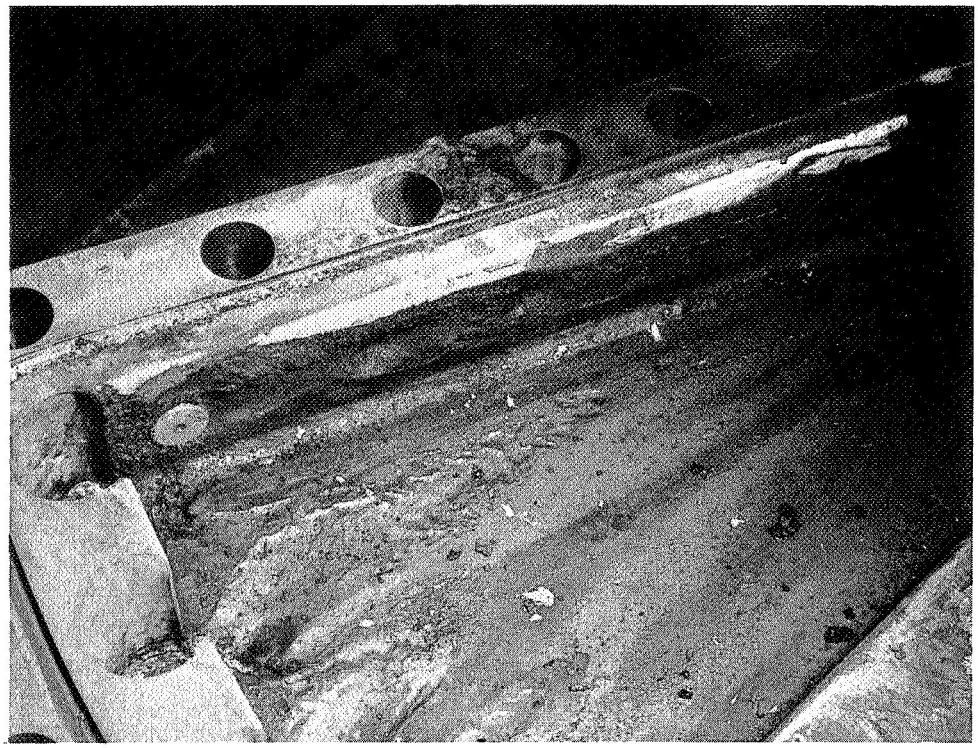

Postfire 1100-D03-0M-006

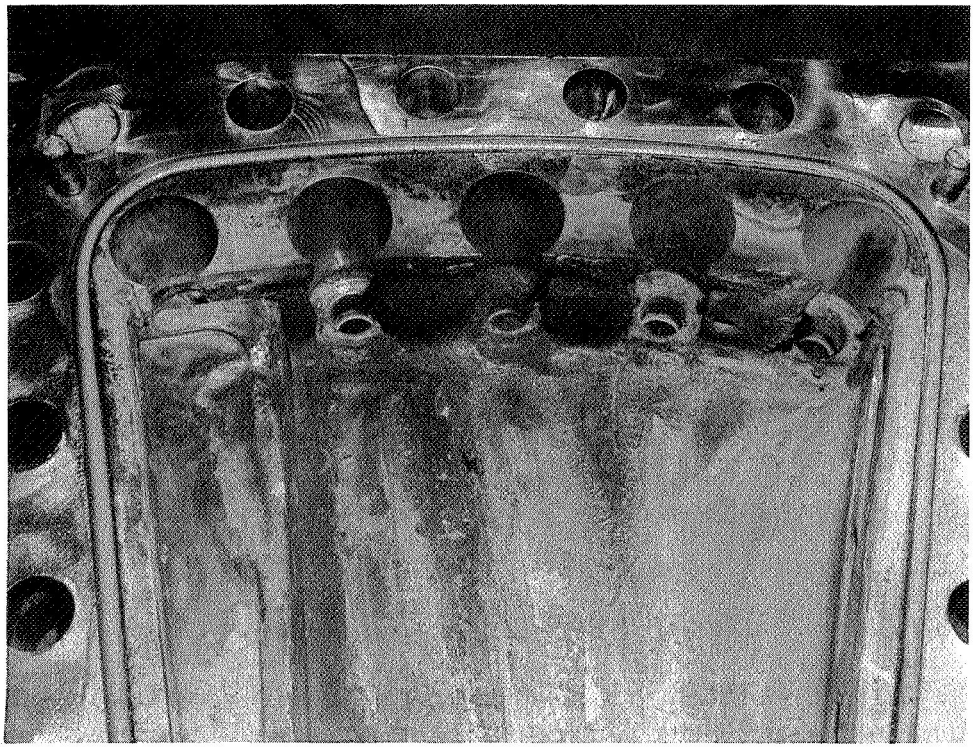

Postfire 1100-D03-0M-014

Transverse Excitation Chamber After Triplet Injector Tests

Figure 40

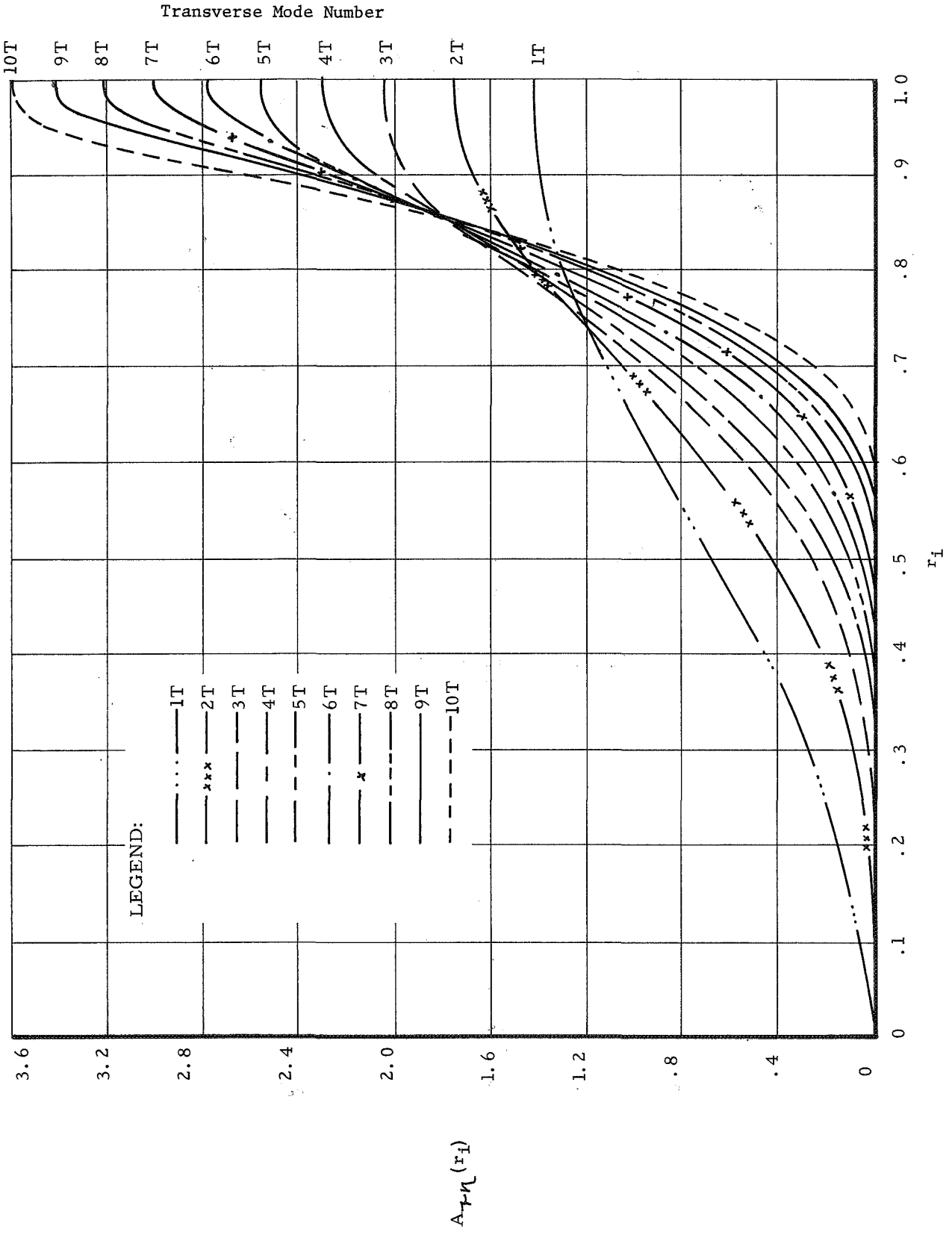

A_{vn} as a Function of Chamber Radius

Figure 41

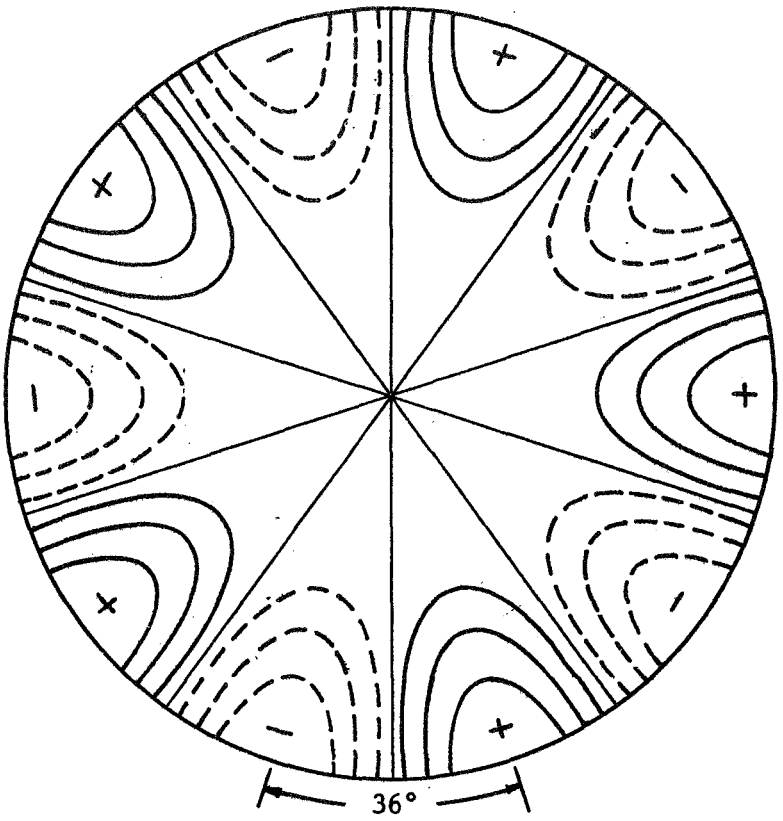

Fifth Tangential Mode in
a Cylindrical Chamber

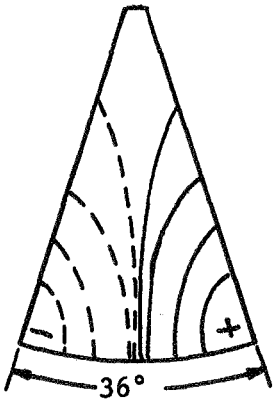

Fundamental Mode of an Excitation Chamber
with a Chamber Angle of 36°

Pressure Characteristics of Transverse Modes in Cylindrical
and Transverse Excitation Chambers

Figure 42

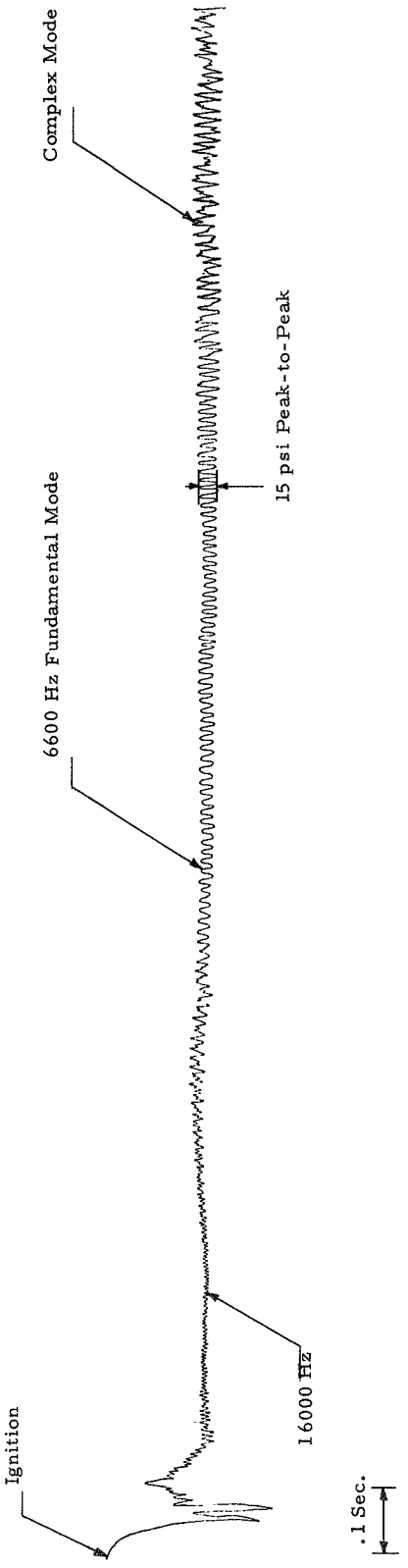

Unfiltered High Frequency Record from Test 3

Figure 43

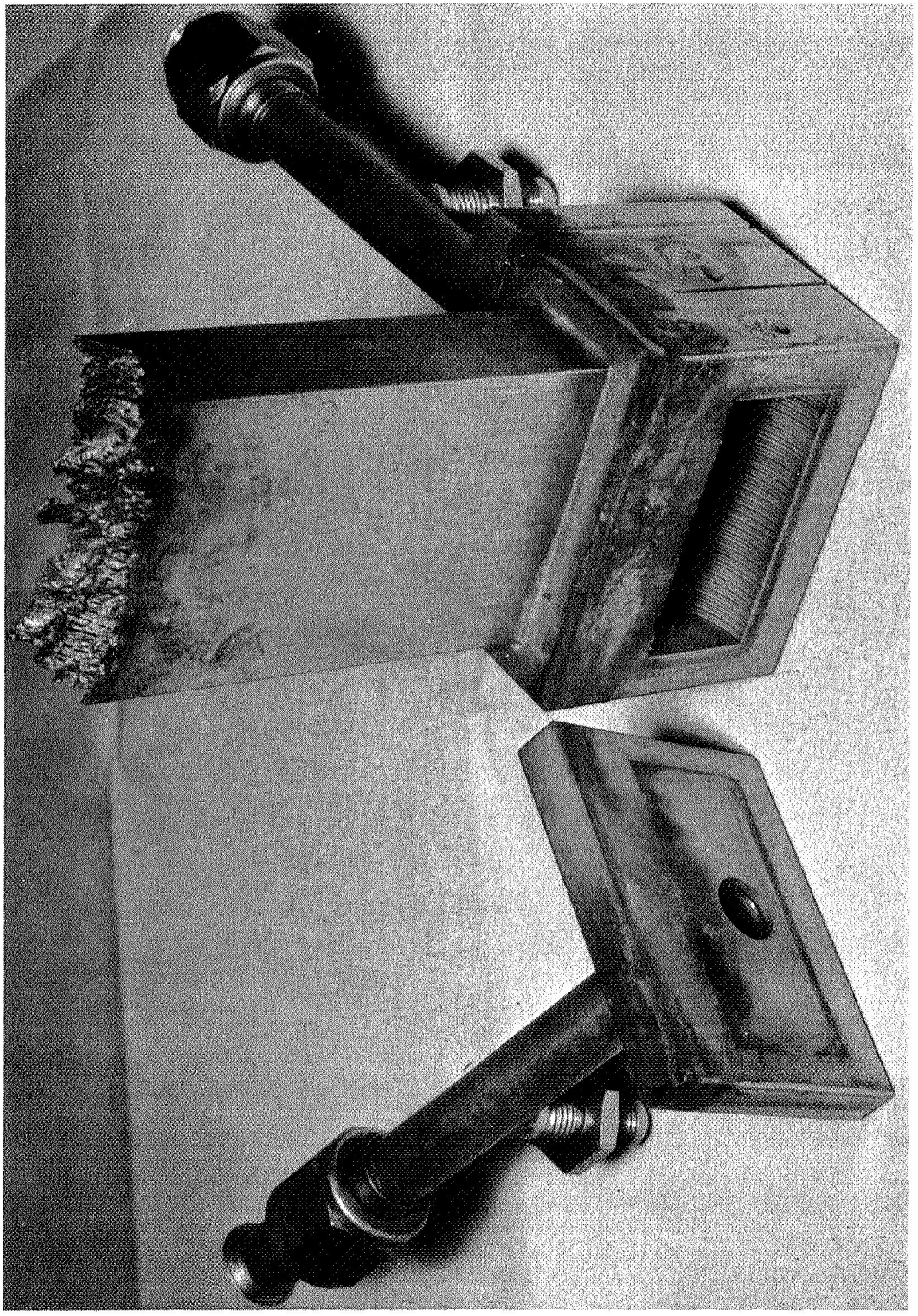

Posttest Condition of HIPERTHIN Injector with Faulty Manifold Braze Joint

Figure 44

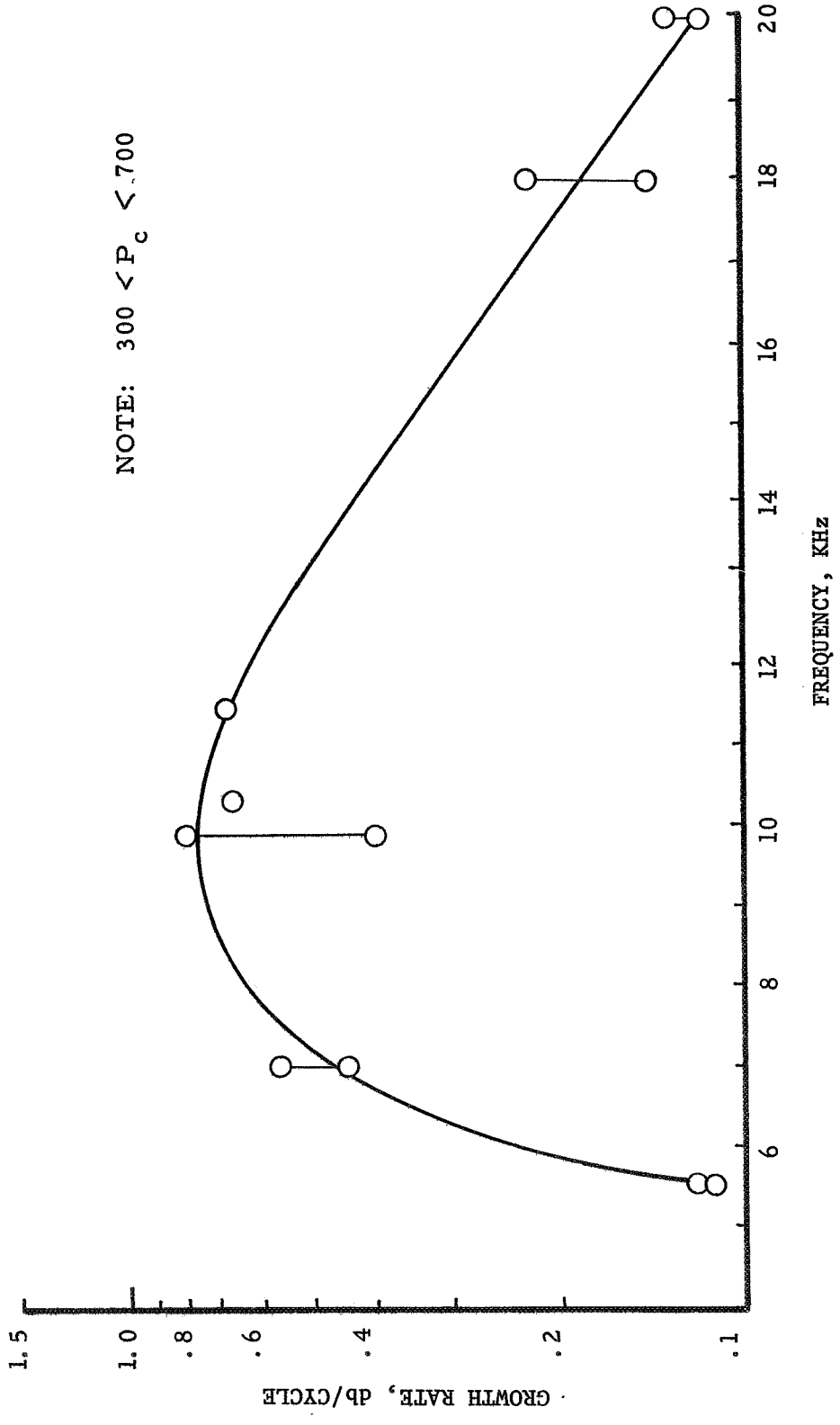

Growth Rate vs Frequency for Selected Data at High Chamber Pressure

Figure 45

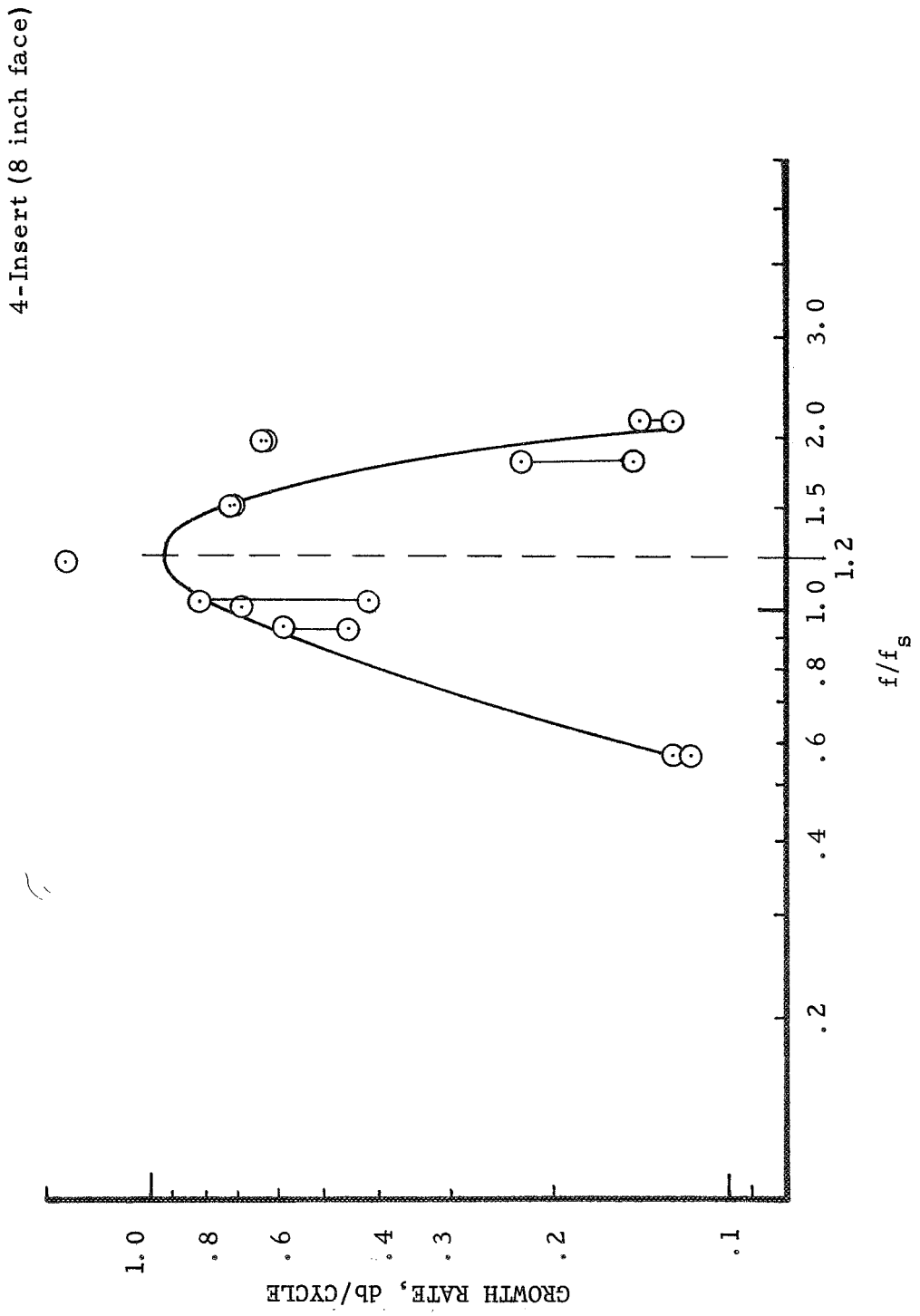

Growth Rate vs Frequency Ratio (Four Insert Injectors)

Figure 46

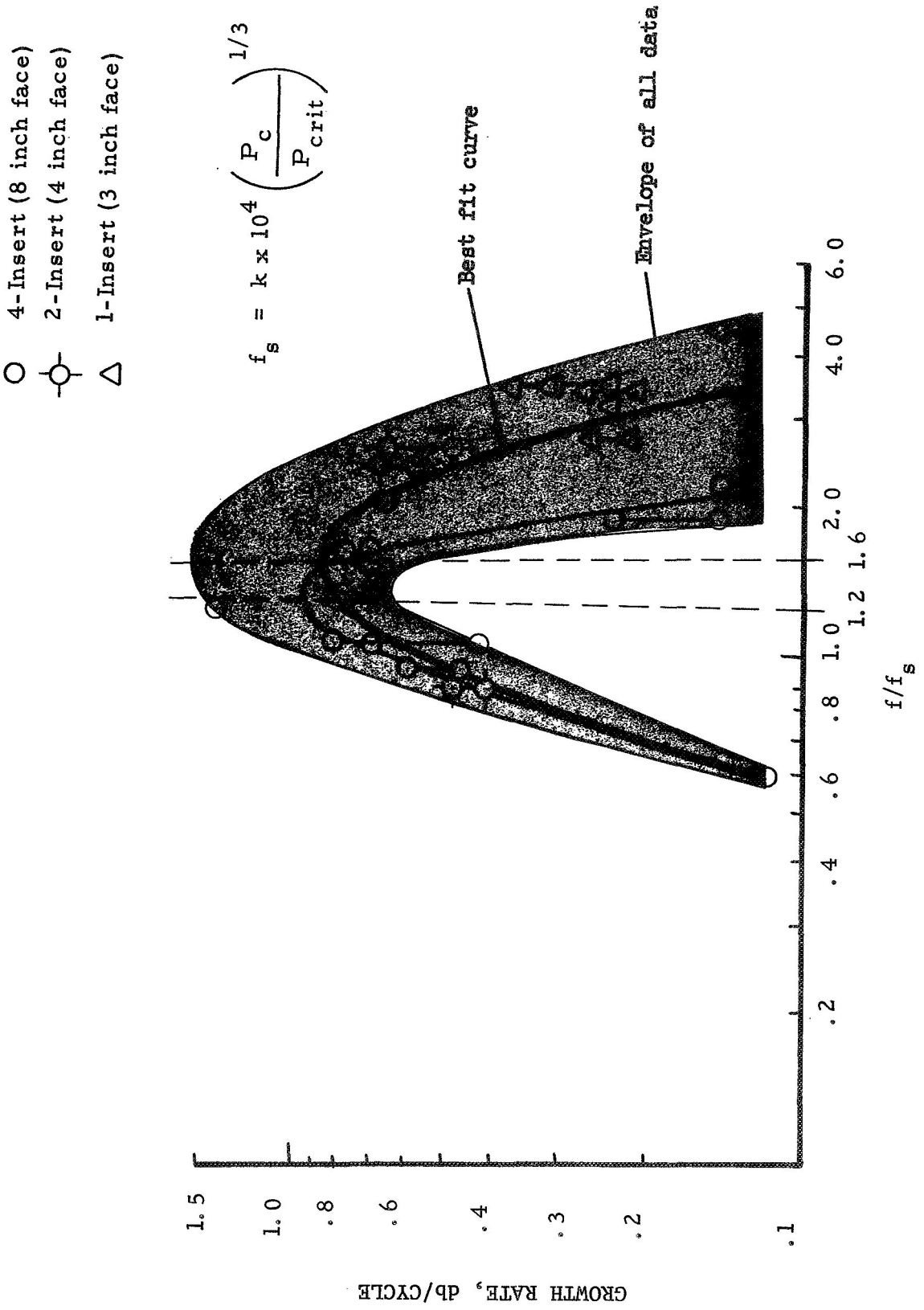

Growth Rate vs Frequency Ratio (All Data)

Figure 47

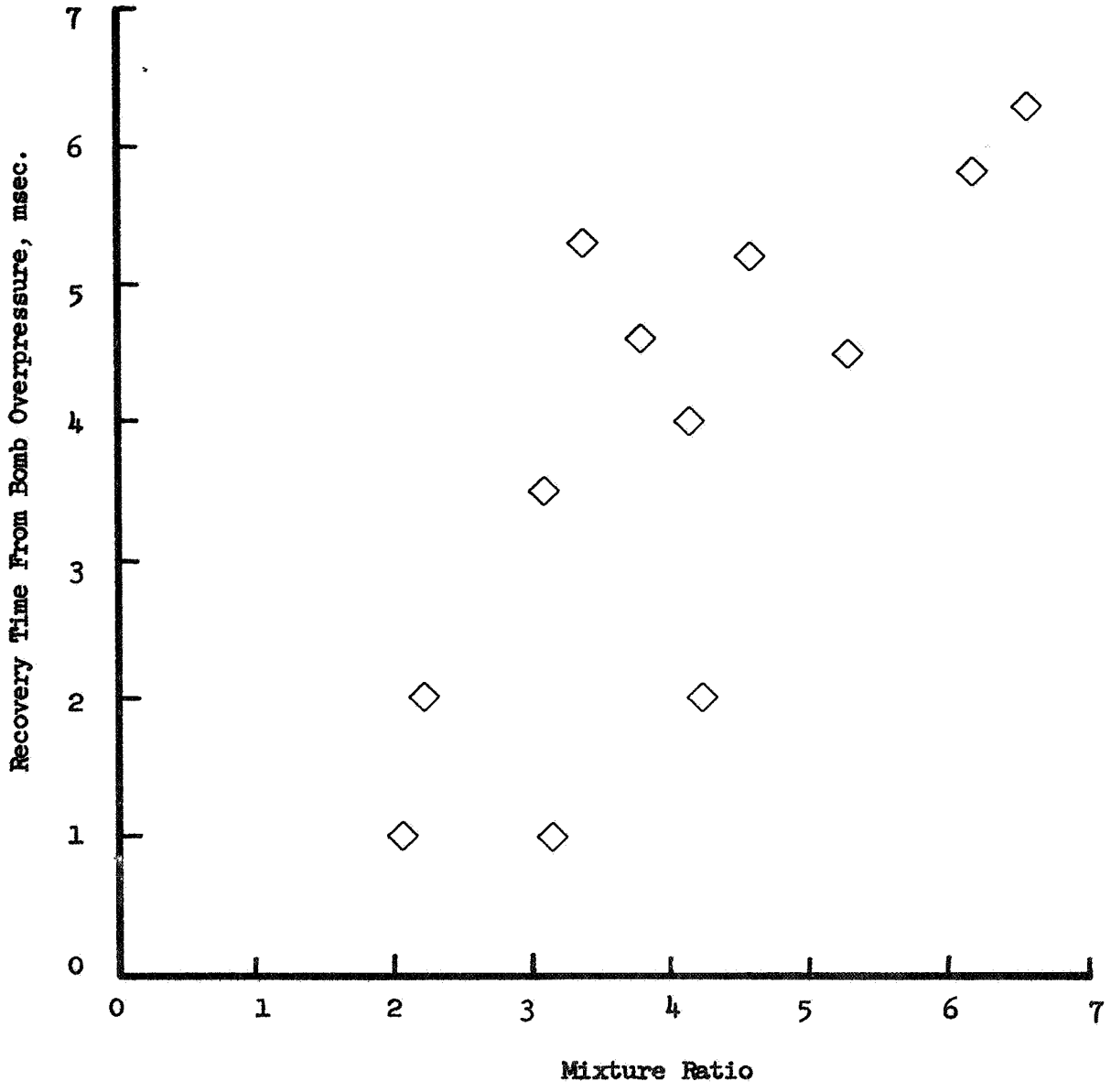

Recovery Time from Bomb Overpressure vs Mixture Ratio - All Data

Figure 48

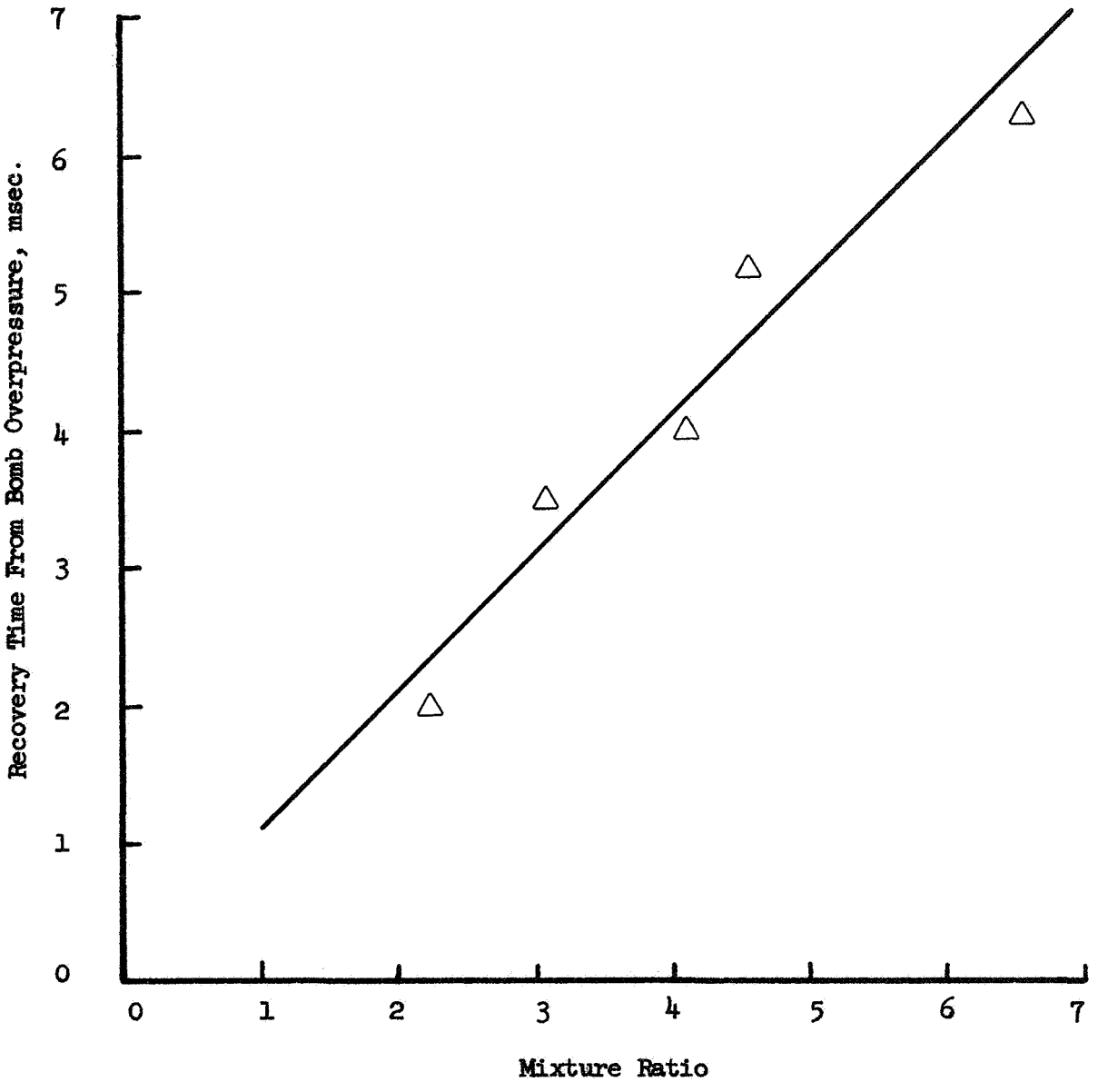

Recovery Time from Bomb Overpressure vs Mixture Ratio - Selected Tests at T_{fuel} 270°R

Figure 49

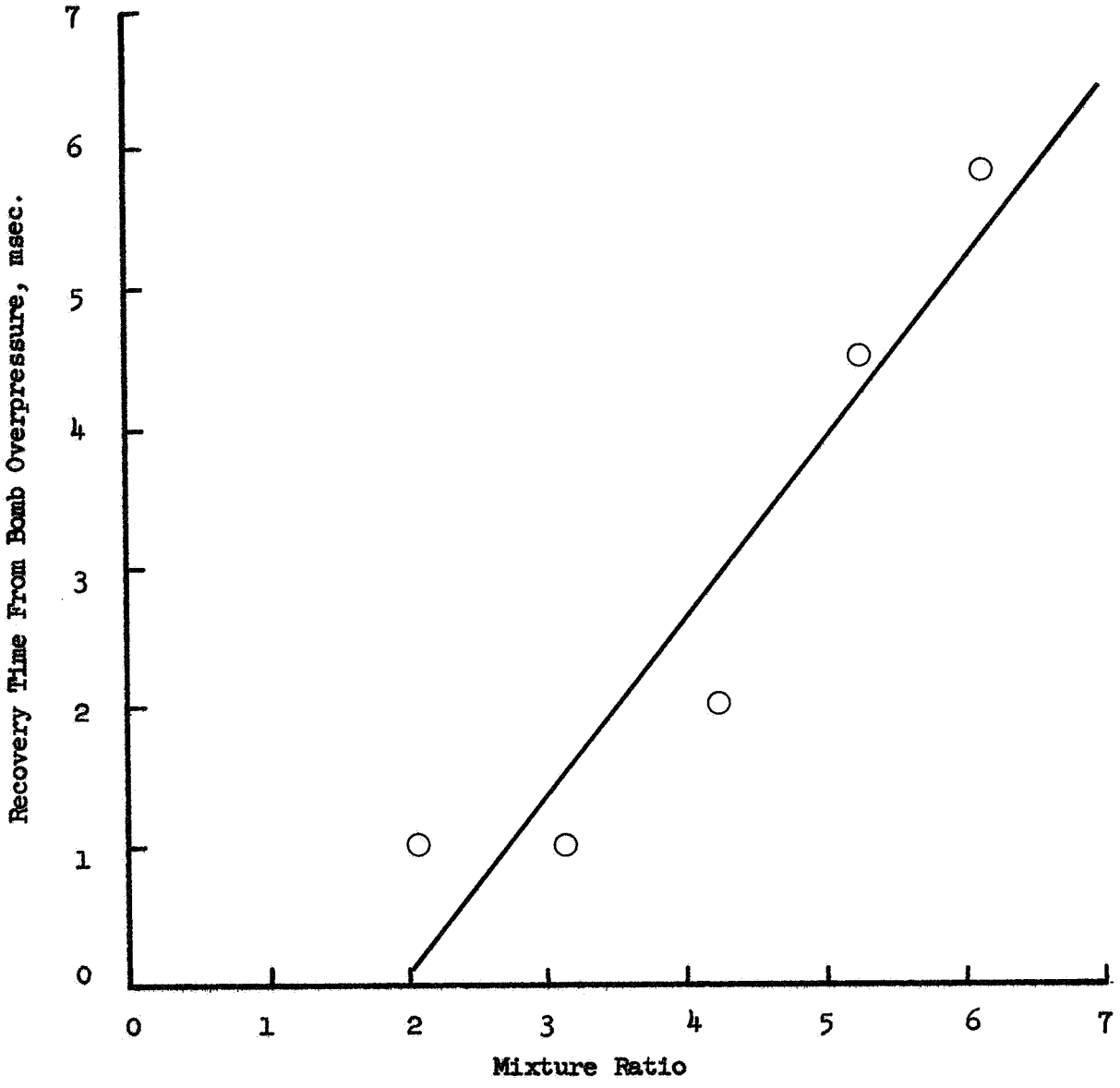

Recover Time from Bomb Overpressure vs Mixture Ratio - Selected Tests at $T_{fuel} \sim 530°R$

Figure 50

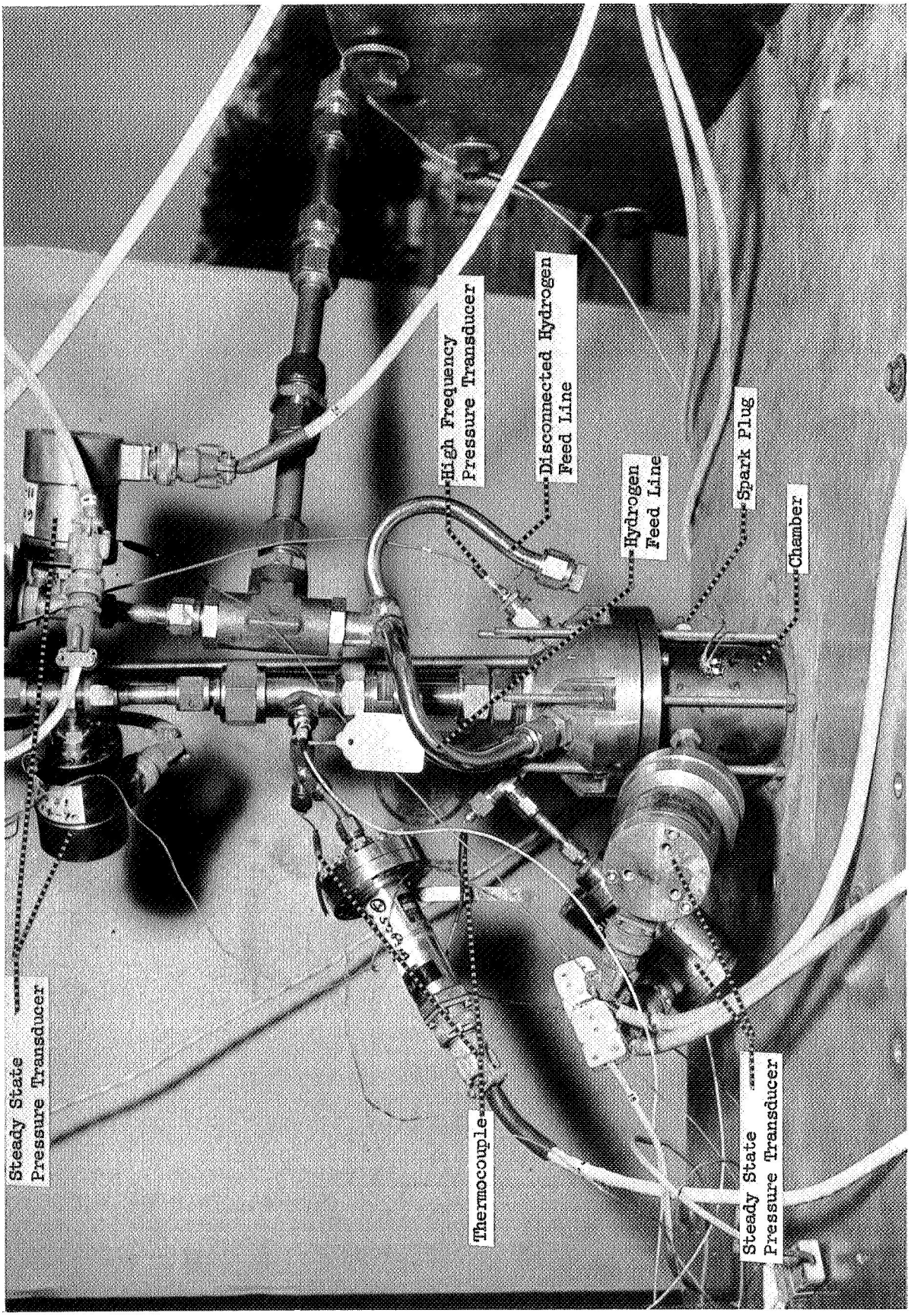

Modified Low Pressure Gas-Gas Hardware on Test Stand

Figure 51

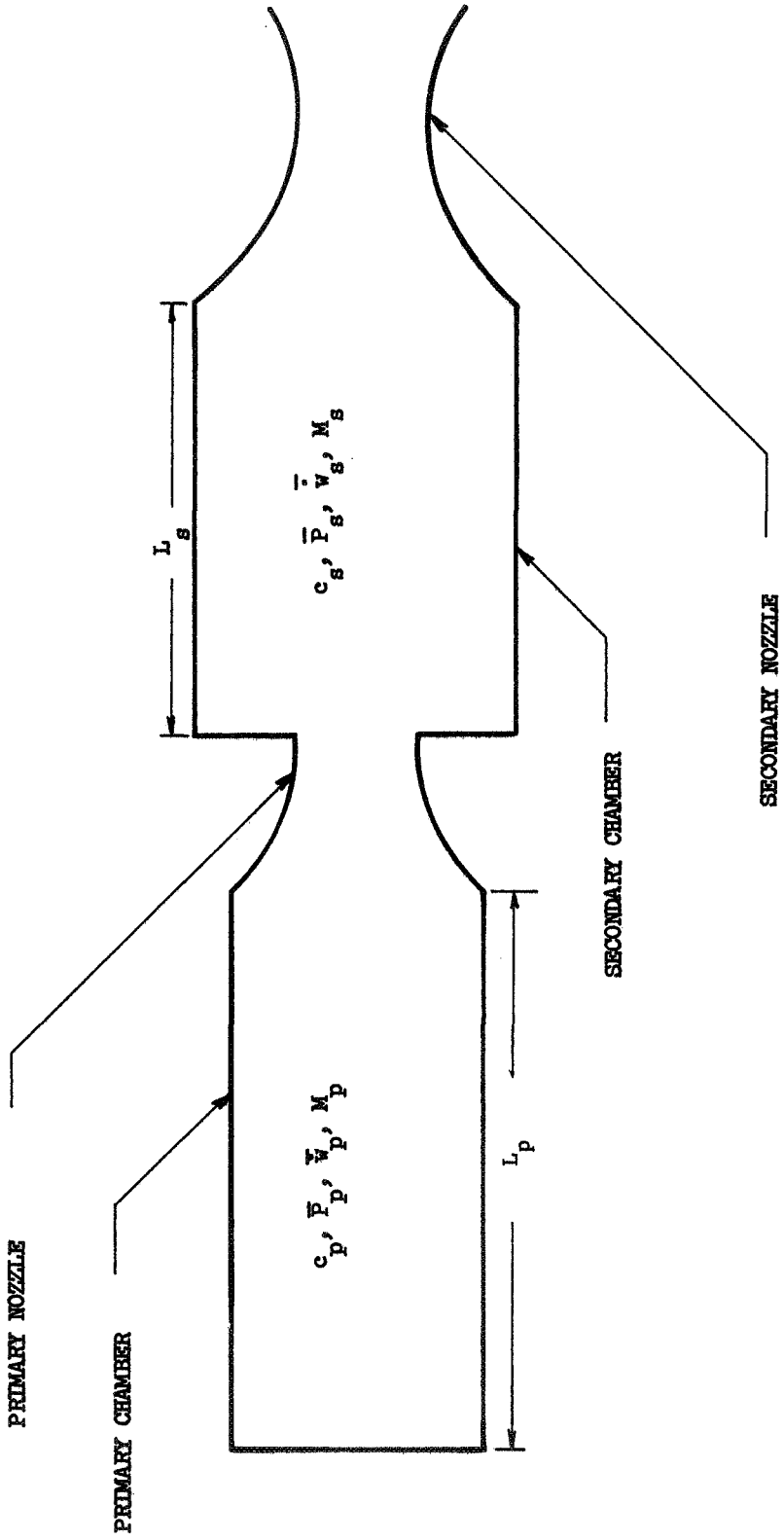

Schematic of Staged Combustion Cycle

Figure 52